ABSTRACT

Title of Dissertation: **Using Electric Fields to Modulate Polymeric Materials: Electro-adhesion, Electro-gelation and Electro-carving**

Wenhao Xu, Doctor of Philosophy, 2023

Directed By: Professor Srinivasa R. Raghavan
Department of Chemical and Biomolecular Engineering

This dissertation concerns the effects of electric fields on aqueous polyelectrolytes (solutions and gels), including those of polysaccharides and proteins. Electrical effects on such polymeric systems have not been studied in detail thus far. In this work, we apply electric fields as stimuli to trigger responses in these materials. We have discovered three novel responses: electro-adhesion of a gel to a solid electrode; electro-gelation of a polymer solution, which allows gels to be made in 3D, and localized electro-disruption of gels, which allows gels to be carved or sculpted.

In our first study, we show that it is possible to adhere a soft ionic conductor (like a polymeric hydrogel) to a hard, electronically conductive electrode using a low DC voltage without any adhesive. When 5 to 10 V DC is applied between a pair of electrodes (e.g., graphite, copper, etc.) spanning a cylindrical hydrogel (e.g., acrylamide, gelatin, etc.), in 3 to 15 min, the gel strongly adheres to either or both electrodes. The ultimate adhesion strength can exceed 150 kPa and is only limited by the strength of the soft material. This hard-soft electro-adhesion applies to not only lab-synthesized hydrogels but also animal or plant tissues, such as beef, pork, apples, bananas, etc. We show that this adhesion results from electrochemical reactions that form chemical bonds between the polymers in the gel backbone and the electrode surface. Hard-soft electro-adhesion

can be used to assemble hybrid materials with hard and soft compartments, which could be useful in robotics, energy storage, underwater adhesion etc.

Next, we demonstrate how an electric field can be used to gel a polymer solution with spatial control — thereby, we can 'print' gels in 3D. When a solution of alginate (an anionic biopolymer) is subjected to a DC electric field (~ 10 V) using a platinum (Pt) needle as the anode, a gel is formed right around the anode within seconds. By using a mobile anode, gel "voxels" can be formed sequentially and these merge into 3D structures. Similar electro-gelation can also be done with the cationic biopolymer chitosan, but at the cathode instead of the anode. The mechanism for gelation with both alginate and chitosan involves the polymer chains losing their charge next to the electrode. A loss of charge leads to insolubility, and insoluble domains act as crosslinks and connect the chains into networks. We have built a prototype for a 3D-printer that can translate a 3D design into a robust biopolymer gel formed by electro-gelation.

Lastly, we show that an electric field applied by an electrode can be used like a knife to carve or sculpt hydrogels into 3D shapes. When we apply a DC electric field across certain gels, the gel shrinks near the anode, while water is expelled out of the gel near the cathode. Ultimately the gel shrinks by more than 50% of its original size. Such shrinkage is observed with a range of anionic gels, including both physical gels of biopolymers like agar and alginate as well as covalent gels such as sodium acrylate. If the ionic strength of the gel is high, the shrinkage does not occur. The origin of this effect lies in a combination of electroosmosis as well as pH changes near the electrodes. Finally, we show that with a focused electric field, the shrinkage can be limited to a specific location in a gel, thereby allowing us to electro-carve gels in 3D.

Using Electric Fields to Modulate Polymeric Materials: Electro-adhesion, Electro-gelation and Electro-carving

by

Wenhao Xu

Dissertation submitted to the Faculty of the Graduate School of the
University of Maryland, College Park, in partial fulfillment
of the requirements for the degree of
Doctor of Philosophy
2024

Advisory Committee:

Prof. Srinivasa R. Raghavan, Dept. of Chemical & Biomolecular Engineering, Chair
Prof. Neil Blough, Dept. of Chemistry & Biochemistry
Prof. Daniel Falvey, Dept. of Chemistry & Biochemistry
Prof. Yuhuang Wang, Dept. of Chemistry & Biochemistry
Prof. Robert M. Briber, Dept. of Materials Science & Engineering, Dean's Representative

This dissertation is dedicated to wonderful world,
for all the splendid phenomena and science
that it has been displaying in front of my eyes.

Acknowledgements

I express my deepest gratitude to my advisor Prof. Srinivasa Raghavan for allowing me to pursue doctoral studies in Complex Fluids group. This successful endeavor would not have existed without his continual encouragement to explore different research topics. His patience, vision, research approach, ability to mentor students, and methodology to present research work with utmost clarity have deeply inspired me. I wish to carry forward these invaluable lessons throughout my scientific career. In all, I could not have asked for a better advisor and mentor for my doctoral studies.

Besides my advisor, I would like to thank the rest of my committee: Prof. Neil Blough, Prof. Daniel Falvey, Prof. Yuhuang Wang, and Prof. Robert Briber for their valuable ideas and feedback on my research projects. I would like to extend my sincere appreciation to Prof. Peter Kofinas and Prof. Po-Yen Chen for their advice and discussions related to this work.

I am also thankful to my groupmates from Dr. Raghavan's group, both present and past, for all the help I received for my research activities. Specifically, I would like to thank Dr. Leah Borden, Dr. Nikhil Subraveti, Faraz Ahmed Burni and Morine Nader, for all the productive suggestions and discussion from them. I would also like to thank Dr. So Hyun Ahn for her kind guidance on lab instruments when I first joined the group. I am also thankful to Dr. Niti Agrawal, Dr. Ben Thompson, Dr. Jaeho Lee, Dr. Hema

Choudhary, Medha Rath, Mahima Srivastava, Futoon Aljirafi, Christine Zhou, Eylul Utlu, Samantha Grasso, Wei-Yi Chu, Ireen Philip and Paula Atienza.

Finally, I would like to express my gratitude to my family and especially my parents. Words cannot express my thankfulness for their love, support, and sacrifices. The value of education that they instilled in me at my young age is the primary foundation for where I am today.

Table of Contents

List of Figures

List of Abbreviations

DC	Direct current
3D	Three-dimensional
AAm	Acrylamide
$EA^{[HS]}$	Hard-soft electro-adhesion
AC	Alternating current
SA	Sodium acrylate
DMAA	*N*,*N*-dimethylacrylamide
NIPA	*N*-isopropylacrylamide
HEMA	2-hydroxylethyl methacrylate
DMAEMA	2-(dimethylamino)ethyl methacrylate
QDM	[2-(methacryloyloxy)ethyl]trimethylammonium chloride
BIS	*N*,*N*'-methylenebis(acrylamide)
PEGDA	Poly(ethylene glycol) diacrylate
PVA	Poly(vinyl alcohol)
Ca^{2+}	Calcium ions
Cu^{2+}	Copper(II) ions
Zn^{2+}	Zinc ions
$–COO^{–}$	Carboxylate groups
H_2O	Water
APS	Ammonium persulfate

KPS	Potassium persulfate
TEMED	*N*,*N*,*N*',*N*'-tetramethylethylenediamine
$CaCl_2 \cdot 2H_2O$	Calcium chloride dihydrate
NaCl	Sodium chloride
HCl	Hydrochloric acid
Cu	Copper
Pb	Lead
Sn	Tin
Ni	Nickel
Fe	Iron
Zn	Zinc
Ti	Titanium
DI	Deionized
FTIR	Fourier-transform infrared
ATR	Attenuated total reflectance
E^o	Standard reduction potential
WE	Working electrode
CE	Counter electrode
G^{bulk}	Gel slice from the bulk
G/+	Gel slice next to the anode
G/–	Gel slice next to the cathode
Al	Aluminum

DLP	Digital light processing
Al^{3+}	Aluminum ions
H^{+}	Hydrogen ions
LVE	Linear viscoelastic
EDC	1-ethyl-3-(3-dimethylaminopropyl)carbodiimide
NHS	*N*-hydroxysuccinimide
HEK293T	Human embryonic kidney 293T
Pt	Platinum
OH^{-}	Hydroxide ions
H_2	Hydrogen
NaOH	Sodium hydroxide
Na^{+}	Sodium ions
4D	Four-dimensional

Chapter 1
Introduction and Overview

1.1 Problem Description and Motivation

Soft polymeric materials such as hydrogels and capsules are widely applied in drug delivery, tissue engineering, soft robotics, and wearable devices.[1-5] They have unique advantages over traditional hard materials, especially in terms of biocompatibility and responsiveness to external stimuli.[6-14] Possible stimuli that can modulate polymers include pH, solvent, temperature, and light, but our particular interest in this work is in electric fields. Electricity is the most widely used form of energy in modern society. An electric field can be turned on and off with spatial and temporal resolution (i.e., at a given location and time) that is difficult to achieve with other stimuli. Also, compared to other stimuli, electric fields can generally trigger a faster response.[15]

Current knowledge regarding the effects of electric fields on soft polymeric materials is still limited. Some studies have focused on conductive polymers, where the charge carriers are electrons, but such polymers are costly and generally not biocompatible.[4,16,17] Responses of polyelectrolyte solutions and gels under electric fields have also been reported in literature, including by our lab. For example, on the application of a DC field to a polyelectrolyte solution, *electro-deposition* has been shown, where the polymer deposits as a thin film on either the cathode or anode due to pH gradients in the solution.[18] Alternatively, polyelectrolyte gels can change their volume (swell or shrink) or undergo a transformation in shape (i.e., a gel strip can bend and curl)

when a field is applied.[19-22] Another example involves *electro-adhesion*, which is a field-induced adhesion of a cationic and an anionic gel.[23-27]

Our lab has contributed recent studies regarding the effects of electric fields on polymeric materials. In particular, we have shown that gels of alginate (an anionic biopolymer) could be formed in various 3D-shapes upon applying a DC field.[28] This approach, termed *electro-formation*, works by inducing electrophoresis of crosslinker cations out of a template into an alginate solution (see next section for details). Unlike the electrodeposition technique[18] reported by others, which was limited to thin films, our electro-formation could be extended to 3D structures, albeit those would be replicas of a template. In the present work, we will seek to improve on our previous work by eliminating the requirement of a template. In a different study, we have shown that electro-adhesion could be induced not only between two gels but also between a cationic gel and various biological tissues.[29] Lastly, we have demonstrated that physically crosslinked hydrogel capsules could be disintegrated by applying a field.[15]

Our previous work has discovered a variety of new and interesting phenomena when electric fields are applied to aqueous polymeric materials. This is an area that has been relatively unexplored, partly because it is very complex, involving electrochemistry, interfacial effects (at electrodes), and electrophoresis (field-induced migration of ions and polyelectrolytes). We believe this is a rich area and that are still many significant responses that could be induced in polymeric materials by electric fields.

1.2 Proposed Approach

The overall goals of this work are to explore phenomena involving electric fields and aqueous polymeric materials (hydrogels and solutions). We aim to modulate the properties of the material, either in the bulk or at an interface. In this regard, we have discovered and developed three new phenomena, which are described in this dissertation:

1.2.1 Electro-Adhesion of Gels to Hard Conductive Solids

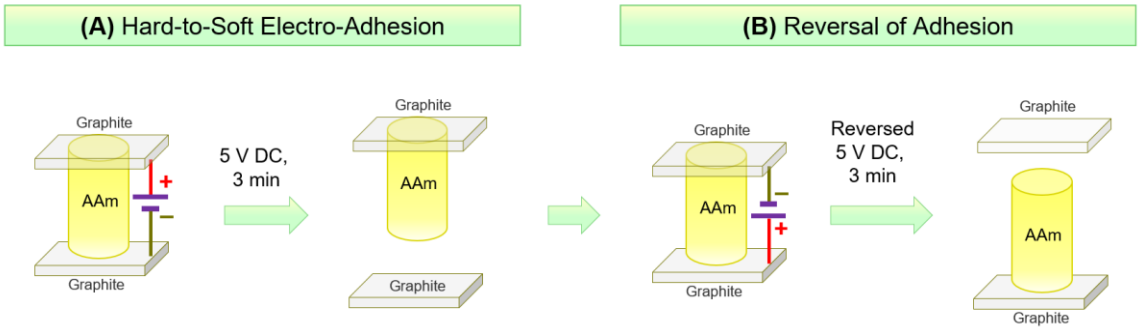

Figure 1.1. Reversible electro-adhesion of an acrylamide (AAm) gel onto graphite. (A) AAm gel adheres to graphite at the anode when 5 V DC is applied for 3 min. (B) When reversed 5 V DC is applied for 3 min, the anode detaches and the cathode adheres.

In Chapter 3, we demonstrate that soft, aqueous materials (e.g., hydrogels, fruit or animal tissue) can be adhered to hard, electrically conductive materials (e.g., copper or graphite) without the use of an adhesive. This is illustrated by Figure 1.1 for the case of graphite and a covalent gel of acrylamide (AAm). The adhesion is induced by a low DC electric field applied across the hard-soft pair. It endures after the field is removed and we term it as hard-soft electro-adhesion or $\mathbf{EA}^{[\mathbf{HS}]}$. $\mathbf{EA}^{[\mathbf{HS}]}$ works with chemical gels like AAm, physical gels like gelatin and alginate, and even soft, everyday objects like fruit (bananas, apples) and animal tissue (beef, pork). Depending on the gel chemistry, adhesion occurs at the anode (+), cathode (–), both electrodes, or neither. If adhesion is

observed only to one electrode, it can typically be reversed by switching the polarity of the electrodes and re-applying the field. We show that **EA[HS]** arises via electrochemical reactions that generate chemical bonds between the hard material (electrode) and the polymers in the gel network.

1.2.2 Electro-Gelation of Biopolymer Solutions as a Route to 3D-Printed Gels

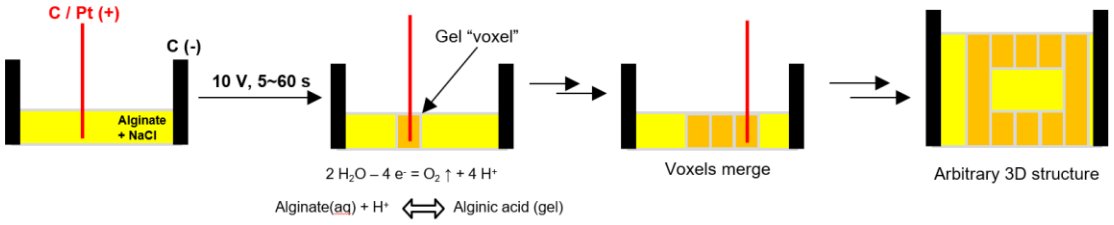

Figure 1.2. Electro-gelation of alginate and its use to make alginate gels in 3D shapes. When a DC electric field is applied, the alginate solution converts into a gel around the anode. The gelled elements ("voxels") fuse to form 3D structures. By moving the anode in 3D, gels of arbitrary shapes can be formed.

In Chapter 4, we describe the local gelation of a polymer solution triggered by an electric field. This allows us to 3D-print hydrogels. In conventional 3D-printing of gels, polymer (or monomer) solutions are extruded out of nozzles and immediately gelled. The nozzle is moved in 3D to achieve a specific shape. In our method, we instead use a needle-like electrode to locally gel the anionic biopolymer alginate (Figure 1.2). The gel forms right around the anode (working electrode) in a small volume. By controlling the position of the anode, alginate gels can be printed as 3D volume elements ("voxels"), which merge into one 3D structure. A similar electro-gelation can also be done with the cationic biopolymer chitosan, but at the cathode instead of the anode. The mechanism for gelation in both alginate and chitosan involves the polymer chains losing their charge

next to the electrode. A loss of charge leads to insolubility, and insoluble domains act as crosslinks and connect the chains into networks.

1.2.3 Electro-Carving Hydrogels into 3D Shapes

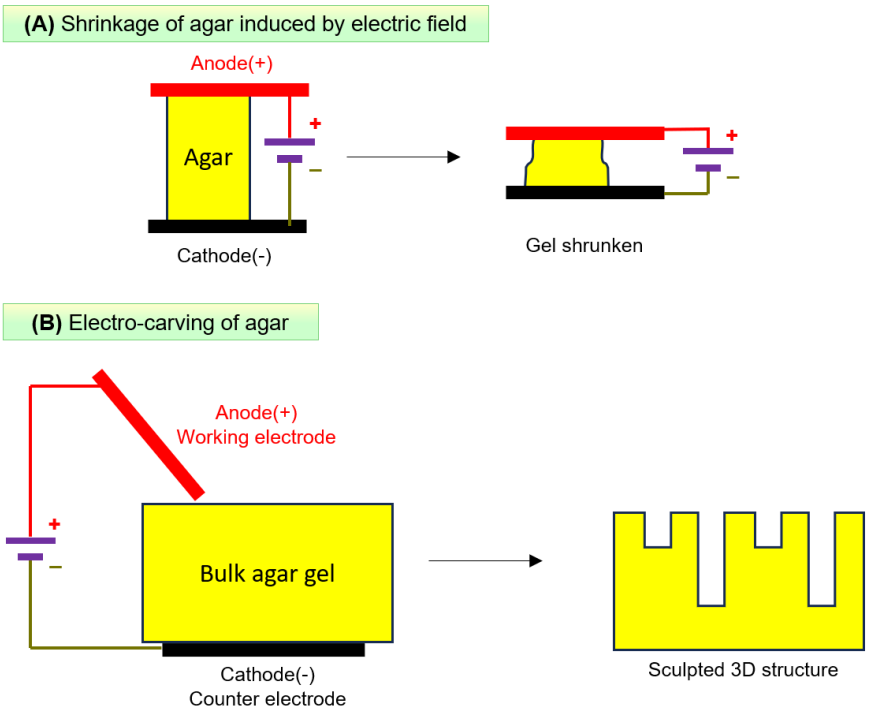

Figure 1.3. Electro-carving hydrogels. (A) Agar gels shrink at the anode when a DC electric field is applied. (B) By focusing the field using a rod-shaped working electrode, the gel can be carved into 3D structures.

Finally, in Chapter 5, we demonstrate the use of electric field to locally liquefy a hydrogel and thereby carve or sculpt it into a 3D shape. When we apply a DC electric field across certain gels, the gel shrinks near the anode, while water is expelled out of the gel near the cathode. Ultimately the gel shrinks by more than 50% of its original size (Figure 1.3A). Such shrinkage is observed with a range of anionic gels, including both physical gels of biopolymers like agar and alginate as well as covalent gels of monomers

like sodium acrylate. If the ionic strength of the gel is high, the shrinkage does not occur. The origin of this effect lies in a combination of electroosmosis as well as pH changes near the electrodes. By focusing and intensifying the electric field using a rod-shaped electrode, the shrinkage can be limited to a specific location in a gel, thereby allowing us to electro-carve gels in 3D (Figure 1.3B).

1.3 Significance of This Work

In this dissertation, we describe new ways to modulate polymeric materials using electric fields. Each part of our work has a fundamental basis, and thus the intellectual merit behind our study lies in advancing the underlying science. Moreover, our focus in Chapters 4 and 5 has been to leverage the spatial and temporal precision of an electric field. In addition, our work can potentially lead to a variety of applications, which constitute its "broader impacts". Significant points pertaining to Chapters 3-5 are:

- In Chapter 3, we show that electric fields generate long-lasting adhesion between a soft hydrogel and a hard conductive solid. Thereby, we can join materials with very different mechanical properties without any adhesive. The resulting hybrids combine the elasticity of soft materials as well as the weight-supporting ability of hard materials, which could be useful in robotics, energy storage, body implants, etc. The fundamental basis for this adhesion lies in electrochemical reactions between an electrode and a gel backbone. This is a rare example where the electrode exchanges electrons with not small molecules but polymer chains in the network.

- Chapter 4 demonstrates local electro-gelation of biopolymer solutions. While the chemistry for such gelation is known, we have focused on exploiting it in a manner conducive to 3D-printing. We have built a prototype device modified from a regular 3D-printer that can take in a 3D shape as input and make a robust biopolymer gel in that shape by electro-gelation. Compared to conventional 3D-printing, our method can achieve faster printing speed and more robust gels, while avoiding nozzles, pumps, inks, and UV light or heat to convert the liquid ink to a gel. All in all, electro-gelation provides a simpler and less costly way to make hydrogels in 3D. hydrogel 3D-printing strategies.

- Lastly, the electro-carving technique in Chapter 5 provides an alternative way for fabricating 3D-structured hydrogels. Top-down strategies (i.e., eliminating excess parts from bulk materials) can sometimes be more effective and convenient than bottom-up strategies (i.e., building up from scratch as in 3D-printing). However, traditional top-down methods for hard materials like mechanical carving and smithing cannot be applied to hydrogels due to their soft nature. We demonstrate that by focusing electrical stimuli, shrinkage of a hydrogel can be triggered at specific locations. Thereby a gel can be carved into 3D shapes by our technique.

Chapter 2

Background

2.1 Polymeric Hydrogels

This dissertation centers on the properties of polymeric materials, especially hydrogels. Hydrogels are crosslinked networks of polymer chains with water entrapped in the network.[30-32] Polymers are basically random coils when dissolved in water. When the random coils are connected to each other by crosslinkers, they form a sample-spanning network and the sample then becomes a hydrogel (Figure 2.1). The crosslinks can be either physical or chemical bonds, i.e., the polymer chains can be crosslinked either by intermolecular interactions, such as van der Waals forces, hydrogen bonding, electrostatic interactions, etc., or by covalent bonds. The properties of a hydrogel depend on the chemical nature of the polymer, the concentration of polymer chains and also the crosslink density.

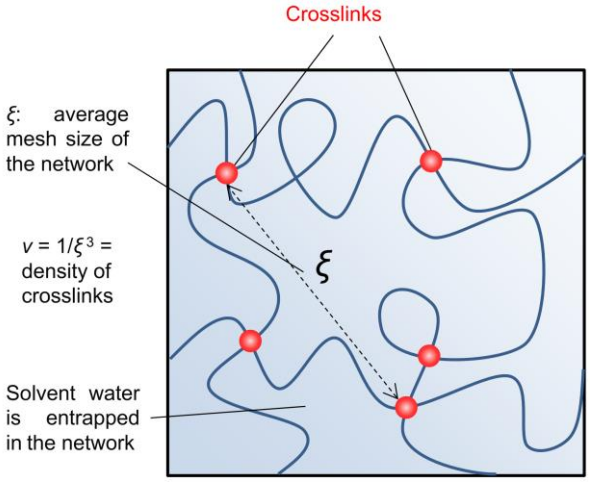

Figure 2.1. Schematic of a polymer hydrogel showing its internal nanostructure. The hydrogel is a crosslinked network of polymer chains. The network is swollen with water.

Swelling of a gel in a solvent is an equilibrium between the osmotic pressure inside the gel and the elastic pressure of the polymer chains.[33] For non-ionic gels, the swelling extent is predicted by Flory-Rehner equation:

$$-\left[\ln\left(1-\phi_p\right)+\phi_p\right]=\chi\phi_p^2+V_s\cdot\nu\cdot\left(\phi_p^{\frac{1}{3}}-\frac{\phi_p}{2}\right) \quad (2.1)$$

Here, ϕ_p is the volume fraction of the polymer in the swollen gel, χ is the polymer-solvent interaction parameter, V_s is the molar volume of the solvent, and ν is the density of crosslinks in the gel. The left side of the equation corresponds to the entropy of mixing, the first term on the right is the enthalpy of mixing, and the second term is the elastic entropy of the polymer network. If the interaction between polymer and solvent is more favorable, $\chi < 0.5$ and if the polymer-polymer or solvent-solvent interaction is more favorable, $\chi > 0.5$. One trend from the above equation is that if $\chi < 0.5$, ϕ_p will be low, implying that the gel will swell appreciably in the solvent. Secondly, with lower density of crosslinks ν, again ϕ_p will be low and the gel will swell significantly. Another point to note is that ionic gels swell much more than non-ionic gels due to the high osmotic pressure arising from the presence of counterions and also from the electrostatic repulsions between polymer backbones.[33]

One of the appealing features of hydrogels is their ability to respond to external stimuli, which can include pH, solvent composition, ionic strength, light, temperature, etc.[6-14] In this dissertation, we will focus on the effects of electric fields on hydrogels. When an electric field is turned on, external forces are imposed on any charged species, be it ionic polymer chains or the small-molecule ions (counterions or those arising from

the dissociation of salts). Depending on the type of field (DC or AC), the field strength, and the geometry of the experiment, hydrogels in solution could experience different effects.

2.2 Synthetic Gels and Free-Radical Polymerization

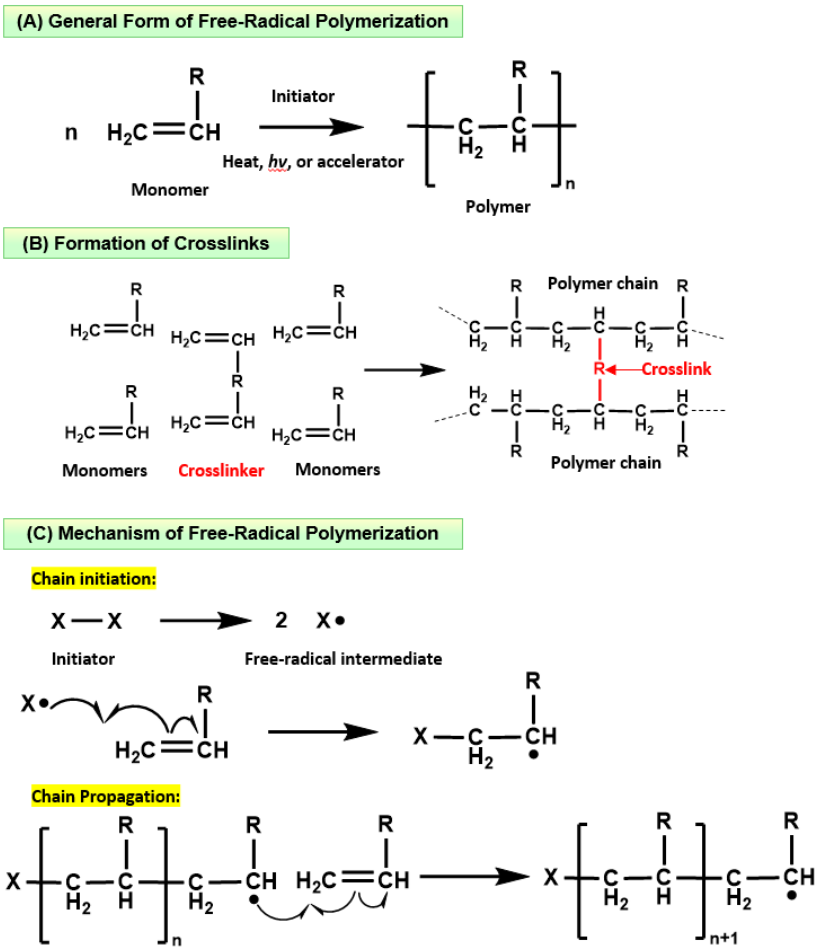

Figure 2.2. Free-radical polymerization. (A) In the typical case, monomers with double bonds polymerize into chains. (B) A crosslinker with two double bonds crosslinks two chains. (C) Mechanism of the polymerization: chain initiation and chain propagation.

This dissertation involves a variety of different hydrogels, including both chemically and physically crosslinked ones. Chemical gels are typically synthesized by

free-radical polymerization. This chemical reaction opens the π-bonds in double bonds of small molecule monomers, and connects multiple monomers into a long polymeric chain (Figure 2.2A). If all the monomers have only one double bond, the reaction results in linear polymers instead of a 3D network. To make a gel with a 3D polymer network, crosslinkers with two or more double bonds are required (Figure 2.2B). The crosslinker molecules connect adjacent polymer chains with covalent bonds. In this way, linear chains are covalently crosslinked into a 3D network, thus forming a gel. Commonly used monomers and crosslinkers for hydrogels include various acrylic acid derivatives, as shown in Figure 2.3.[34]

The kinetics of free-radical polymerization typically involves three steps: chain initiation, chain propagation and chain termination (Figure 2.2C). An initiator is required to generate free radicals that initiate the reaction. Typically, the initiator has a weak covalent bond (e.g., peroxide or azo) that cleaves to generate free radicals when triggered by heat, light or chemical accelerators. These free radicals attack the double bonds of the monomer, resulting in new free radicals with one more monomer than the previous one. By repeating the propagation process, monomers are connected in series, with the end of the chain still being a free radical. Finally, the free radicals are quenched by each other or by inhibitors and thus the chain is terminated. Inhibitors react with free radicals and form non-radical molecules or stable radicals that do not propagate. Trace amounts of inhibitors are added to monomers to prevent their polymerization on the shelf. Oxygen is also a common inhibitor, and so free-radical polymerizations in the aqueous phase usually requires an inert (nitrogen) environment to avoid the interference of oxygen.[34]

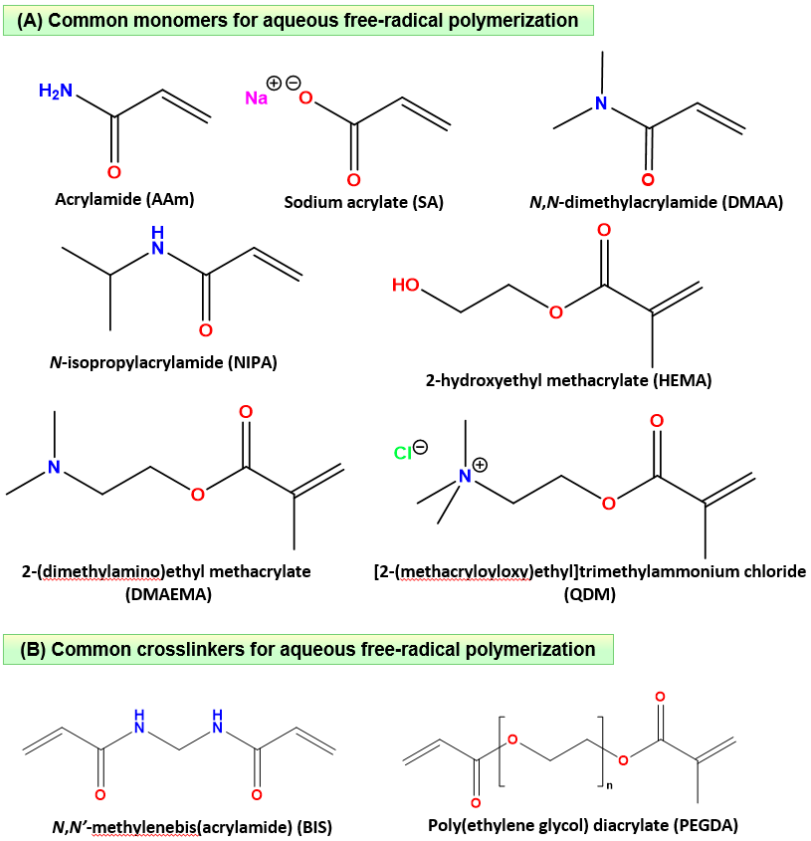

Figure 2.3. Monomers and crosslinkers used to make hydrogels by aqueous free-radical polymerization. (A) Monomers. (B) Crosslinkers.

Synthetic polymers can also be physically crosslinked instead of being chemically crosslinked, one typical example being poly(vinyl alcohol) (PVA). Commercially available PVA is a linear water-soluble polymer. A PVA solution is viscous, but not a gel. However, it can be gelled by freeze-thaw cycling. When a PVA solution is frozen, the crystallizing ice takes up the space, forcing PVA chains to form domains via hydrogen bonding. Then when the frozen solution is thawed at room temperature, the domains of PVA are still preserved. By repeating the freeze-thaw cycle, more domains are formed. The domains act as crosslinks between the linear chains, thereby leading to a gel network.[35]

2.3 Biopolymers and their Hydrogels

Hydrogels can also be made by crosslinking biopolymers obtained from natural sources.[36] Biopolymer-based hydrogels have advantages over their synthetic counterparts in terms of their inherent biocompatibility, abundance, safety, and low cost. Biopolymers involved in this dissertation include alginate, gelatin, chitosan, and agar.

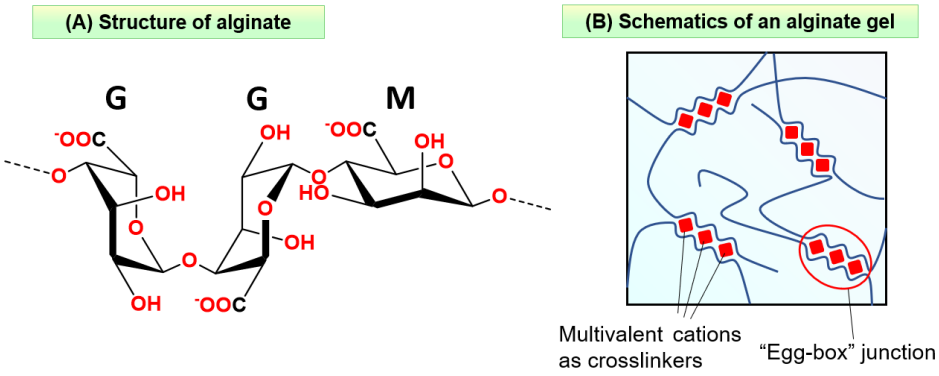

Figure 2.4. Alginate and its hydrogels. (A) Chemical structure of alginate. (B) An alginate hydrogel crosslinked by multivalent cations such as Ca^{2+}.

Sodium alginate is an anionic polysaccharide derived from brown algae. It is composed of 1,4-linked β-D-mannuronic (M) and α-L-guluronic (G) residues, which are typically found in blocks along the polymer chain (Figure 2.4A).[37] Being an anionic polymer, sodium alginate is soluble in water. To gel this polymer, it is contacted with multivalent cations such as Ca^{2+}, Cu^{2+}, Zn^{2+} etc. The carboxylates ($-COO^-$) on the G blocks form complexes with the cations, and such "egg-box" junctions crosslink the chains into a gel network (Figure 2.4B).[37,38] Due to its easy and fast gelation, high biocompatibility and low cost, sodium alginate has been widely used in applications such as cell encapsulation and 3D-bioprinting.

Gelatin is a mixture of polypeptides derived from denaturing of its parent protein collagen. Collagen, being the most abundant structural protein in animal kingdom, constitutes ~ 30% of an animal's total proteins. Collagen- and gelatin-derived products are widely used in food, pharmaceutical and cosmetic applications. For instance, Jell-O, one of the most common desserts worldwide, is basically a gelatin gel. A collagen molecule consists of three polypeptide chains, each one being a left-handed α-helix. The three α-chains further intertwine into a right-handed triple super-helical fibril. Collagen from different sources also varies in sequence and structure. To make gelatin from collagen, the triple helix formed by the peptide chains is disassembled, and slight hydrolysis of the peptide bonds also occurs. Gelatin is known to be thermo-responsive. It dissolves in water when heated to ~ 40 °C, slightly higher than physiological temperature. When a gelatin solution is cooled, the triple helical structure recovers to some extent, and the triple-helical junctions crosslink gelatin into a gel. When the gel is heated up, the crosslinks disassemble, and the gel "melts" and becomes a solution.[39,40]

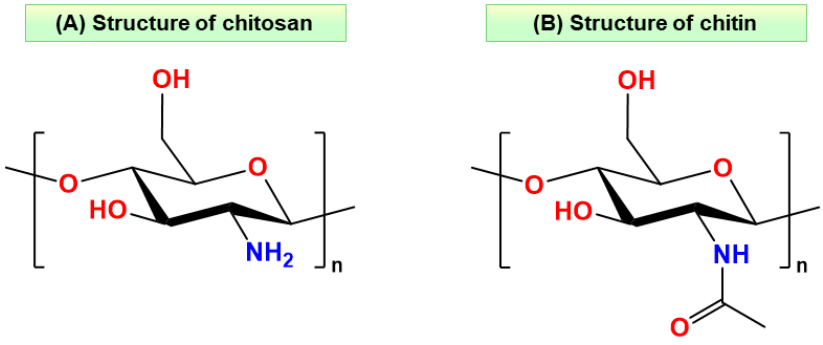

Figure 2.5. Chemical structure of chitosan and chitin. (A) Chitosan. (B) Chitin.

Chitosan is a polysaccharide derived from its natural precursor chitin. Chitin is a long-chain polymer of β-(1→4)-linked *N*-acetyl-D-glucosamine. It is the main

component of the exoskeleton of arthropods like crabs, shrimps and insects, and also the primary polymer in the cell walls of fungi. Chitosan is made by deacetylation of chitin (Figure 2.5), with the degree of deacetylation ranging from 60% to 100%. The amine groups of chitosan have a pK_a around 6.3, and so chitosan is not fully protonated around neutral pH. It only dissolves in water under acidic conditions. To gel the chitosan solution, there are multiple methods. Cationic chitosan can be crosslinked by micelles formed by anionic surfactants, or by multivalent anions such as tripolyphosphate. Also, adding a chitosan solution to a base will deprotonate chitosan and convert it into a gel.[41]

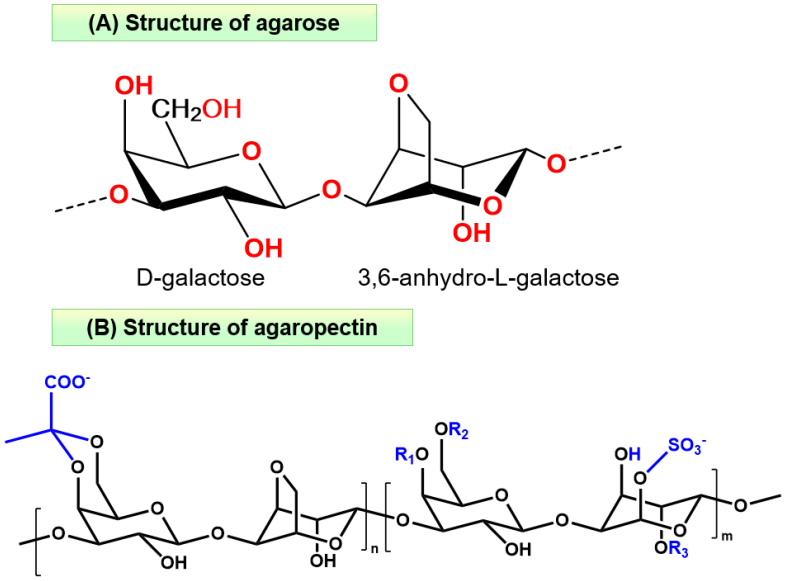

Figure 2.6. Chemical structures of the two components of agar. (A) Agarose. (B) Agaropectin.

Agar is a polysaccharide extracted from red algae. It is composed of two components: non-ionic agarose and anionic agaropectin. Agar is well-known for its application as a vegetarian alternative to gelatin in desserts, and also agar gels are used

for microbial cell culture. Agarose has a wide range of applications in drug delivery, disease treatment, tissue engineering, etc., while agaropectin is of less interest. Agarose is a linear polymer of 1,3-linked β-D-galactose and 1,4-linked 3,6-anhydro-α-L-galactose residues in an alternating sequence (Figure 2.6). Agar and agarose are insoluble in water at room temperature, but dissolve near boiling temperature (80 to 90°C). When a hot agar or agarose solution is cooled, it forms a gel at 30 to 45°C. Agar and agarose gels are thermo-reversible, which means the gels can be converted back into a solution when heated to ~ 80°C. This makes it easy to mold agar or agarose gels into various shapes.[42,43]

2.4 Electric-Field-Induced Effects on Polymeric Materials

A DC electric field generates two effects on charged species in water.[44] One is electrophoresis, which is the migration of charged species (ions, ionic polymer chains, colloidal particles, etc.) along the direction of the field. The other is electrochemical reactions, which are redox reactions that occur at the interfaces of ionic conductors (i.e., the electrolyte) and electronic conductors (i.e., the electrodes). By redistribution of ions and generation or consumption of species, further effects on polymers can be triggered.

Figure 2.7 depicts some of the possible effects of DC fields on polyelectrolyte gels, as described in the literature. Gel strips have been shown to bend under a field (Figure 2.7A).[20] This has been attributed to osmotic gradients originating from the electrophoresis of ions or pH gradients due to electrolysis of water. Next, Figure 2.7B depicts reversible adhesion of oppositely charged gels triggered by an electric field.[24,29] This is believed to arise from the migration and entanglement of cationic and anionic

polymer chains across the interface. Lastly, Figure 2.7C shows that certain spherical gels/capsules can be disrupted by an electric field, which is attributed to electrophoresis causing changes in crosslink density within the capsule.[15]

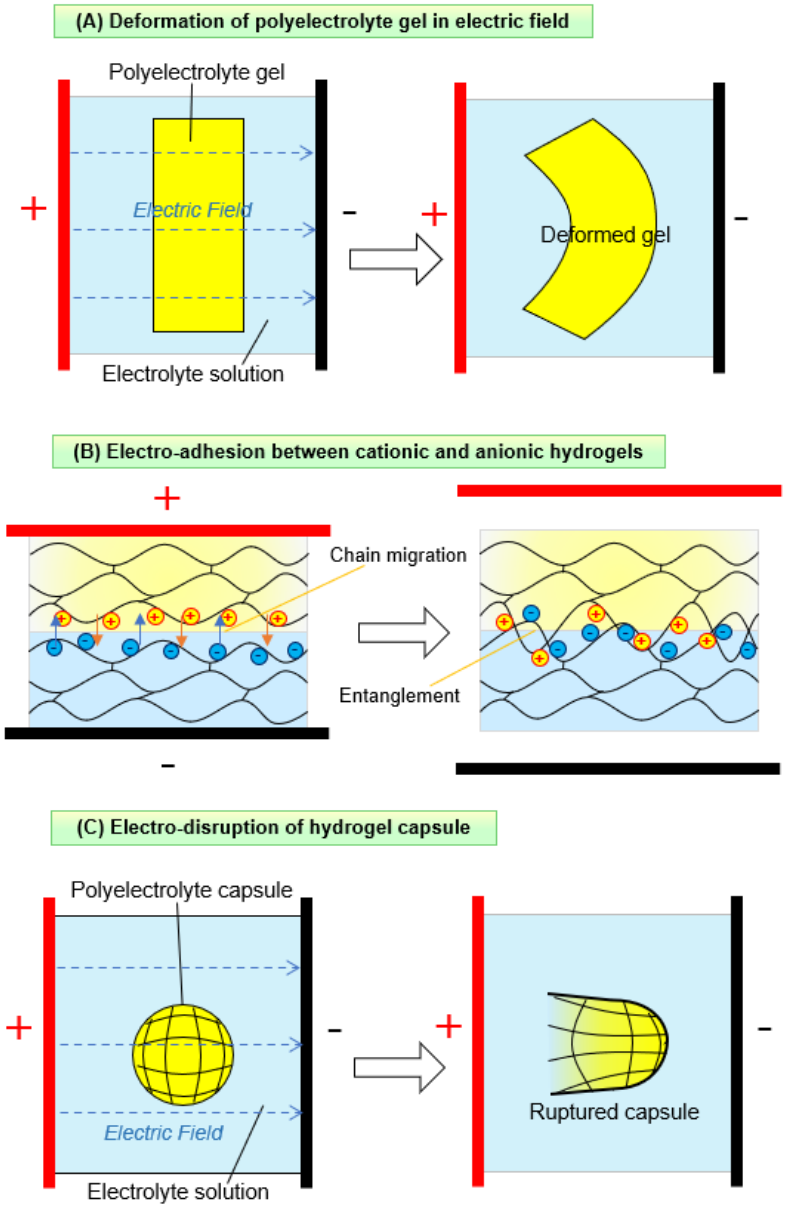

Figure 2.7. Schematics of electric-field induced effects on hydrogels. (A) Anisotropic swelling of a polyelectrolyte gel induced by electric field; **(B)** Electro-adhesion of a cationic and an anionic gel; **(C)** Electro-disruption of a polyelectrolyte capsule induced by electric field.

Chapter 3
Electro-Adhesion of Gels to Hard Conductive Solids

3.1 Introduction

This chapter is concerned with both soft and hard solids. Common examples of soft solids are *hydrogels*, which are three-dimensional networks of polymer chains swollen with water.[30-32] The networks can be crosslinked by chemical (covalent) bonds or physical (non-covalent) bonds such as hydrogen-bonds. Examples of the latter include gelatin gels, which are a popular dessert (Jell-O) in many parts of the world.[39,40] Other examples of soft, aqueous materials include plant products (fruits and vegetables), aquatic animals, and the tissues in our body.[45,46] Indeed, typical biological cells are soft and gel-like, with a water content around 70%.[45,47] Yet, the architecture of vertebrate animals, including humans, shows the need to combine soft tissues with hard structural elements, i.e., bones, vertebrae, and the skeleton.[45,48] The hard elements are needed to support the weight of the animal, provide structural integrity, and transmit force. The need to combine soft and hard elements also comes into the fore when designing soft robots or actuators.[49,50] Researchers have realized that, for a robot to exert forces, soft, force-generating elements (akin to muscle) must be interfaced with stiff, load-bearing elements (akin to bone) via elements of intermediate stiffness (akin to cartilage).[50]

Motivated by some of the points mentioned above, several researchers have attempted to adhere soft hydrogels to hard solids (e.g., metals, plastic, wood, glass).[51-59] However, to achieve adhesion, typically the chemistry of either the hydrogel or the hard

surface has to be modified. One common modification has been inspired by the chemistry of mussels and is *via* catechol groups.[60-62] Mussels stick to rocky surfaces by secreting filaments rich in catechols, which form strong coordination bonds with the surfaces. Accordingly, catechols can be introduced into gel backbones to make gels adhere to hard surfaces.[61,62] Other chemistries have also been exploited to induce strong gel-solid adhesion. For instance, Sekine *et al*.[54] functionalized acrylamide (AAm) gels with azide groups and contacted the gels with glass surfaces decorated with alkyne groups. A cycloaddition reaction between the azides and alkynes ensued, leading to strong adhesion. In most of the above cases where a gel is bonded to a hard solid, the adhesion is permanent, i.e., the two cannot be easily detached at a later time if needed. Thus, to sum up the literature, gel-solid adhesion has been achieved mostly for chemically tailored gels or surfaces, and once the gel is adhered to the solid, their adhesion is generally permanent and irreversible.

Recently, there has also been interest in triggering adhesion (i.e., achieving 'adhesion on command') via an external stimulus such as electric fields.[24,27,29] For example, a DC field can induce adhesion between a cationic and an anionic gel.[24] When the gels are subjected to 10 V DC for ~ 10 s, they become stuck — and the adhesion endures after the field is removed. This gel-gel *electro-adhesion* (EA) is believed to be due to the electrophoretic migration of polymer chains across the gel-gel interface. In a similar vein, we have shown that cationic gels can be electro-adhered to animal tissues, which are known to be anionic.[29] This gel-tissue EA again has all the above hallmarks (it is a permanent adhesion induced by 10 V DC within seconds). Interestingly, both gel-gel

and gel-tissue EA can be reversed at a later point simply by placing the adhered pair under 10 V DC and reversing the polarity. Thus, EA occurs between soft, aqueous materials of opposite charge, and it is strong, durable, and reversible.

Electric fields have also been used to stick hard and soft materials, but such adhesion typically decays and disappears quickly when the field is switched off.[63-67] For example, a metal can be stuck to a soft dielectric material (such as an elastomer or a non-aqueous gel) when a DC field > 120 V is applied across the pair.[67] This phenomenon is also called electro-adhesion, but it is conceptually very different and has an electrostatic origin (i.e., the Johnson-Rahbek effect[65]). When the field is turned off, the materials quickly lose this electrostatic adhesion — thus, this phenomenon allows metallic grippers in a robot to pick up objects and then release them.[63,67] Note that this electrostatic effect cannot lead to permanent adhesion in the absence of the field. To our knowledge, the only example of enduring hard-soft adhesion induced by an electric field was the recent study of Qiu *et al*.[68] The authors contacted a hydrogel with glass as well as two iron electrodes and applied a DC field of ~ 6 V for several hours. The glass (but not the electrodes) adhered to the gel, and this was attributed to the formation of iron(III) hydroxide nanoparticles at the gel-glass interface. This finding seems to be restricted to a particular choice of electrodes (and to thin gels) and so is not generalizable.

In this chapter, we report our discovery that hard electronic conductors (e.g., metals or graphite) can be electro-adhered to a range of soft aqueous materials, including hydrogels, fruit, and animal tissue. Our studies into these hard-soft combinations arose as

an offshoot of our earlier work on gels and tissues. The experiments are very simple. For example, two graphite slabs are placed on either side of a cylindrical hydrogel (5 cm tall) and 5 V DC is applied across the combination for ~ 3 min. After this period, one of the graphite slabs is found to be strongly stuck to the hydrogel (see Figure 3.1). This adhesion endures long after the field is removed (gel-graphite pairs have remained adhered for months). We term this phenomenon as *hard-soft electro-adhesion* or **EA**$^{[HS]}$ and we emphasize that it is conceptually different from all previous uses of the term 'electro-adhesion'. Adhesion can be achieved in just a few seconds if the gel has a high ionic conductivity. The adhesion is very strong: the strength of the adhesion is limited mostly by the strength of the gel and is shown to exceed 150 kPa.

Over the course of this study on **EA**$^{[HS]}$, we have examined numerous hard-soft material pairs. On the soft side, **EA**$^{[HS]}$ works with chemical gels like AAm, physical gels like gelatin and alginate, and even soft objects like fruit (bananas, apples) and animal tissue (beef, pork). Cationic, anionic, and non-ionic gels can all be bonded to hard solids by this method. On the hard side, **EA**$^{[HS]}$ is achieved with many metals (e.g., copper, lead, tin, nickel, iron, or zinc). Depending on the gel chemistry, adhesion occurs at the anode (+), cathode (–), both electrodes, or neither. If **EA**$^{[HS]}$ is observed only to one electrode, generally it can be reversed by switching the polarity of the electrodes and re-applying the field. With regard to the mechanism behind **EA**$^{[HS]}$, we show that it arises due to electrochemical reactions that generate bonds between the hard electrode and the polymers in the gel network. Overall, this phenomenon is remarkable in its simplicity and wide applicability; in fact, one wonders why it has not been discovered earlier. We close

with examples of hybrid materials created by **EA**$^{[HS]}$ that highlight its utility in robotics, energy storage, biomedical implants, and underwater adhesion.

3.2 Experimental Section

Materials. The following monomers were from Sigma-Aldrich: acrylamide (AAm), *N*,*N*-dimethylacrylamide (DMAA), sodium acrylate (SA), *N*-isopropyl-acrylamide (NIPA), 2-hydroxyethyl methacrylate (HEMA), 2-(di-methylamino)ethyl methacrylate (DMAEMA), *N*,*N*′-methylene-bis(acrylamide) (BIS) and [2-(methacryloyloxy)ethyl]trimethylammonium chloride (QDM, 75% solution in H_2O). Other chemicals used for making hydrogels were also from Sigma-Aldrich, including the initiators ammonium persulfate (APS) and potassium persulfate (KPS) and the accelerant *N*,*N*,*N*′,*N*′-tetramethylethylenediamine (TEMED). Polymers used in this study were also from Sigma-Aldrich and included alginate (i.e., alginic acid sodium salt, from brown algae, medium viscosity), agarose (Type IA, low EEO), gelatin (from porcine skin, gel strength 300, Type A), and poly(vinyl alcohol) (PVA, MW 85–124k, 99+% hydrolyzed). Other chemicals included calcium chloride dihydrate ($CaCl_2$•$2H_2O$, from Sigma-Aldrich), sodium chloride (NaCl, from LabChem) and hydrochloric acid (HCl, from BDH). Graphite sheets (~ 1.5 mm thickness) were from Saturn Industries. Dyes used to color-code the gels were methyl orange from TCI America, and methylene blue and rhodamine B from Sigma-Aldrich. Laponite XLG was a gift from Southern Clay Products. Cu, Pb, Sn, Ni, Fe, Zn and Ti were purchased from RotoMetals. All the meat, fruits and vegetables were purchased from Whole Foods. Deionized (DI) water was used in all experiments.

Hydrogel Synthesis. AAm, DMAA, SA, NIPA, QDM, DMAEMA and HEMA gels were prepared by free-radical polymerization. For a typical gel, 20% monomer, 0.03-0.06% BIS (crosslinker), and 2.0 μL/g TEMED (accelerator) were dissolved in DI water. After sufficient mixing, 0.02-0.06% initiator (APS or KPS) was quickly mixed into the solution. Then the solution was placed under a nitrogen atmosphere for at least 30 min, whereupon it was polymerized into a gel. For laponite-crosslinked AAm gels, 3% laponite XLG particles were used as crosslinker instead of BIS. Gels were typically made in 30 mL cylindrical vials and when taken out of the vial, they had a cylindrical form with a size close to the vial dimensions, i.e., a height of 5 cm and a diameter of 2 cm. Such cylindrical gels were used in the adhesion studies shown in Figures 1, 3, and 4. For other experiments, the same gels were also made in Petri dishes. For all electro-adhesion experiments, it was necessary to include salt in the gel to ensure ionic conductivity. For this purpose, 1% NaCl was typically added to the monomer solution prior to polymerization.

Alginate gels were made by a new method that involves diffusion of calcium cations (Ca^{2+}). 3% alginate was dissolved in DI water in a vial. Then the solution was frozen at –20°C overnight. The vial was then broken and the frozen solid was removed. 7% $CaCl_2 \cdot 2H_2O$ was dissolved in water and the cylindrical frozen solid (~ 2 cm diameter and 5 cm height) was then placed in this solution at room temperature on a stir plate. As the solid melted, Ca^{2+} came into contact at the interface and the cations diffused inwards to

crosslink the alginate chains. Within 6 h, an alginate gel in the shape of a cylinder was obtained, and this was used in Figure 3.4.

PVA gels were made by freeze-thaw cycling.[69] 20% PVA (with 1% NaCl for ionic conductivity) was dissolved in DI water at ~ 90°C. Upon cooling to room temperature, a viscous solution was obtained. This solution was then subjected to two freeze-thaw cycles. For each cycle, the solution was frozen at –20°C overnight and then thawed at room temperature. The freeze-thaw cycling induced the PVA to form a robust gel due to the formation of crystallites at junctions between the chains.[69]

Gelatin gels were made by dissolving 20% gelatin together with 1% NaCl in DI water at 50°C. Upon cooling to room temperature, the solution was converted into a gel due to the formation of triple-helical junctions between the gelatin chains.[39,40] Similarly, agarose gels were made by heating 5% agarose together with 1% NaCl in DI water at 90°C. Upon cooling to room temperature, the agarose chains bind to each other via hydrogen-bonds, resulting in a gel.[43]

The hybrid AAm/QDM gel was made using a method modified from our previous work.[35] The QDM gel was first made in a 90 × 10 mm Petri dish, as described above. After the QDM gelled, a pre-gel solution of AAm was added onto the top. Then the sample was placed again under a nitrogen atmosphere until the AAm also gelled. The AAm and QDM layers were strongly bonded with each other since the pre-gel solution would diffuse into the QDM gel, making the resulting AAm gel network penetrate with

the existing QDM network. Then the hybrid gel was cut into appropriate shape with a razor blade for adhesion experiments.

Electro-Adhesion Experiments. Two polished slabs or strips of the hard material (graphite or metal) were placed in contact on either end of the gel (or other soft material) to be tested, as shown in Figure 3.1. The two slabs were connected as electrodes to the positive and negative terminals of a BK Precision 9104 DC power supply. A DC voltage of typically 5 to 10 V was applied for 3 to 15 min. If the duration of exposure to the electric field was relatively long, the gels were covered with Parafilm during the experiment to minimize water evaporation. After stopping the field, the electrodes were examined for adhesion to the gel. Next, the polarity was reversed (i.e., the previous anode became the cathode, and vice versa) and the field was reapplied. The electrodes were then examined again for adhesion to the gel.

Pull-off Adhesion Strength Tests. The data shown in Figure 3.2 are for the strength of $\mathbf{EA}^{[HS]}$ between AAm gels and graphite. For these measurements, AAm gels were made in Petri dishes, from which they were cut into cuboids with a square cross-section (1 × 1 cm) and a height of 1 to 1.6 cm. The gel was then electro-adhered to a graphite slab (2 × 1.5 × 0.2 cm). After adhesion, the gel was cut open using a razor blade with ~ 0.2 cm thickness left on the graphite slab. This gel-graphite pair was then taken for pull-off testing on an AR2000 rheometer (TA Instruments) using 40-mm parallel-plates. The back side of the graphite was stuck to the bottom plate using either double-sided tape or an epoxy glue. On the top plate, a zinc sheet was first affixed using double-sided tape or

epoxy glue. Then, the gel was stuck to the sheet using a cyanoacrylate glue. With this setup, the pull-off test mode was selected on the Rheology Advantage Instrument Control AR software. During the test, the top plate was pulled upward at a constant rate (typically 1.0-9.3 μm/s; the stiffer the gel, the lower the rate) and the normal-force transducer was used to record the normal force as a function of the gap (distance). The force was converted to stress by dividing by the contact area between the gel and the graphite. The stress at the point of failure was taken as the pull-off strength for a given gel-graphite pair.

Infrared Spectra. Infrared spectra were collected using a Fourier transform infrared (FTIR) spectrometer (Thermo Nicolet NEXUS 670) in attenuated total reflectance (ATR) mode. Samples examined were those at gel-electrode interfaces. Samples were directly placed on the ATR window in the instrument and absorption spectra were measured over a wavenumber range of 650-4000 cm^{-1} with a resolution of 4 cm^{-1}. Each sample underwent 32 scans, and the resulting spectra was averaged.

Statistics. For the data in Figure 3.2, at least three samples were tested for each data point. No outliers were excluded. Mean values are shown in the plots and error bars correspond to standard deviations. Statistics were calculated and plotted using Excel and SigmaPlot.

3.3 Results and Discussion

3.3.1 Reversible Adhesion of Graphite to AAm Gels

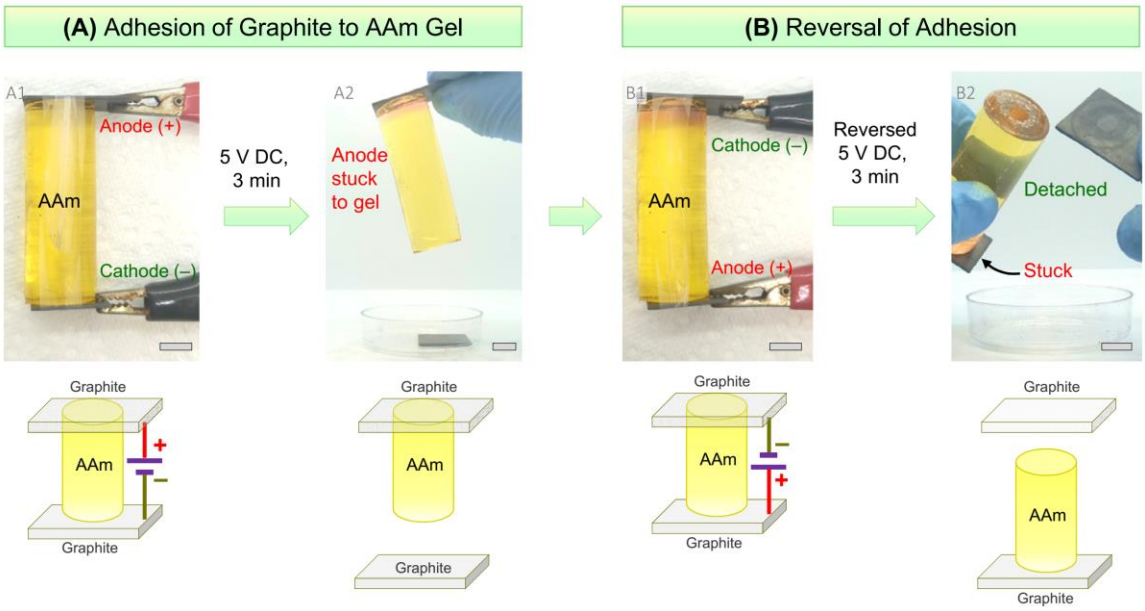

Figure 3.1. Reversible electro-adhesion of graphite to an acrylamide (AAm) hydrogel. Photos and schematics are shown for each case. First, graphite slabs are placed on either end of the AAm gel cylinder (dyed yellow) and 5 V DC is applied for 3 min (A1). The graphite anode (+) becomes strongly adhered to the gel (A2), allowing the pair to be lifted up in mid air. Next, the graphite slabs are again contacted with the gel, and the polarity is reversed, i.e., the adhered slab is now the cathode (–). Upon applying 5 V DC for 3 min, the adhered slab is detached while the bottom one (new anode) is now adhered to the gel. Scale bars are 1 cm.

We first tested the adhesion between graphite and acrylamide (AAm) gels (Figure 3.1). The AAm gel was made by free-radical polymerization using 20% AAm, with *N*,*N*′-methylenebis(acrylamide) (BIS) (1.5% of the AAm) as the crosslinker. Salt (1% NaCl) was added to the gel for ionic conductivity. We typically prepared gels in the shape of a cylinder (2 cm diameter, 5 cm tall, total weight ~ 30 g). This geometry allowed us to easily check if a hard solid was strongly adhered to the gel: as shown in the figure, when adhesion occurs, the solid is able to hold the gel in mid-air. The graphite slabs were cut

from a larger piece to a size of 3 × 2 × 0.2 cm. As a control, when a graphite slab and the AAm gel were pressed into contact, there was no adhesion and the two could be separated right away. Next graphite slabs are placed on the top and bottom of the gel (Figure 3.1A, Panel A1) and these are connected to a DC power supply. The graphite slabs thus serve as electrodes, i.e., one is the anode, connected to the positive terminal of the power supply, and the other is the cathode, connected to the negative terminal. With this setup, 5 V DC is applied across the gel for 3 min. After the DC field is stopped, the graphite anode is found to be strongly adhered to the AAm gel. Panel A2 shows the anode lifting up the gel in mid-air.

The above result was surprising and unexpected. Qualitatively, we noted right away that a strong adhesion had been induced between the gel and the slab. If we tried to wrench apart the gel and the slab, typically the gel would break and pieces of the gel would be left behind on the graphite surface. The adhesion persisted indefinitely so long as the gel did not lose water (i.e., if the graphite-gel pair was stored in a closed container). We have preserved such adhered pairs in the lab for months and they still remain adhered. If the gel is left to dry in air, it shrinks considerably and then the adhesion to the slab weakens gradually due to a size mismatch.

A continuation of the experiment between graphite and AAm gel is shown in Figure 3.1B. We take the graphite-gel pair and place back the unadhered graphite slab on the other side. Then we apply the DC field in the reverse direction, i.e., we switch the polarity (Panel B1). The previously adhered graphite anode is now the cathode (–) while

the other graphite slab serves as the new anode (+). With this configuration, we apply 5 V DC for 3 min (Figure 3.1B). After the DC field is stopped, the previously adhered graphite is found to have detached (Panel B2). Conversely, the previously unadhered slab is now stuck to the gel. These results imply that graphite adheres to AAm gels if it is the anode in a DC circuit, but not if it is the cathode. Moreover, this implies that the adhesion can be reversed as and when desired by applying the DC field with reversed polarity.

3.3.2 Factors that Affect the Adhesion Strength

The phenomenon shown by Figure 3.1 is termed as *hard-soft electro-adhesion* or $\mathbf{EA}^{[HS]}$. What are the main factors that affect $\mathbf{EA}^{[HS]}$? To determine this, we conducted pull-off testing on adhered graphite-AAm pairs, and the results are presented in Figure 3.2. The gel pieces for these tests were made as cuboids with a base of 1 × 1 cm and a height of 1.6 cm. From the experiments, we obtained the pull-off adhesion strength, which is the tensile stress required to separate the gel from the graphite slab (i.e., the stress at break).

First, we present the effect of varying the electric field strength on graphite-AAm $\mathbf{EA}^{[HS]}$ (Figure 3.2A). The DC voltage was varied from 0 to 5 V across the AAm gels. The gel composition was fixed at the one used in Figure 3.1 and in each case, the voltage was applied for 30 s. Below 1 V, the adhesion strength is negligible (i.e., it is comparable to contact adhesion). At 2 V, $\mathbf{EA}^{[HS]}$ is noticeably stronger than contact adhesion. In this case, when the gel is pulled off from the graphite, an *adhesive failure* occurs,[70] i.e., the gel and graphite separate at their interface. This mode of failure was consistently

observed when the adhesion strength was low (< 20 kPa). When the voltage is increased to 3 V, the adhesion strength increases to 40 kPa. In this case, a *cohesive failure* occurs,[70] i.e., the failure occurs in the middle of the gel. Such failure was always observed when the adhesion strength was high (> 30 kPa). It indicates that the adhesion is so strong that it exceeds the gel strength. Consequently, we find that the measured adhesion strength due to $\mathbf{EA}^{[HS]}$ levels out as the voltage is increased above 3 V.

Next, we varied the time over which the electric field was applied (Figure 3.2B). The AAm gel was the same as above and the voltage was fixed at 5 V. Over the first 30 s, the adhesion of the gel to graphite strengthens with increasing time, indicating that $\mathbf{EA}^{[HS]}$ accumulates as the voltage is applied. Thereafter, the adhesion plateaus. We again observed an adhesive failure for the initial points (< 20 kPa in adhesion strength) and a cohesive failure for the subsequent ones. The results indicate that for a 1.6 cm-tall gel sample, strong adhesion can be achieved within a minute of applying the field. For the taller gels studied in Figure 3.1 (5 cm height), a longer time (~ 3 min) was needed to achieve strong $\mathbf{EA}^{[HS]}$. This is why we applied the field for a time of 3 min in Figure 3.1.

The salt (electrolyte) concentration in the gel also plays an important role in $\mathbf{EA}^{[HS]}$ (Figure 3.2C). For a gel that is non-ionic like AAm, in the absence of salt, the ionic conductivity is very low. It is only with the addition of salt that the gel becomes conductive. A conductive gel is needed to complete the DC circuit. As the salt in the gel increases, the current through the circuit increases. This has an effect on the adhesion strength, as shown in Figure 3.2C. For these experiments, we used the same 20% AAm

gel and applied a voltage of 5 V for 5 s. NaCl was used as the salt and its concentration in the gel was varied. The results show that the adhesion strength of the gel to graphite increases monotonically with increasing NaCl. A key corollary of this result is that if the gel has high salt, it can be stuck by **EA**$^{[HS]}$ to hard solids in a very short time. For example, a tall (5 cm) AAm gel with 15% NaCl can be adhered strongly to graphite in only 5 s. We will return to this result later under Figure 3.8.

We also studied the effect of gel properties on **EA**$^{[HS]}$. A first key variable is the concentration of polymer chains, which can be altered via the AAm monomer content used during synthesis. The gels so far all had 20% AAm with the crosslinker BIS at 1.5% of the AAm. We kept the same BIS:AAm ratio and varied the AAm from 10 to 50%. As the AAm increased, the gels transformed from soft to stiff. We loaded each gel with 1% NaCl and studied their adhesion to graphite induced by 5 V DC for 30 s. Figure 2D shows that the adhesion strength increases with polymer concentration. One point to note here is that the values for the 10, 20 and 30% AAm gels correspond to the maximum value of adhesion strength at 5 V. That is, the time of 30 s was sufficient for these gels to reach a plateau in adhesion strength vs. time (as found in Figure 3.2B). For the 40 and 50% AAm gels, increasing the time in the field beyond 30 s to 3 min increased the adhesion strength (open symbols in Figure 3.2D). For the 50% AAm gel, the bar graph in Figure 3.2E contrasts the **EA**$^{[HS]}$ adhesion strength, which is ~ 150 kPa, with the value for contact adhesion, which is ~ 15 kPa. The comparison implies that **EA**$^{[HS]}$ can be 10× the strength of contact adhesion if the gel is strong. Figure 3.2F shows a 100 g weight

embedded in a 20% AAm gel and then stuck to graphite by **EA**[HS]. The pair can be held up vertically, which vividly shows the high strength of **EA**[HS].

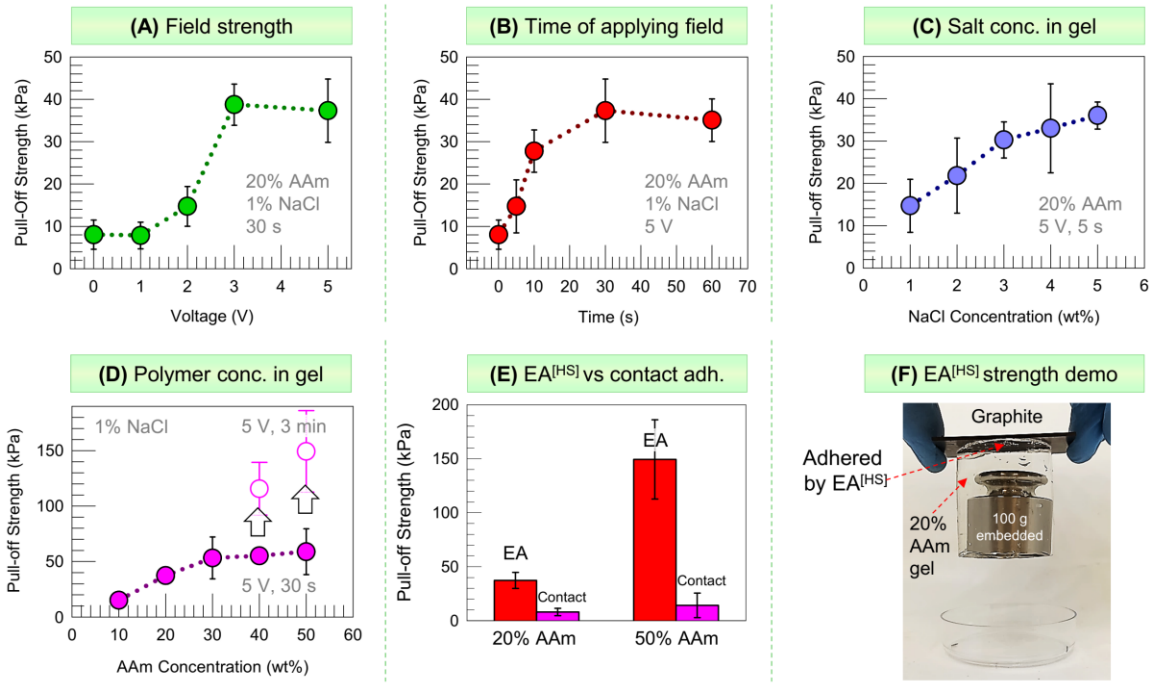

Figure 3.2. Factors that affect the adhesion strength achieved by EA[HS] between graphite and AAm gels. The pull-off adhesion strength is shown in each graph. Mean values are plotted and the error bars represent standard deviations from $n \geq 3$ measurements. (A) Varying the voltage; (B) Varying the time over which the voltage is applied; (C) Varying the concentration of salt (NaCl) in the gel; (D) Varying the concentration of monomer (AAm) used to make the gel. The filled symbols correspond to 30 s of applying the voltage and the open symbols to 3 min. (E) The EA[HS] values from (D) for 20 and 50% AAm are compared with the values for contact adhesion. EA[HS] is much stronger. To illustrate the strength of EA[HS], (F) shows that a graphite-gel pair (gel is 20% AAm) can support an additional weight of 100 g.

3.3.3 Adhesion to Various Hard Materials

Apart from graphite, what other hard materials can undergo **EA**[HS] to gels? To examine this aspect, we performed tests with AAm gels and different metals (Figure 3.3). The gels are similar to those in Figure 3.1: 20% AAm with 1% NaCl and in the form of a 5-cm-tall cylinder. Each metal is in the form of rectangular strips (~ 3 × 1 cm) with 0.2 to

0.8 mm thickness. The metal strips are placed on either side of a gel cylinder and 5 V DC is applied for up to 15 min. All metals showed negligible contact adhesion with the gel (i.e., there was no adhesion in the absence of the field). Upon applying the field, **EA**$^{[HS]}$ is induced with several metals on the anode (+) side, but there is no adhesion to the cathode (–) side. When adhesion occurs, the metal-gel pair can be lifted up in the air, and this adhesion persists afterward.

The results of anodic adhesion to AAm are shown in Figure 3.3. Graphite, copper (Cu), lead (Pb) and tin (Sn) all adhere to AAm gels, while nickel (Ni), iron (Fe), zinc (Zn) and titanium (Ti) do not. We have arranged all the above in an electrochemical series,[44] whereupon a pattern emerges. Metals that do not adhere to AAm have negative standard reduction potentials $E°$, indicating that they are more reactive,[44] i.e., they easily lose electrons and thereby get oxidized. Conversely, materials that do adhere to AAm are *relatively inert*.[44] These have positive (or not so negative) $E°$, with a cut-off value for adhesion being around –0.2 V. The correlation between adhesion and the electrochemical series suggests that **EA**$^{[HS]}$ arises due to electrochemical reactions at the interface. At the anode, where the half-reaction is oxidative, the DC field causes the gel to react electrochemically with the inert metal (instead of electrolyzing the metal into cations). We should note that the result from Figure 3.3 is for AAm gels only. Some metals on the left of Figure 3.3 like Zn and Fe do undergo **EA**$^{[HS]}$ to other gels, as will be discussed below.

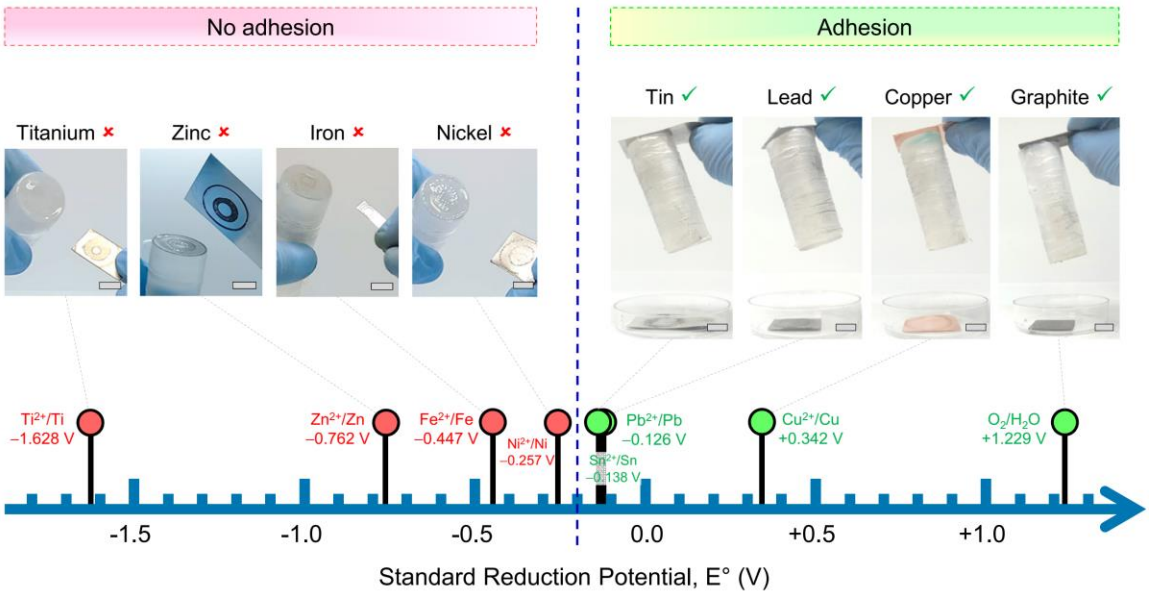

Figure 3.3. Adhesion results at the anode for various hard materials to AAm gels by EA[HS]. The results are shown in an electrochemical series with the standard reduction potential *E*° for each material. Photos are shown for each case. Strips of each material are placed on either end of a cylindrical AAm gel and 5 V DC is applied for up to 15 min. Adhesion occurs only to the anode (+). Materials that adhere are all on the right side of the series, i.e., their *E*° > – 0.2 V, indicating that they are relatively inert. In all these cases, the material-gel pair can be lifted up in the air. Materials that do not adhere have more negative *E*°, indicating that they are more reactive (easily oxidized). Scale bars are 1 cm.

3.3.4 Adhesion to Various Hydrogels

Next, what other hydrogels can be stuck by **EA**[HS] to hard solids? To study this, we tested graphite along with gels of different chemistry. Some were chemical gels made by free-radical polymerization (similar to AAm but with different monomers) — the crosslinks in these gels are covalent bonds. Others were physical gels, e.g., gels of polysaccharides or proteins where the crosslinks are physical, non-covalent bonds (e.g., ionic or hydrogen-bonds). The geometry was the same as in Figure 3.1: each gel in the

form of a 5-cm-tall cylinder, while graphite was in the form of thin slabs. 5-10 V DC was applied for up to 15 min and adhesion was assessed visually as shown in Figures 1 and 3.

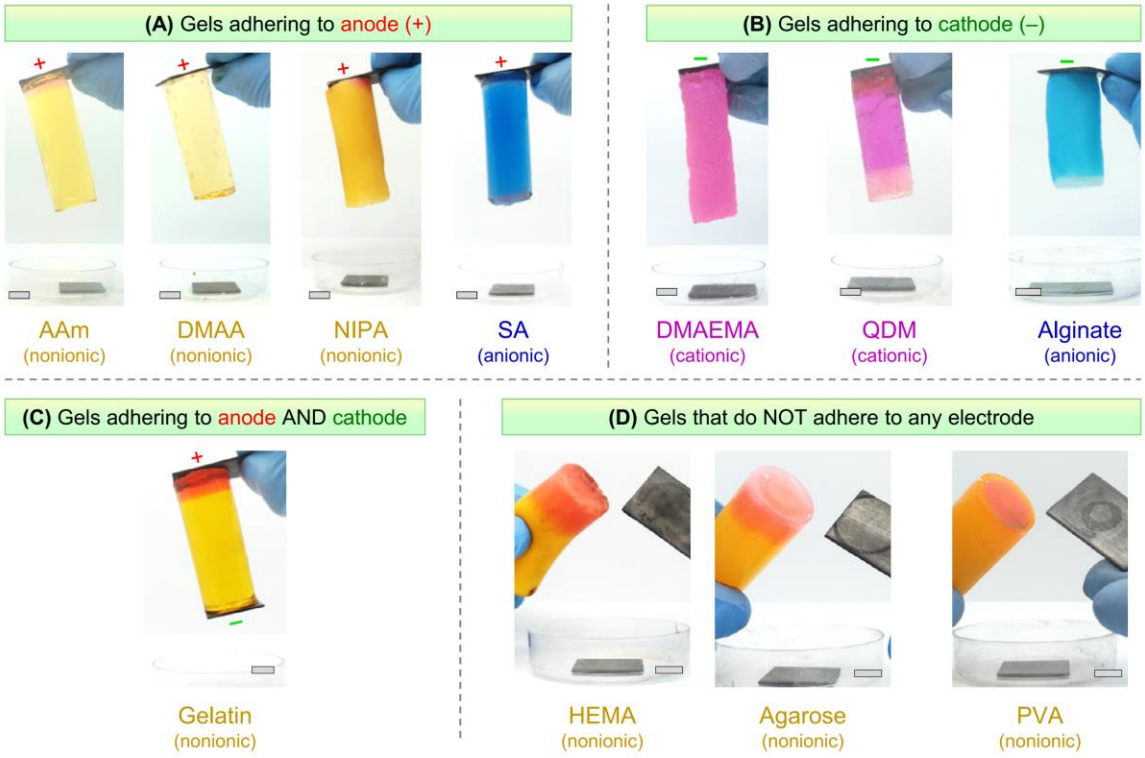

Figure 3.4. Adhesion results for graphite to various gels by EA[HS]. The results are shown through photos. Gels are imbued with dyes and are thus color-coded as follows: non-ionic gels in yellow, anionic gels in blue and cationic gels in pink. Strips of graphite are placed on either end of a cylindrical gel and 5-10 V DC is applied for 15 min. (A) Gels that adhere only to the anode (+); (B) Gels that adhere only to the cathode (–); (C) Gelatin is the only gel that adheres to both electrodes; (D) Gels that do not adhere to either electrode. Scale bars are 1 cm.

The results for graphite-gel adhesion are presented in Figure 3.4. **EA**[HS] is seen in many, but not all, cases, and the results are quite complex. We have color-coded the gels based on their ionic nature (nonionic, anionic, cationic) using traces of water-soluble dyes. First, the gels in Figure 3.4A all adhere to graphite only at the anode (+). These include AAm and other chemical gels made from the acrylic acid derivatives *N*,*N*-

dimethyl-acrylamide (DMAA), *N*-isopropylacrylamide (NIPA), and sodium acrylate (SA).[31,32] Note that AAm, DMAA, and NIPA gels are nonionic whereas SA is anionic.

Next, the gels in Figure 3.4B all adhere to graphite only at the cathode (–). These include two cationic gels made by free-radical polymerization of the monomers [(2-methacryloyloxy)ethyl]tri-methylammonium chloride (QDM) and 2-(dimethylamino)ethyl methacrylate (DMAEMA).[27,29] Cathodic adhesion also occurs with gels of the anionic polysaccharide alginate, which is made by crosslinking sodium alginate with divalent calcium (Ca^{2+}) cations.[27] Thus, both cationic and anionic gels adhere to cathodes. In the case of QDM gels, in addition to graphite, several metals (Cu, Pb, Sn, Ni, Fe and Zn) all adhered at the cathode. Note that this includes metals with both positive and negative reduction potentials.

Next comes the curious case of gelatin (Figure 3.4C). Gelatin is a denatured form of the protein collagen and forms thermoreversible gels in water driven by hydrogen-bonding of the protein chains into triple helices at crosslinking points.[39,40] We find that gelatin undergoes **EA**$^{[HS]}$ to graphite at *both the cathode and the anode*. This is the only gel in our studies to show this behavior. The fact that gelatin adheres to both electrodes also implies that this adhesion cannot be reversed by re-applying the field with reversed polarity.

The last category of gels is those in Figure 3.4D — these do not stick to graphite at either the anode or cathode. Gels in this category include the nonionic chemical gel

made from 2-hydroxyethyl methacrylate (HEMA) and two other nonionic physical gels: those of the synthetic polymer poly(vinyl alcohol) (PVA)[69] and the polysaccharide agarose.[43] The fact that some gels do not adhere to hard materials is an important point to note. This means that **EA**$^{[HS]}$ is not due to a simple, universal reaction between water and any solid surface. It depends on the chemistry of both the gel and the hard material.

3.3.5 Adhesion to Animal and Plant Tissues

Apart from hydrogels, are there other soft materials that can be adhered to hard ones by **EA**$^{[HS]}$? We explored this point with a variety of animal and plant-based soft materials, especially those that are available as edible foods. Adhesion was attempted to graphite slabs using 5 V DC for up to 15 min. In the cases of fruit or vegetables, the sample was cut open and the graphite was contacted with the fleshy interior. (Note that the outer skins of many fruits are hydrophobic and may have negligible ionic conductivity.[71])

The results on **EA**$^{[HS]}$ with biological tissues are interesting, but again rather complex (Figure 3.5). Some tissues adhere to graphite only at the anode (+) (Figure 3.5A) and these include vegetables (tomato, garlic) as well as tissues from animals: cow muscle (beef shank) and chicken muscle (segment from the thigh). Some others adhere to graphite only at the cathode (–) (Figure 3.5B) and these include fruit (apple) and pig muscle (pork shoulder). It is generally recognized that animal cells and tissues have an anionic character,[29,45] but as can be seen here, the animal tissues we tested show wide differences in **EA**$^{[HS]}$. Three of the plant materials we tested (banana,

onion, and potato) adhere to both electrodes, similar to gelatin gels (Figure 3.5C). Lastly, there were several plant-based materials that did not adhere to either electrode (Figure 3.5D), including grape, blueberry, raspberry, cucumber, orange and pear.

The results in Figures 3–5 indicate that **EA**[HS] works with a range of both hard and soft materials. The common requirement for the hard material is that it *has to be an electronic conductor*, which includes graphite and metals. As for the soft material, it has to be *an ionic conductor*, which means it has to contain water and salt.

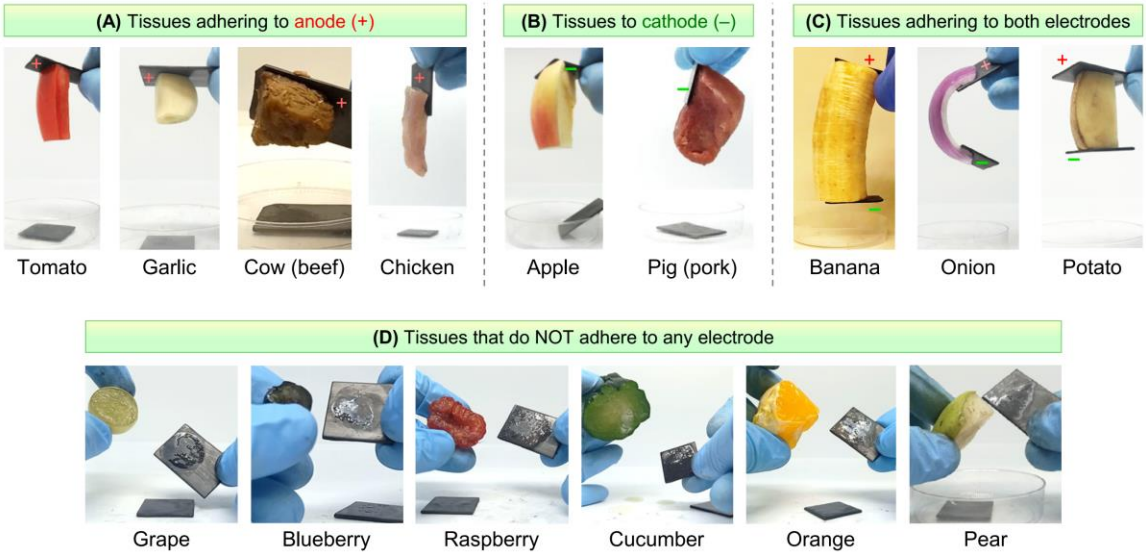

Figure 3.5. Adhesion results for graphite to various plant and animal tissues by EA[HS]. The results are shown through photos. Strips of graphite are placed on either end of a given soft material and 5 V DC is applied for 15 min. (A) Tissues that adhere only to the anode (+); (B) Tissues that adhere only to the cathode (–); (C) Tissues that adheres to both electrodes; (D) Tissues that do not adhere to either electrode.

3.3.6 Adhesion in Various Configurations

The versatility of **EA**[HS] can be further shown by sticking hard and soft materials in other geometries or configurations, three of which are shown in Figure

3.6. First, we use a thin strip of AAm gel as an adhesive to stick two Cu sheets (Figure 3.6A). For this, an AAm gel (20% AAm, with 1% NaCl) is cut into a rectangular (3 × 1 cm) strip with a thickness of 2 mm. The Cu strips are also similarly sized (but thinner), as shown in Figure 3.6A, Panel A1. From Figure 3.3, we have seen that Cu strips adhere to AAm gels at the anode, whereas neither Cu nor graphite stick to AAm at the cathode. With this knowledge at hand, we first place a Cu strip perpendicular to the AAm gel at one end and make this strip the anode (+) (Panel A1). At the other end of the gel, we place a graphite slab and make it the cathode (–). We then apply 5 V for 5 min, inducing $\mathbf{EA}^{[HS]}$ between the Cu anode and the gel. Then, a second Cu strip is placed over the gel (on the opposite side, parallel to the first Cu strip) and is made the anode (Panel A2). $\mathbf{EA}^{[HS]}$ between the second Cu and the gel is then induced (Panel A3). The overhanging portion of the gel is cut off and we finally have the two Cu strips stuck together by the AAm gel that is sandwiched between them (Panel A4).

Another interesting demonstration is done with gelatin gels and graphite (Figure 3.6B). As noted earlier, gelatin gels adhere to graphite both at the anode and the cathode. We therefore attempt a single-step adhesion of gelatin and graphite pieces into a closed ring. For this, we begin with eight graphite slabs (3 × 1 × 0.2 cm size) and eight gelatin gel strips (3 × 1 × 0.2 cm size) and arrange them in a ring using Parafilm (Panel B1). Note that a portion of a given gel strip bridges adjacent graphite slabs (Panel B2). This is essentially a series configuration of hard and soft materials. We connect positive and negative terminals to two ends of the ring and apply a DC

voltage of 40 V for 15 min. Each gel strip has one graphite slab connected to it as the anode and another as the cathode. Due to **EA**[HS], all graphite-gel pairs adhere strongly, and the result is a robust ring. Panel B3 shows the ring being lifted up in the air by a metal tube. This shows that the ring can be manipulated as a single object. The ring stays intact without loss of adhesion indefinitely (as long as the gels remain hydrated).

A further possibility is to use EA to adhere different gels and electrodes step by step, thereby generating unusual configurations, such as a chain (Figure 3.6C). To make such a chain, a series of steps must be followed, and in each step, a given gel strip is contacted with a working electrode (WE) and a counter electrode (CE) and 10 V is applied for 2 min. The gel, the electrodes and the direction of the electric field are chosen so that the gel only adheres to the WE but not the CE. Specifically, in the case of an AAm gel, it does not adhere to graphite at the cathode. Thus, a graphite cathode can be the CE while Sn, Pb, Cu, and graphite can be the anode (WE). In the case of a QDM gel, it does not adhere to graphite at the anode. Therefore, a graphite anode can be the CE while Sn, Ni, Fe, and Zn can be the cathode (WE). With these considerations, we start with a first gel strip, contact it with a WE and CE, and induce **EA**[HS] between the gel and the WE. Next, this gel is contacted with a second WE and CE. By leaving the first adhered WE in open circuit, we can adhere the second WE without affecting the already adhered pair. Thereby, a second (and different) metal is adhered to the gel strip on its other end. In this way, different gels and different electrodes are connected serially in a chain (Figure 3.6C). Graphite, Cu, Pb, and Sn

are connected by AAm gel strips, while Sn, Ni, Fe and Zn are connected by QDM gel strips.

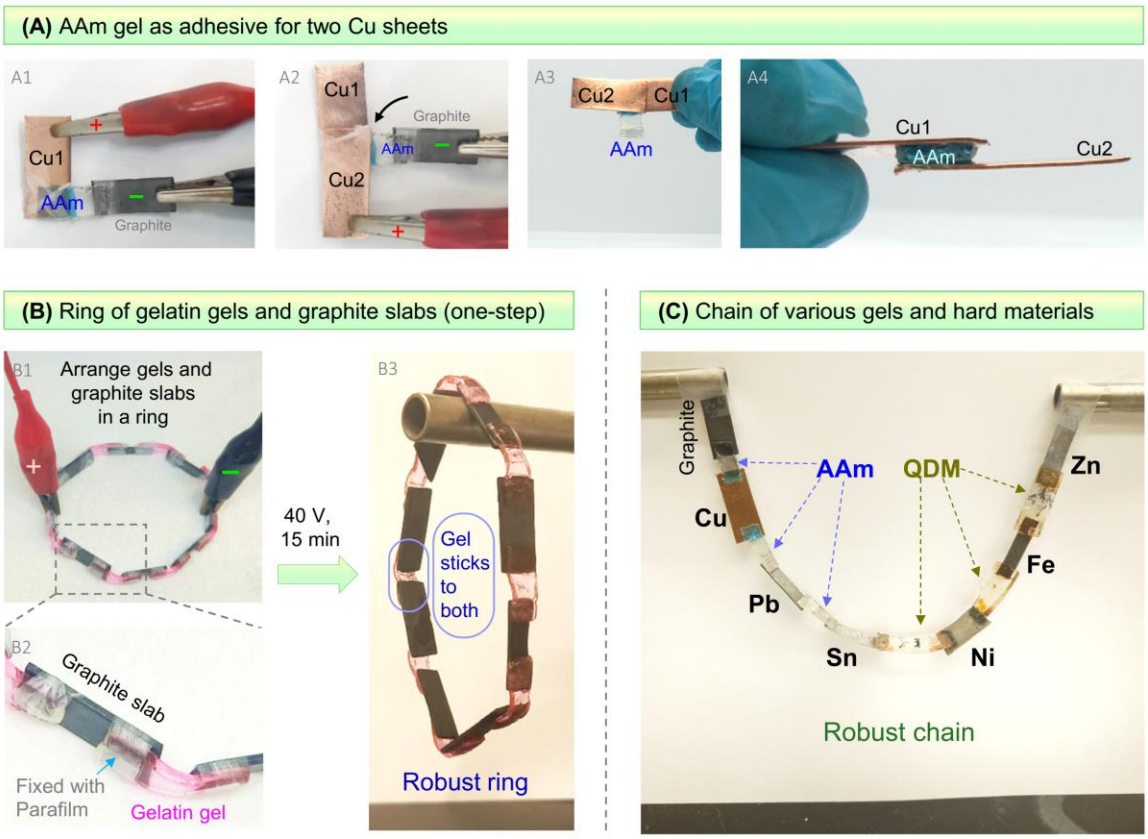

Figure 3.6. Use of EA[HS] to adhere hard and soft materials in various configurations. (A) A thin AAm gel is used as an adhesive between two Cu sheets, labeled Cu1 and Cu2. AAm is first stuck to Cu1 using graphite as a counter electrode and then the AAm is stuck to Cu2. (B) A ring of alternating gelatin gels and graphite strips is bonded together in a single step. This is possible because gelatin adheres to graphite at both electrodes. (C) A robust chain of eight different hard materials connected by AAm and QDM gels.

3.3.7 Mechanism for EA[HS]

We now turn to the crucial question regarding the mechanism, i.e., why does such adhesion occur? As discussed in the Introduction, **EA**[HS] is conceptually distinct from all previous uses of the term ‘electro-adhesion’. It arises between a hard electronic conductor

and a soft, ionic conductor. Once induced by the DC electric field, the adhesion persists thereafter. Adhesion is induced with both chemical and physical gels (Figure 3.4). Moreover, adhesion can be achieved to gels that are cationic, anionic, or non-ionic. Some anionic gels like SA stick to graphite only at the anode (Figure 3.4A), whereas other anionic gels like alginate stick to graphite only at the cathode (Figure 3.4B). Thus, electrostatic or ionic interactions cannot be a decisive factor in the mechanism behind **EA**$^{[HS]}$.

Our results on **EA**$^{[HS]}$ to AAm gels with different metals follow a significant trend (Figure 3.3). Metals adhere only at the anode to these gels, and those that do have positive reduction potentials, while those that do not have negative reduction potentials. This correlation with the electrochemical series strongly indicates that adhesion is caused by electrochemical reactions between the metal and the gel at the anode. Metals that do not adhere are those that get oxidized first at the anode. This oxidation (electrolysis) of the metal dominates over any competing processes, which explains why there is no adhesion. Conversely, metals that do adhere are relatively inert, allowing the polymer chains of the gel network to get oxidized first at the anode. We hypothesize that such oxidations result in chemical bonds between the metal surface and the polymer chains, leading to adhesion. The precise nature of the bonds will vary depending on the chemistry of the gel. When the polarity is inverted (i.e., the adhered surface is now made the cathode), the reactions at the electrode are reductive, which serves to undo the bonds between the metal surface and the polymer chains. As a result, the gel can now be detached from the metal.

To test our hypothesis, Fourier Transform Infrared spectroscopy (FTIR) in the attenuated total reflectance (ATR) mode was conducted on the graphite-AAm pair (Figure 3.7A). The IR spectrum for a bulk AAm gel is dominated by the water present in it,[72,73] as can be seen from the bottom two curves. Water shows a broad peak at 3300 cm^{-1} for O–H stretching, one peak at 1636 cm^{-1} for H–O–H scissoring, and one below 600 cm^{-1} for O–H bending. For the AAm gel, all these peaks appear, and there is an additional strong peak at 1659 cm^{-1} for the stretching of the C=O bond in the amide group.[72,73] For a polished graphite surface without any contact with gels, IR absorption occurs over the range of wavelengths, but with no clear peaks. Next, graphite electrodes were contacted with the AAm gel and 5 V DC was applied for 15 min. As expected, the graphite anode adhered to the AAm gel by $\mathbf{EA}^{[HS]}$ while the cathode did not. We used a razor blade to cut slices of the gel next to each electrode as well as in the bulk (middle), i.e., far from the electrode interfaces.

Figure 3.7A shows that the AAm gel slice from the bulk (G^{bulk}) has nearly the same IR spectrum as the one before adhesion (compare the blue and orange curves). This indicates that any changes to the gel happen only at the interfaces with the electrodes. Next, we turn to the gel slice next to the anode (G/+). This gel still has some graphite attached to it and this graphite cannot be washed off with water. The IR spectrum for G/+ is the top (purple) curve in Figure 3.7A and it is an overlap of the spectra for graphite and the gel. More importantly, the C=O stretching peak of the amide group has disappeared, while one additional peak now appears at 1582 cm^{-1}. These data indicate that there must

have been electrochemical reactions induced by the field that consume the amide group. In turn, these reactions appear to generate new bonds that are hard to identify.

To further examine our hypothesis, we conducted FTIR on the graphite-agarose pair (Figure 3.7B). As shown by Figure 3.4D, this is a combination for which **EA**$^{[HS]}$ does not occur. The initial agarose gel has the water peaks as well as additional minor peaks at 1045 and 1073 cm^{-1}. Next, the agarose gel was contacted with graphite and 5 V DC was applied for 15 min. A razor blade was then used to cut slices of the gel from the bulk (middle), the anode interface and the cathode interface. Because there is no adhesion, the gel slices at the interfaces have no graphite clinging to them. IR spectra of the three gel slices (top three curves in Figure 3.7B) are nearly identical and show no new peaks. This indicates that no electrochemical reactions have occurred at the interfaces (at least none that alter the chemistry of the gel). We emphasize the contrast between Figure 3.7A and 3.7B. For graphite-AAm, where **EA**$^{[HS]}$ occurs, IR shows *evidence of chemical changes to the gel at the adhering electrode* after the field is applied. For graphite-agarose, where no such adhesion occurs, there is no evidence of any chemical changes. This strengthens our hypothesis that adhesion arises due to electrochemical reactions between the adhering electrode and the gel. The precise nature of the bonds between the electrode and gel will depend on their chemistries.[51,60]

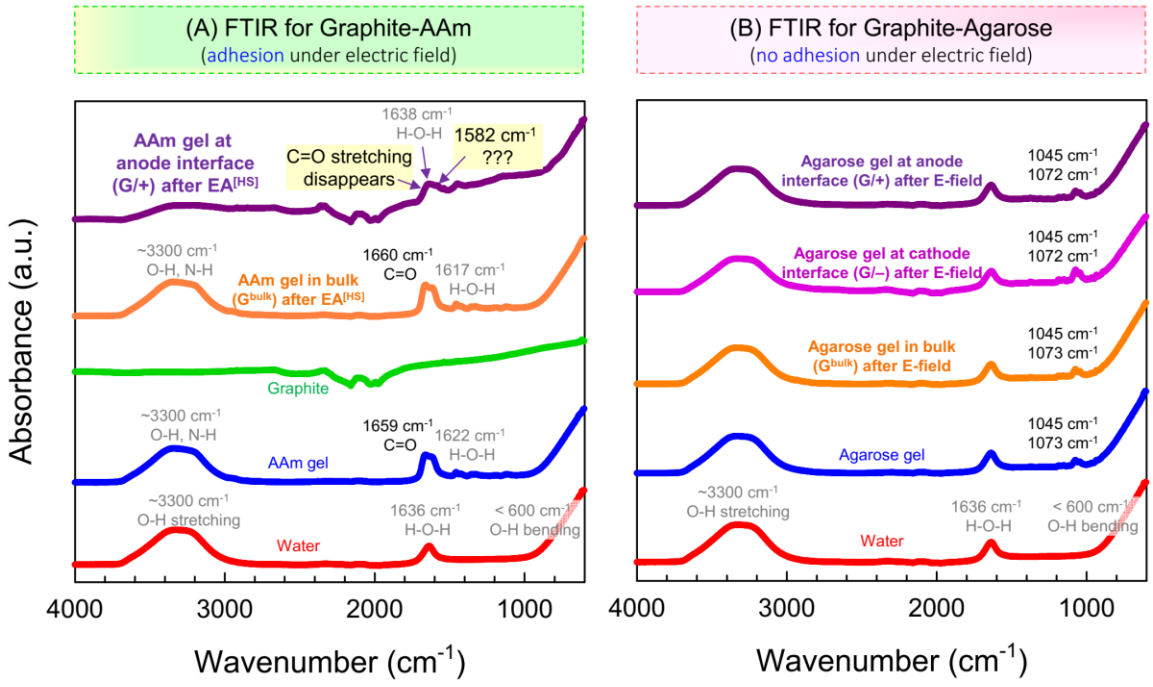

Figure 3.7. Probing the mechanism for EA[HS] using FTIR. Spectra are shown for the cases of (A) graphite-AAm gel and (B) graphite-agarose gel. AAm adheres to graphite at the anode by EA[HS], whereas agarose does not adhere to either electrode. Gel slices next to the electrodes or in the bulk are analyzed. No chemical changes are detected in (B) from the IR spectra. In (A), only the gel slice near the anode (denoted as G/+, purple curve) shows evidence of new bonds.

3.3.8 Applications

We close this paper with a few demonstrations that leverage the use of **EA**[HS]. First, we show in Figure 3.8 an electro-gripper to pick up and drop off gels. We stuck a graphite slab to the end of a glass rod using epoxy glue and used this graphite as the working electrode (WE). Two pieces of aluminum (Al) foil serve as the counter electrodes. Two DC power sources (not shown in the figure) are used for adhesion and detachment, respectively. The gel cylinder (~ 5 cm tall) is made with 20% AAm gel and contains 15% NaCl. The high salt ensures a high ionic conductivity and thereby a short

adhesion time. Initially, the gel is placed on the first Al foil (Figure 3.8A). The graphite WE is placed in contact with the gel and 5 V is applied for 5 s (Figure 3.8B): note that the graphite is the anode (+) while the Al is the cathode (–). Even with this short time, the graphite strongly adheres to the gel by **EA**[HS], allowing the two to be lifted up in the air (Figure 3.8C). The gel-graphite pair is then placed on the second Al foil and a reverse voltage of 5 V is applied for 15 s (Figure 3.8D), with the graphite as the cathode (–) and the Al as the anode (+). In this time, the graphite detaches from the gel and can be lifted off, leaving the gel on the Al foil (Figure 3.8E). In this way, the gel is picked up from one spot and dropped off at another. This setup could provide a simpler alternative for grippers in robotics[63,66], as it does not require the robot's fingers or hands to have any joints or specific shapes to hold an object.

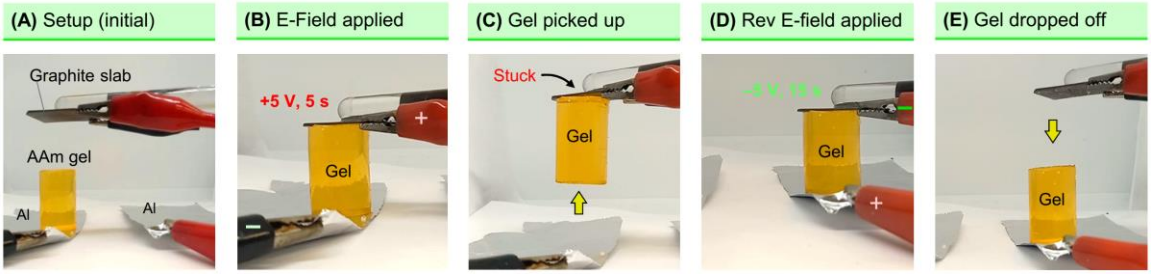

Figure 3.8. Electro-gripper based on EA[HS]. (A) A graphite slab is stuck to a glass rod and connected to DC power. Two pieces of Al foil serve as the counter electrodes. An AAm gel to be picked up is placed on one foil. (B) The graphite slab is contacted with the gel and serves as the anode (+). 5 V is applied for 5 s. (C) The gel is stuck to the graphite slab and is picked up. (D) The gripper moves the gel to the other foil. The graphite is now made the cathode (–) and 5 V is applied for 15 s. (E) The gel detaches from the graphite and is dropped off.

Another potential application of **EA**[HS] is in making new kinds of batteries. Battery designs often have two hard solids (as electrodes) and an electrolyte between them. The electrolyte can be a soft solid, such as a gel in an ion-conductive solvent. We assembled a primary battery with a hydrogel electrolyte using our **EA**[HS] technique (Figure 3.9A). The gel is a hybrid composed of two layers, with the top layer being AAm and the bottom being QDM. This hybrid gel was made using a strategy modified from our previous study[35] (see Experimental Section for details). Cu and Zn were chosen as the electrodes. The logic behind these choices is that AAm adheres to Cu anodes by **EA**[HS] (Figures 3.3, 3.6A) while QDM adheres to Zn cathodes by **EA**[HS] (Figure 3.6C). We proceeded to place a Cu strip in contact with the AAm side and a Zn strip with the QDM side. The gels both had 1% NaCl in them, as usual, for ionic conductivity. Then, with Cu as the anode and Zn as the cathode, we applied 10 V for 30 s. Both the metals adhered to the gels, as expected (Figure 3.9A). During this process, Cu was electrolyzed into Cu^{2+} within the AAm gel (note that the gel turns blue as a result). The overall assembly serves as a primary battery (Figure 3.9B). The open-circuit potential, with Cu as the cathode (+) and Zn as the anode (–), is ~ 0.9 V. This output was stable for hours (Figure 3.9B), which shows that our simple setup provides the basic function of a battery. More sophisticated battery designs, including flexible and rechargeable batteries, can be assembled in the future using **EA**[HS].

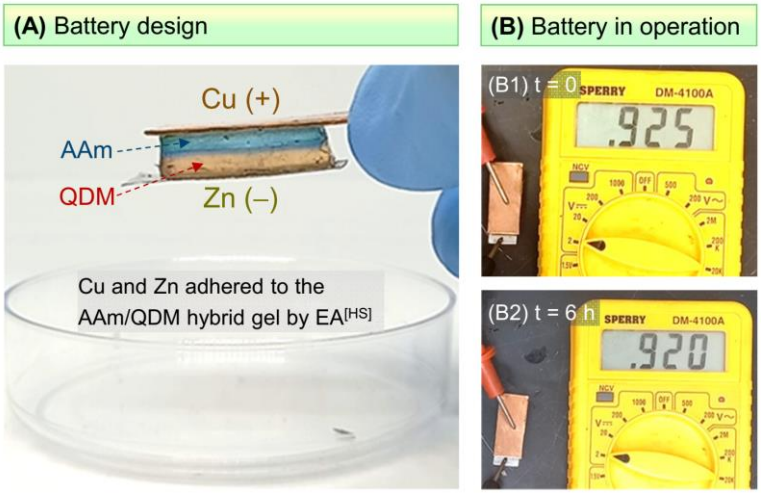

Figure 3.9. Primary battery created by EA[HS]. (A) The battery has Cu and Zn strips as electrodes flanking a hybrid AAm/QDM gel (with 1% NaCl in it) as the electrolyte. The metal strips are adhered to the gel using **EA**[HS]. (B) Under open-circuit conditions, with Cu as the cathode (+) and Zn as the anode (–), the battery delivers a potential of ~ 0.9 V (B1) and this remains stable after 6 h (B2).

A third potential application of our **EA**[HS] technique is in bio-inspired actuators and soft robotics. By combining flexible hydrogels with rigid solid materials, we can fabricate robots with a stiff, bone-like skeleton as well as soft, muscle-like elements. Figure 3.10 shows a simple example of a load-bearing hard-soft structure made using **EA**[HS]. Two graphite slabs (5 × 5 cm) are joined by **EA**[HS] to four pillars made of flexible AAm gels. To make the gels flexible, they are crosslinked by nanoparticles of the synthetic clay laponite, instead of the molecular crosslinker BIS.[35] Each gel is made in the shape of a long cuboid (0.5 × 0.5 × 3 cm) and the gels are all robust and elastic. The gels are fixed as pillars on the four corners between the two slabs (Figure 3.10A). We then placed weights on the top slab to examine the ability of the structure to support a load. The structure is negligibly affected when 20 g is placed (Figure 3.10B) whereas 50

g makes the pillars buckle and bend (Figure 3.10C). When the load is increased to 100 g (Figure 3.10D), the gel pillars buckle and the top slab is pushed down to the bottom one. When this weight is removed, the gel pillars retract to their original state and so the top slab moves upward (Figure 3.10E).

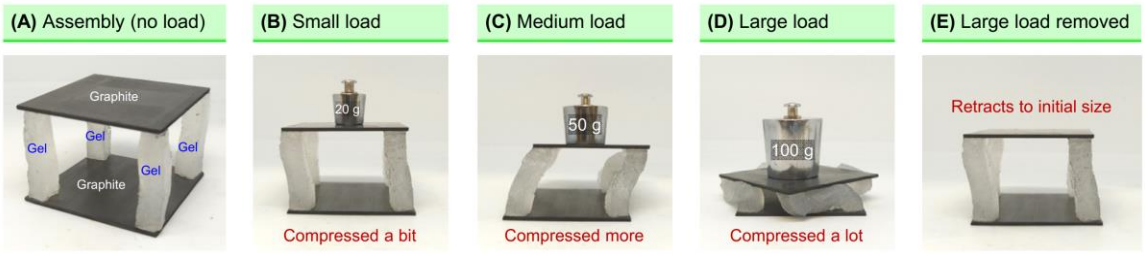

Figure 3.10. Load-bearing assembly fabricated by EA[HS]. (A) Four flexible gel pillars are electro-adhered between two graphite slabs. Different weights are loaded on the top. (B) 20 g causes minimal compression. (C) 50 g causes the pillars to buckle and bend. (D) 100 g makes the pillars buckle until the top slab is compressed down to the bottom one. (E) When the 100 g load is removed, the assembly retracts to its original state.

The results in Figure 3.10 show the utility of combining hard and soft elements in the same structure. Hard elements alone will not be compressible or deformable, whereas soft elements alone could get crushed by a load. The combination, however, is able to bear a load without damage. Moreover, as the pillars retract after load removal (Figure 3.10E), the elastic energy stored in the deformed gels gets released, and in the process, the structure can do work (e.g., push an object). During all these steps, the *strong adhesion* induced by **EA**[HS] between the hard slabs and the soft pillars persists and endures. This demonstrates that EA can indeed be leveraged in making actuators and robots. Similar hard-soft assemblies could also be useful in the body where metal implants like stainless steel or titanium are widely used. The ability to adhere a gel (or

tissue) to metal could be useful in reinforcing these implants and also to control the interface between the implant and bodily fluids.

A final point is that the adhesion induced by **EA**$^{[HS]}$ between a hard and a soft solid can also be achieved underwater. This is demonstrated in Figure 3.11 using Cu sheets and an AAm gel. First, in Figure 3.11A, we bring a Cu sheet into contact with a strip of AAm gel while being immersed in water. We make Cu the anode (+) and complete the circuit with graphite as the cathode (–), similar to the arrangement in Figure 3.6A. The gel is the same as in Figure 3.8 and has high salt content (15% NaCl), which ensures a short adhesion time. We then apply 5 V for 60 s, thus inducing **EA**$^{[HS]}$ between the metal and the gel (Figure 3.11B). Note that the graphite as cathode does not adhere to the gel and is not shown in the figure. Next, we stick a second Cu sheet to the opposite side of the AAm gel strip. For this, the second Cu sheet is made the anode, graphite is again the cathode, and the adhered Cu sheet is left in open circuit. 5 V is again applied for 60 s to induce **EA**$^{[HS]}$. The result (Figure 3.11C) is that the two Cu sheets are stuck together by the AAm gel, similar to the earlier result in Figure 3.6A. However, in the present case, the entire assembly is underwater — thus *the gel is able to serve as an underwater adhesive*. Achieving adhesion underwater has proven to be a huge challenge in recent years because many flowable adhesives cannot be spread onto solid surfaces that are immersed in liquids like water. Even if spreading can be achieved, the solid-solid adhesion ends up being quite weak because the bonds between the solids are influenced by the water molecules around them. Here, we are able to surmount this problem because the gel is not

inherently adhesive to the metal: the adhesion is only switched on when the gel and metal are contacted under the field.

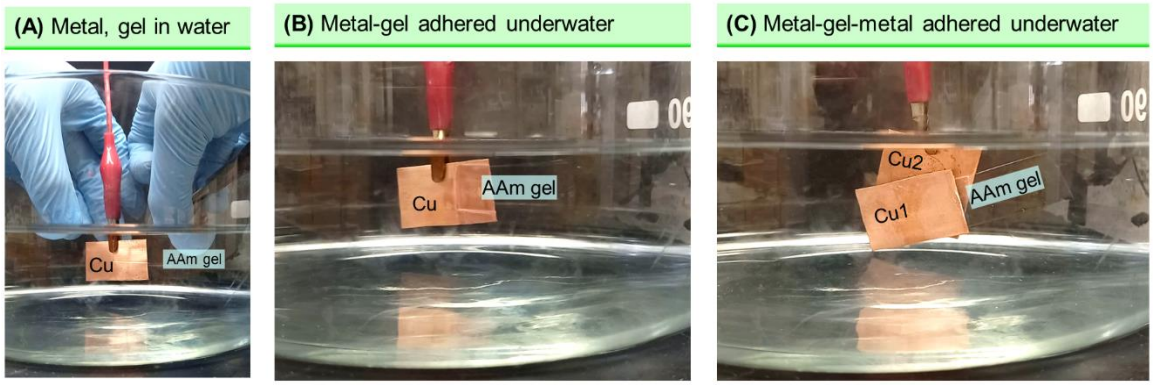

Figure 3.11. Underwater adhesion of metal and gel by EA[HS]. (A) A Cu sheet and an AAm gel are contacted underwater. With the Cu as anode and graphite as the cathode (not shown), **EA**[HS] is induced between the metal and the gel. (B) After the field is switched off, the pair remain adhered. (C) Next, a second Cu sheet is adhered on the opposite side of the gel by **EA**[HS]. The gel thus serves as an underwater adhesive between the two metal sheets.

3.4 Conclusions

In summary, we have reported a simple method for adhering hard materials to soft, aqueous materials. The hard material must be an electronic conductor like a metal or graphite, allowing it to serve as electrodes in a simple electrochemical setup. The soft material must be an ionic conductor, which typically means it must have water and ions (salt). Examples of such materials include hydrogels as well as plant-based tissues (fruits and vegetables) and animal-based tissues (meat from cows, pigs, and chickens). Our method, which we term *hard-soft electro-adhesion* or **EA**$^{[HS]}$, is to bring the hard and soft material into contact and apply a low DC electric field (e.g., 5 V) for a short time (e.g., 3 min). Depending on the nature of the hard and soft materials, adhesion is induced at the anode (+), cathode (–), both electrodes, or neither. This adhesion endures after the field is removed. If adhesion is observed only to one electrode, switching the polarity of the field typically reverses the adhesion. The adhesion strength increases with increasing voltage, time in the field, and ionic conductivity of the gel. The ultimate adhesion strength is limited only by the strength of the gel. Metals that can be adhered via **EA**$^{[HS]}$ to AAm gels (all at the anode) have reduction potentials above a critical value. This correlation to the electrochemical series suggests that **EA**$^{[HS]}$ is due to chemical bonds between the gel and the anode induced by electrochemical reactions. Support for this conclusion comes from FTIR data. Finally, the versatility of this phenomenon is shown through various examples. **EA**$^{[HS]}$ could enable applications in robotics, energy storage, and underwater adhesion.

Chapter 4
Electro-Gelation of Biopolymers to 3D-Print Hydrogels

4.1 Introduction

3D-bioprinting, or additive manufacturing of hydrogels, has been a hot topic in recent years.[74-76] By using stimuli to solidify bio-ink at specific location and time, it builds up hydrogels from scratch, allowing arbitrary 3D-shaped hydrogels to be made. Compared to conventional material-shaping strategies, such as mold-casting and smithing, 3D-printing has its advantages such as more flexibility, less consumption of materials and so on.[77-81] Therefore, 3D-printed materials are widely used in different applications, such as biomedical, food, pharmaceutical, tissue engineering, drug delivery, etc.[80-84]

3D-bioprinting strategies reported in literature could be divided into four categories[75]: ink-jet bioprinting[85,86], extrusion bioprinting[87,88], digital light processing (DLP) bioprinting[89,90] and laser-assisted bioprinting[91-93]. The former two, ink-jet and extrusion bioprinting, are based on extrusion of bio-ink from a nozzle. Temperature, pH or light can be used as the stimuli to trigger gelation of the bio-ink. Typically, nozzle extrusion methods are relatively simpler and more flexible, and the corresponding printers are at lower cost. However, clogging of nozzles is always an issue. Depending on the bio-ink, the printers could only work under a certain range of pressure and limited speed. Also, due to the drop-by-drop or line-by-line printing mode, the structure integrity of the printed structures is poor.[76,94]

DLP and laser-assisted printing use photopolymerization as the solidification method. Light is focused on specific locations in a reservoir of bio-ink to induce gelation. Since the nozzle is no longer needed for directing spatial solidification, there is no worry about clogging the nozzle. And the resolution is not limited by the physical size of the nozzle tip and can be precise to the order of wavelength of light, i.e., 1 μm or even less. For DLP-based bioprinting specifically, the solidification process is continuous so that the structure integrity is excellent. However, light-assisted printing also faces some challenges. For photopolymerization, the material is limited to photo-sensitive polymers, and additional chemicals such as initiators are required. The printer is generally more costly, since it requires either a complex optical system or a laser generator. In one word, the current 3D-printing techniques are still finding a balance among various considerations including printing speed, resolution, structural integrity, cost and so on.[76,90,94]

To address these concerns, we seek to use another stimulus to trigger gelation of the bio-ink instead of commonly used temperature, pH or light as stimuli.[75] Our choice is the electric field. Electro-responses of biopolymers have been widely reported in literature, among which one common example is alginate.[18,22] Alginate is an anionic polysaccharide. It is known to form so-called "egg-box junctions" with various multivalent cations, such as Ca^{2+}, Cu^{2+}, Zn^{2+}, Al^{3+}, etc.[37,38] When electrolyzing an alginate solution with calcium carbonate nanoparticles suspended, the nanoparticles neutralize H^+ generated from the anode (+) while dissolving and releasing Ca^{2+}. Thereby

alginate gets crosslinked by Ca^{2+} and deposited onto the anode (+) as Ca^{2+}-alginate gel.[18] The resulting alginate gel, being a thin film, is not shaped into a 3D structure. Our lab developed a strategy to fabricate 3D-shaped Ca^{2+}-alginate gels.[28] Using an agarose gel containing Ca^{2+} as a shape mold, electrophoresis of Ca^{2+} out of the mold into an alginate solution makes Ca^{2+}-alginate gels in the shape of a replica of the mold. This method is simple and fast, and it fabricates fairly strong gels. Yet this is not really 3D-printing since it requires a mold, so the difficulty of shaping 3D structures comes to fabrication of the mold. To the best of our knowledge, so far there is no 3D-bioprinting technique using an electric stimulus reported in literature.

Herein, we introduce a method to 3D-print alginate gels using an electric field to trigger solidification, which we term as "electro-gelation". When an alginate solution is electrolyzed, on the anode (+) H^+ is generated and thus alginate gets protonated and becomes alginic acid. Since alginate loses its charge, it forms a cylindrical gel around the positive electrode. By using a moving anode (+) as the working electrode, multiple gel cylinders can be formed in the same container. These gel cylinders serve as building blocks or voxels which compose the final structure. Despite the voxel-by-voxel printing process, the adjacent voxels well merge together, resulting in good structural integrity. The resolution depends on voltage and time, and can be further fine-tuned by applying a reversed field around the gel after it is printed. Various 3D structures are printed, demonstrating printability of arbitrary structures. We also demonstrate the printability of a cationic biopolymer chitosan by deprotonating it at the cathode (–) as the working

electrode. This suggests that 3D-bioprinting by electro-gelation could potentially be applicable to any biopolymer whose solubility varies under different pH conditions.

4.2 Experimental Section

Materials. The following chemicals were from Sigma-Aldrich: alginate (i.e., alginic acid sodium salt, from brown algae, medium viscosity), calcium chloride dihydrate ($CaCl_2$•$2H_2O$), and chitosan (medium molecular weight). Platinum wire (26 gauge, 99%, 6 inches) was purchased from uGems. Graphite rods (fine extruded, 0.094"OD×12"L) were purchased from Graphite Store. Other chemicals include sodium chloride (NaCl, from LabChem) and acetic acid (glacial, from Fisher Scientific).

3D-Printing by Electro-Gelation. The electro-gelation 3D-bioprinter is modified from a commercially available 3D-printer. A Duet3D Duet 3 6HC 3D-printer controller board is connected to a Creality Ender-3 220×220×250 mm X-Y-Z stage to control the movement and also to a BK Precision 9104 DC power supply to control the applied voltage. A cable connects the controller board to a lab computer to receive commands. G-code is modified for this setup to set the voltage and movement. A 90×50 mm crystalizing dish is located on the printing platform of the stage as the container for bio-ink. Three graphite rods as the counter electrodes are fixed on the inner wall of the container. The working electrode, either a graphite rod or a platinum wire, is fixed on the moving head of the stage, in place of a nozzle as in extrusion-based 3D-printers. Depending on the chemistry of bio-ink, the working electrode is connected to either terminal of the DC power source (positive terminal for alginate and negative terminal for chitosan), and the counter electrodes to another terminal. G-code commands can be either pre-programmed or directly sent from the computer. By inserting the working electrode into the bio-ink in the container and

applying voltage, cylindrical gels are formed around the electrode. Using the cylindrical gels as voxels, 3D structures are built.

Rheology of Printed Hydrogels. Rheological experiments on the alginate gels (Figure 4.2) were performed at 25°C on an AR2000 stress-controlled rheometer (TA Instruments) using 20-mm parallel plates. Gels were cut into discs of diameter 20 mm and thickness 2 mm. Dynamic stress-sweeps were first performed to identify the linear viscoelastic (LVE) region of the sample. Dynamic frequency sweeps were then conducted at a constant strain amplitude within the LVE region.

Cell Viability Tests. Cylindrical gels (~ 20 mm diameter × 3 mm height) were printed by electro-gelation by applying 10 V for 5 min. These gels were incubated in a 2 wt% calcium chloride solution and then washed with DI water until neutral pH. Following this step, the gels were subjected to conjugation with rat tail collagen. This process involved immersing them in a solution containing 200 mM 1-ethyl-3-(3-dimethylaminopropyl)carbodiimide (EDC) and 50 mM *N*-hydroxysuccinimide (NHS) for 30 minutes, followed by incubation in a 30 µg/mL rat tail collagen solution for 12 hours. After conjugation, the gels were washed with DI water and transferred to a 12-well plate. A small amount of agar solution was added to the bottom of the 12-well plate, so that when it cooled down and gelled, it anchored the printed alginate gel on the bottom of the 12-well plate.

Human embryonic kidney 293T (HEK293T) cells were cultured in Dulbecco's modified Eagle's medium supplemented with high glucose (4500 mg/L), L-glutamine (4 mM), pyruvate (1 mM), penicillin-streptomycin (1%), and fetal bovine serum (10%). The cells were trypsinized, suspended in medium, and 200,000 cells were pipetted onto each printed gel. Subsequently, 2 mL of medium was added to each well and changed daily throughout the experiment. After cell culture for 2 days, Calcein AM and Ethidium homodimer (Thermo Fisher Scientific, Waltham, MA) were utilized for live/dead staining according to the manufacturer's protocol. The stained gels were put under a fluorescent microscope for observation and imaging.

4.3 Results and Discussion

4.3.1 General Approach of Electro-Gelation

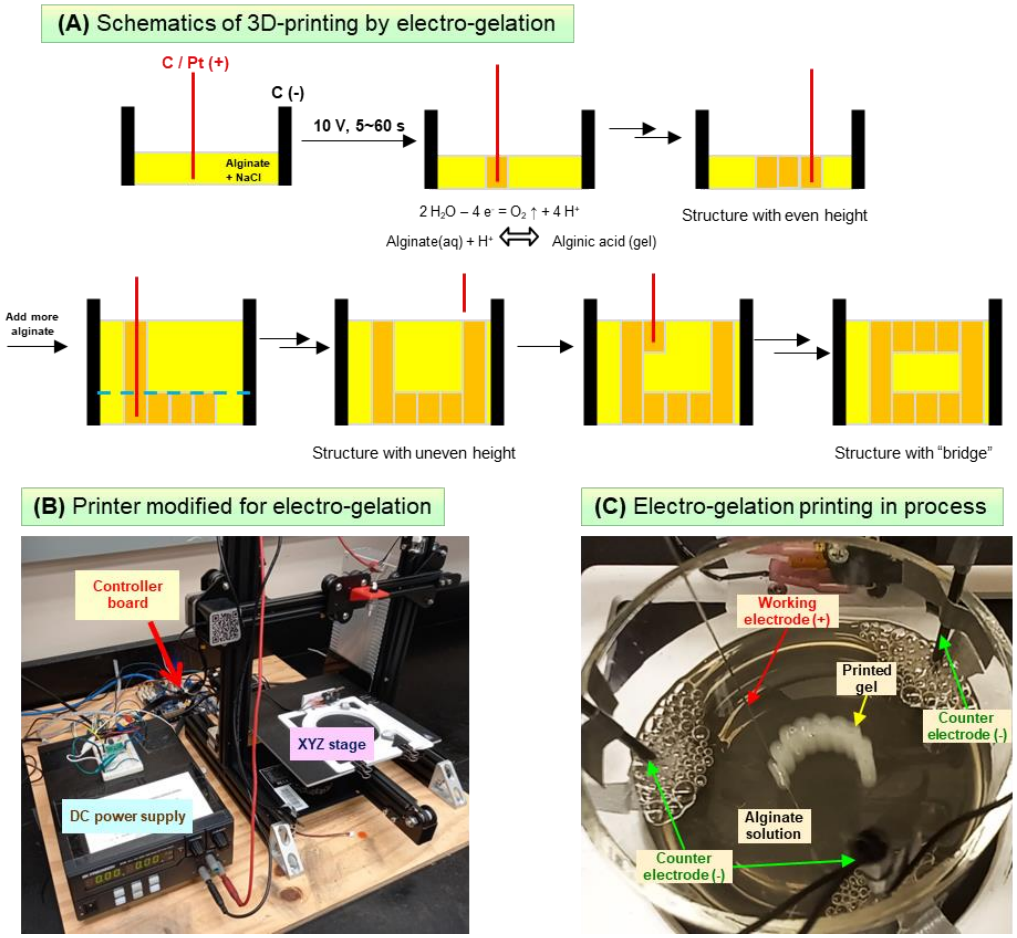

Figure 4.1. Setup of Electro-Gelation 3D-Printing. (A) Schematics of electro-gelation 3D-printing of alginate gels. An alginate solution is electrolyzed with a mobile working electrode and multiple fixed counter electrodes. Gel "voxels" are formed around the working electrode. By merging multiple gel voxels, 3D structures are fabricated. (B) Electro-gelation 3D-printer. (C) Printing in progress.

Figure 4.1A shows the schematics of 3D-bioprinting by electro-gelation. A 2% alginate solution with 1% NaCl is electrolyzed with one working electrode (either a graphite rod or a Pt wire), which is the anode (+), and graphite rod counter electrodes, which are cathodes (–). By applying a voltage of typically 10 V, H_2O in the solution gets

electrolyzed and H^+ ions are generated on the working electrode. Thereby alginate becomes protonated and forms a gel due to loss of charge. A gel cylinder is "grown" in this way around the working electrode. By lifting the working electrode and inserting it again into the solution at another location, multiple gel cylinders can be formed. When one gel cylinder grows and encounters another gel cylinder, they merge into a whole piece without any further assistance. In this way, a 2D pattern with even height at different locations can be made by merging multiple gel cylinders of the same height. To fabricate 3D structures, more alginate solution is added into the container so that taller gel cylinders can be made. Shorter cylinders can also be made at a higher location by controlling how deep the working electrode inserts into the solution. By combining gel cylinders of different heights, arbitrary 3D structures can be made.

To achieve automated 3D-bioprinting by electro-gelation, we fabricated a device for electro-gelation by modifying a commercially available 3D-printer. (Figure 4.1B) The device is composed of three parts: an X-Y-Z stage, a DC power supply and a controller board. The container for alginate solution, with 3 graphite counter electrodes fixed onto it, is located on the stage platform. Instead of a nozzle for extrusion-based 3D-printers, the graphite or Pt working electrode is fixed onto the moving head of the stage. The positive terminal of the DC power supply is connected to the working electrode, while the negative terminal to the counter electrodes. The controller board, connected to PC with a cable, accepts modified G-code commands from the computer and controls the movement of the stage as well as the voltage and time of electrolysis. With this setup, we

are able to automate the printing process as in regular 3D-printing. Figure 4.1C shows a gel during printing process.

4.3.2 Rheology of Alginate Gels Printed by Electro-Gelation

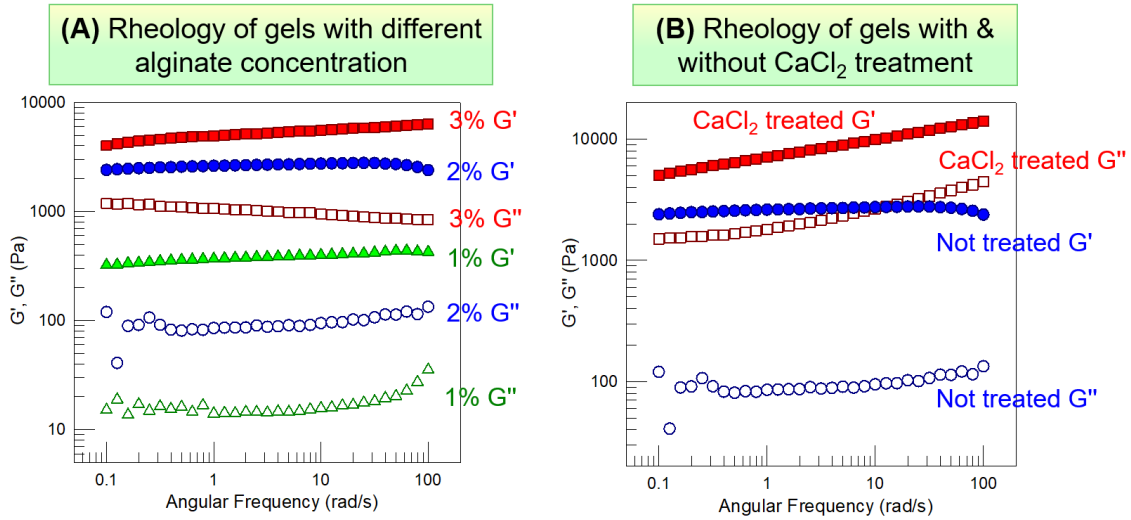

Figure 4.2. Rheology of Printed Alginate Gels. (A) Dynamic rheology of alginate gels with 1%, 2%, and 3% concentration without $CaCl_2$ treatment. As the concentration of alginate increases, the modulus of the gel increases, indicating the gel becoming stiffer. (B) Rheology of 2% alginate gels before and after $CaCl_2$ treatment. Incubating printed gels in $CaCl_2$ solution increases the gel modulus.

Rheology of printed gels is shown in Figure 4.2. Gels printed with alginate solution of different concentration (10, 20, 30%) are compared in Figure 4.2A. The elastic moduli in all cases are much higher than the corresponding viscous moduli, and also keep constant all over the frequency range, which means that all three materials printed are solid gels. With increasing alginate concentration, increasing gel moduli were observed. As one would expect, increasing the polymer concentration should increase the crosslinks formed by intermolecular interactions such as hydrogen bonding and chain entanglement, etc., and thereby increase the stiffness of the gel. To further enhance the

mechanical properties, a printed alginic acid gel is put into 2% $CaCl_2$ solution overnight. As alginate is well-known to form so-called “egg-box” junctions with all kinds of multivalent cations, this post-treatment would convert alginic acid gels into calcium alginate gels with stronger crosslinks. Rheology of printed gels before and after post-treatment is compared in Figure 4.2B. It is shown that post-treatment with $CaCl_2$ solution enhances the mechanical strength of the gel.

4.3.3 Resolution

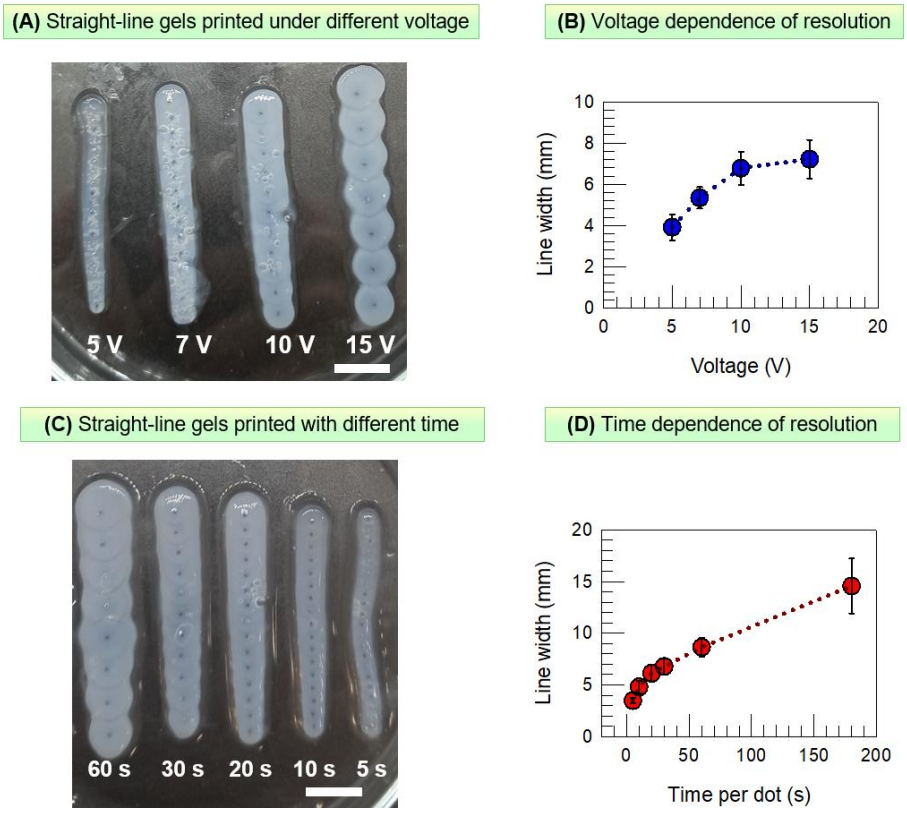

Figure 4.3. Resolution of Straight-Line Gels Printed by Electro-Gelation. (A) & (C) Images of straight lines printed by electro-gelation with (A) different voltage and (C) different time. (B) Voltage and (D) Time dependence of line width printed by electro-gelation. Scale bars are 1 cm.

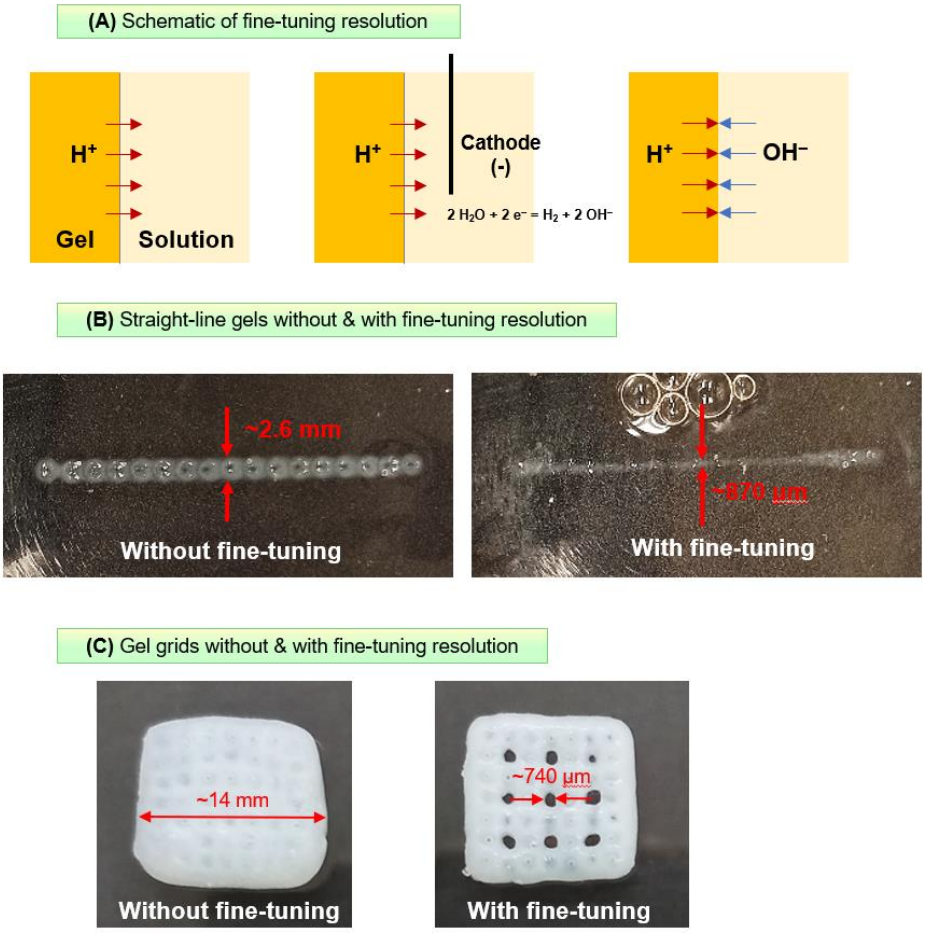

Figure 4.4. Fine-tuning of Resolution. (A) Schematics of fine-tuning step. The working electrode is used as the cathode (–) to electrolyze alginate solution around the printed gel. OH^- is generated around the gel and neutralizes H^+ diffusing out from the gel, preventing further growth of the gel. (B) Straight lines printed before & after fine-tuning resolution. With fine-tuning step, the resolution is refined to < 1000 µm. (C) Gel grids printed with & without fine-tuning resolution. Without fine-tuning, a grid cannot be printed as the holes are filled by gels formed due to diffusion of H^+. With fine-tuning step, holes on the scale of hundreds of microns are preserved.

We also examined different variables that affect printing resolution. Since a working electrode in our setup replaces the extrusion nozzle in regular 3D-printing, the key parameters to resolution become voltage and time of electrolysis instead of pressure of extrusion and moving speed of nozzle. Intuitively, for a 3D structure built by merging gel cylinders as voxels, the resolution depends on size of the gel voxels, which is in turn

determined by the voltage and time of electrolysis. With higher voltage or longer time, more H^+ should be generated and more alginate should be gelled.

The effect of voltage is shown in Figure 4.3A & 4.3B. Straight lines composed of gel cylinders as voxels were printed under different voltages. Each voxel of the straight lines was printed with the same electrolysis time. As one would imagine, higher voltage makes larger voxels, thus results in thicker straight lines. Interestingly, with higher voltage, fewer bubbles get entrapped inside the gel as seen in Figure 4.3A. The effect of time of electrolysis for each voxel is shown in Figure 4.3C & 4.3D. Straight lines were printed under the same voltage of 10 V, while each line has a different time of applying voltage for single voxels. As one would expect, a shorter time leads to a thinner straight line, i.e., finer resolution. The lower limit appears to be ~ 5 s under 10 V, which corresponds to a resolution of ~ 3 mm.

One issue that bothers the resolution has been the diffusion of H^+. Since the solution is solidified by H^+ generated from the working electrode, the gel has a lower pH than the surrounding solution, and thus H^+ diffuses along the concentration gradient from the gel to the solution even after the voltage is stopped. Therefore, the gel still grows slowly without a voltage until the whole gel is taken out of the solution. In order to further fine-tune the resolution, a reversed voltage can be applied around the gel after it is printed. Figure 4.4A shows the schematics of fine-tuning the resolution of printed gels. After a gel is printed, the polarity of the voltage is switched, i.e., the working electrode becomes the cathode (–) and the counter electrodes are anodes (+). Then “virtual voxels”

are “printed” right around the printed gel. OH^- instead of H^+ is generated at the working electrode, so no gel is formed in this step, but the OH^- ions neutralize the H^+ diffusing out of the gel, thereby the uncontrolled growth of the gel is stopped. Figure 4.4B shows a straight line printed followed by the fine-tuning step. The width of the gel is further restricted to ~ 800 μm. Figure 4.4C shows a grid structure printed with and without the fine-tuning step. Without OH^- stopping diffusion, the holes of the grid are finally all solidified by H^+ diffusing out of the gel. Only with fine-tuning of resolution, i.e., inserting the working electrode into each hole of the grid and applying reversed voltage, the holes can be preserved after printing. The dimensions of the holes are ~ 700 μm, close to the dimension of the fine-tuned straight line. This demonstrates that resolution on hundred-micron scale is achievable.

4.3.4 Various 3D Structures Printed by Electro-Gelation

By properly programming the printing process, various 3D structures can be fabricated. (Figure 4.5) Figure 4.5A shows a gel tube printed by electro-gelation. The tube is composed of 16 gel cylinders in a circle, each printed under 10 V for 20 s. The diameter of the tube is defined by the locations of the cylinder voxels, while the height of the tube is controlled by the amount of alginate solution in the container. Such a cylinder can be printed in ~ 8 min, which is much faster than regular 3D-bioprinting.

To print a structure with different height at different X-Y locations, we can control the height of each cylinder by adding or reducing the amount of solution in the container during the printing process. Figure 4.5B shows a square pyramid printed by

electro-gelation. The solution is first added to a depth of 3 mm, and the outermost cylinders are printed. Then we add more alginate solution to the container and print the next outermost cylinders. By repeating this process several times until we reach the center, gel cylinders with gradually increasing height from the edge to the center are printed and merged together to be a pyramid. The slow growth of the gel due to diffusion of protons smoothens the surfaces, making the side surfaces of the pyramid flat and smooth. Therefore, to print a tilt surface, there is no need of fabricating numerous layers to approach a flat surface.

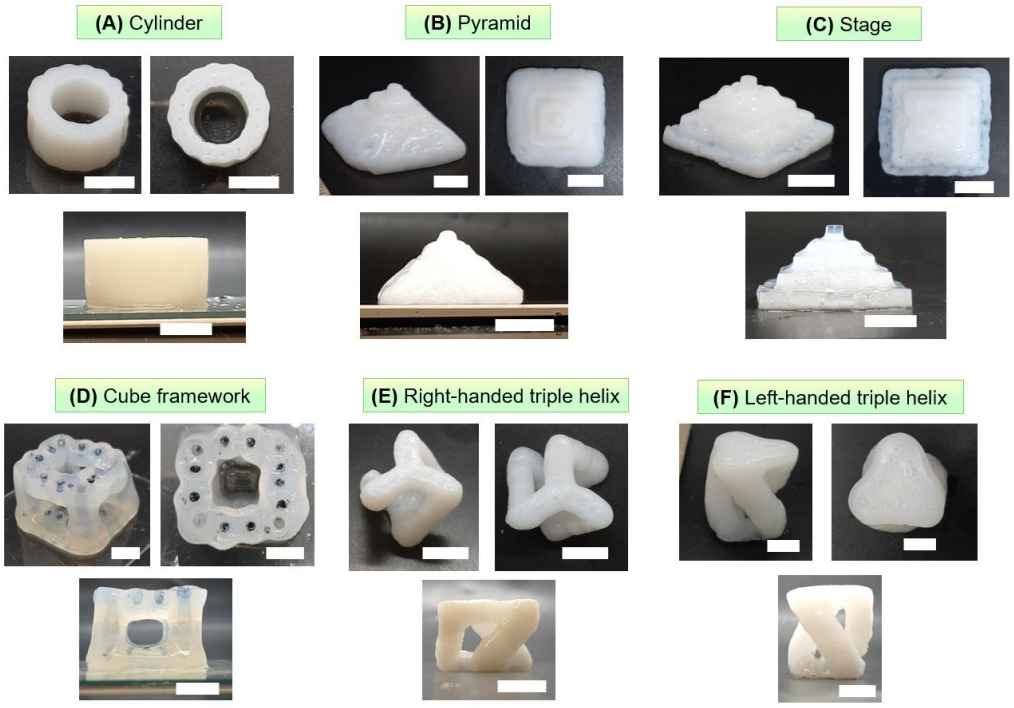

Figure 4.5. Various 3D Structures Printed by Electro-Gelation. (A) Cylinder. (B) Pyramid. (C) Stages. (D) Cube framework. (E) Right-handed triple helix with three-armed-star top & bottom. (F) Left-handed triple helix with triangular top & bottom. Scale bars are 1 cm.

Interestingly, if the pyramid is printed in a reversed order, (i.e., starting at a high solution level, printing the center first, and then gradually reducing the solution and printing the outer layers), the final structure becomes stages instead of a pyramid. (Figure 4.5C) When the solution is reduced, the top of the printed gel is left in the air with no solution around it, allowing no protons to diffuse out. Thereby the corners of the cylinders are preserved in the final structure, making it stages.

Bridged structures can also be printed in a facile manner. In traditional 3D-printing, fabricating a bridged structure could be difficult since gravity forces unsolidified materials to flow down. Therefore, a lot of additive manufacturing of hydrogels is done in supporting materials. A supporting material is either a viscous solution or a shear-thinning gel, which is not miscible with the ink. When the ink is injected into the supporting material, the floating force and viscous force will hold the ink at its position until it solidifies. Thereby the entire 3D structure can be printed without deformation. After printing is completed, the supporting material should be easily removed. In our electro-gelation technique, the alginate solution around the printed gel naturally serves as a supporting material. The solution is viscous and has a similar density to the gel, which enables it to hold the printed gel steady. A cubic framework is printed as a demonstration of fabricating bridged strictures. (Figure 4.5D) First, a low level of alginate solution is added into the container and the bottom square is printed. Then the solution level is increased to 20 mm to print the four pillars. Finally, short gel cylinders connecting the top of pillars are printed by inserting the working electrode only 1 mm depth into the solution. This demonstrates that by controlling the solution level and the location of the

working electrode for each voxel, electro-gelation can print arbitrary 3D structures. More structures such as triple helices are shown in Figure 4.5E & 4.5F.

4.3.5 Printability of Biopolymers Other than Alginate

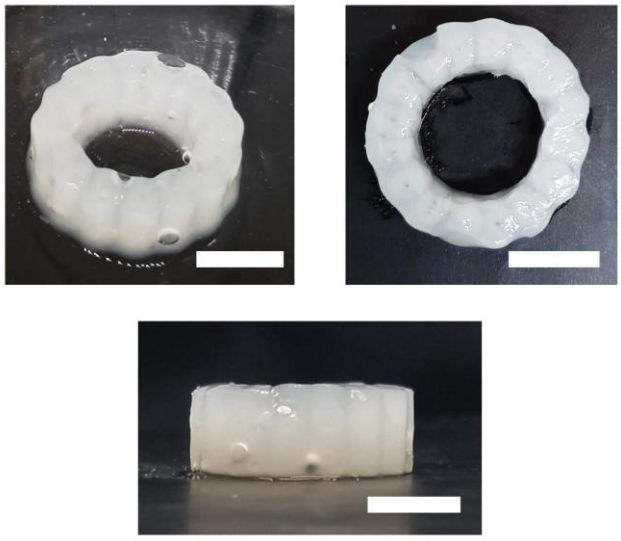

Figure 4.6. Chitosan Gels Printed by Electro-Gelation. Chitosan gels are printed with the same codes as for alginate gels but with a cathode (–) instead of anode (+) as the working electrode. The resulting chitosan gel has the same appearance as the alginate gel in Figure 4.5A, indicating that electro-gelation is applicable to different biopolymers. Scale bars are 1 cm.

Since the anionic polymer alginate gels at the anode (+) due to protonation, is it possible to achieve an opposite process, i.e., gel a cationic polymer at the cathode by deprotonation? We also tested this idea with the cationic polymer chitosan. Chitosan is known to be water-soluble only under acidic conditions. Here, 2% chitosan is dissolved in 0.08 M acetic acid. 1% NaCl is also added for conductivity. A same program for printing alginate gel tube is used to print chitosan, while the working electrode is switched to the cathode (–) instead of the anode (+). The resulting chitosan gel has an

almost identical shape to that of the corresponding alginate gel tube. This implies that electro-gelation could be valid for 3D-printing of various ionic polymers so long as they undergo significant solubility changes due to pH variation.

One interesting thing to notice is that the concentration of acetic acid used for dissolving chitosan is important for printing nice-looking gels. As electrolysis occurs, the pH is increased around the cathode (–) to gel chitosan, while H_2 gas bubbles are also generated at the same time. Consumption of H^+ and generation of H_2 are stoichiometric. If there is excess acid, there will be large amounts of bubbles generated before pH is lowered to the extent where chitosan starts to form gels. The excess bubbles disturb the solution, resulting in irregular shape of the gels. Therefore, the concentration of acetic acid should be just enough to dissolve chitosan, but not excess. We determined that it requires 0.08 M acetic acid to dissolve 2% chitosan, and this acid concentration minimizes bubble generation and thus results in nice-looking gels.

4.3.6 Cell Viability Test on Gels Printed by Electro-Gelation

Lastly, we show that our gels are biocompatible and suitable for cell culture. Printed alginate gels were first treated with $CaCl_2$ to convert into Ca^{2+}-alginate gels. Then the gels were brought to neutral pH in buffer. After that, the surface of the gel was modified with collagen for adhesion of cells. Then human embryonic kidney 293T (HEK293T) cells were loaded onto the gel surface and let grow. After two days of cell growth, we used live-dead assay to examine the liabilities of cells. Figure 4.7 shows the live cells and dead cells. Green spots which indicate cells alive are spread on the gel,

while red spots for dead cells are very few. This indicates that cells can adhere to the gel and survive on the gel surface, which allows our printed alginate gels to be suitable for cell culture.

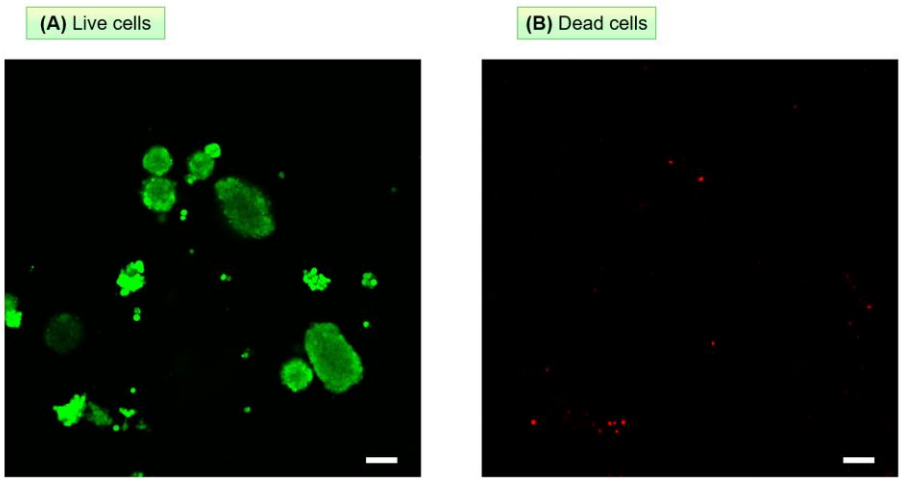

Figure 4.7. Cell Viability Test by Live-Dead Assay. Alginate gels are printed, treated with $CaCl_2$, and modified with collagen. Then cells are adhered onto the printed alginate gels. After incubation for two days, the cells on the gels were dyed with live-dead assay and put under fluorescent microscope. (A) Live cells with green fluorescence. (B) Dead cells with red fluorescence. Scale bars are 100 μm.

4.4 Conclusions

In this study, we demonstrate a nozzle-free 3D-printing technique using an electric field to solidify the bio-ink. By electrolyzing an alginate solution with platinum wire or graphite rod electrodes, H^+ is generated at the anode and protonates the anionic alginate. Thus, alginic acid gels are formed at the anode. By modulating the voltage and time of electrolysis, the size of the resulting gel is under control. Using a moving working electrode, multiple alginate gels can be formed at desired locations. These gels serving as building blocks or "voxels" merge together spontaneously and thereby form 3D structures. This electro-gelation strategy is fast and at low cost compared to regular 3D-bioprinting. The resolution of electro-gelation can be fine-tuned to hundreds of micron scale. Cell studies confirmed that cells can adhere to and survive on printed gels. Electro-gelation could also apply to ionic biopolymers other than alginate, such as chitosan. This strategy may provide a facile alternative to currently available 3D-bioprinting techniques.

Chapter 5
Electro-Carving Hydrogels into 3D Shapes

5.1 Introduction

Shaping materials have been of great importance in daily life, industry and scientific research.[95-97] In human history, people developed a variety of shaping strategies, such as carving[98,99], smithing[100], mold-casting[101], photolithography[102], 3D-printing[74-76], etc. Different shaping methods have different advantages, and they are suitable for different materials.

Among all the shaping techniques, carving or sculpting might be the most ancient method.[103,104] The art of sculpture dates back to ancient Sumer and ancient Egypt civilization, and the use of chipped stone or polished stone as tools even appeared before civilized human society. By eliminating the excess outer part of a bulk material, carving as a top-down strategy avoids building the bulk material from scratch as in 3D-printing. And the resolution of carving can be tuned by fine polishing so that nice sculptures can be made. The structural integrity of the original material is also perfectly preserved. However, to the best of our knowledge, bulk carving is only applied to hard solids like stones. It is difficult to mechanically sculpt soft materials, since soft, elastic materials like hydrogels deform when a force is applied on them.[30] When the force is too high, soft materials may crack or break.

In the past few decades, researchers have developed a variety of strategies to trigger responses on soft materials with stimuli.[6-14] Polymeric materials can swell, shrink,

bend, fold, form a gel or dissociate under various stimuli such as temperature, pH, ionic strength, light, electric field, magnetic field, etc. However, very few of these stimuli can trigger responses at a specific location and time.[15] The resolution of temperature, pH and ionic strength stimuli is limited due to heat transfer and mass transfer. Light can be focused on a precise spot, but the penetration depth of light into a material is limited by absorption and scattering, therefore fabrication methods with light as a trigger, such as photolithography, is generally applied on materials with thicknesses on micro- or nano-scale.[102] To carve a bulk hydrogel into 3D shape, a stimulus with spatial and temporal resolution to trigger disruption is required.

Herein, we report a strategy that uses electric field as the stimulus to "sculpt" hydrogels into 3D shapes. We have found that when an agar gel is electrolyzed by two graphite sheets, half of the gel near the anode (+) shrinks, while water leaks out from the other half near the cathode (–). The gel ultimately shrinks more than a half. The rate of shrinkage increases with increasing field strength and decreasing agar content. High ionic strength prohibits the shrinking phenomenon. The same electrically induced shrinkage also happens on some other gels such as alginate, poly(sodium acrylate) and agarose. We propose a combined effect of electroosmosis and pH variation as the mechanism. Finally, we show that using this phenomenon, electric field can be used as the "knife" to "carve" hydrogels into 3D shapes with appropriate electrodes.

5.2 Experimental Section

Materials. The following chemicals were from Sigma-Aldrich: agar (microbiology tested, plant cell culture tested, cell culture tested, powder), agarose (Type IA, low EEO), gelatin (from porcine skin, gel strength 300, Type A), alginate (i.e., alginic acid sodium salt, from brown algae, medium viscosity), chitosan (medium molecular weight), poly(vinyl alcohol) (PVA, MW 85–124k, 99+% hydrolyzed), sodium acrylate (SA, 97%), *N*,*N*′-methylenebis(acrylamide) (BIS), *N*,*N*,*N*′,*N*′-tetramethylethylenediamine (TEMED), potassium persulfate (KPS). Other chemicals include sodium chloride (NaCl), calcium chloride dihydrate ($CaCl_2$•$2H_2O$), acetic acid, sodium hydroxide (NaOH), hydrochloric acid (HCl), Alizarin Red S. Graphite plates were from Saturn Industries. Deionized (DI) water was used in all experiments.

Hydrogel synthesis. Agar and agarose gels were made by dissolving typically 1% corresponding polymer in water at ~90 ℃. If any NaCl needed to be included in the gel, it was also dissolved along with the polymer. Upon cooling down to room temperature, the solution was converted to a hydrogel due to the formation of hydrogen bonding and entanglement of agar or agarose chains. Gelatin was made with a similar method. Upon heating to ~ 50 ℃, gelatin dissolves in water. Upon cooling down to room temperature, the gelatin chains forms triple-helix junctions, thereby converting the solution to a gel.

Alginate gels were made by crosslinking with calcium ions. 3% alginate was dissolved in DI water in a vial. Then the solution was frozen at –20°C overnight. The vial was then broken and the frozen solid was removed. This cylindrical solid was then placed in a 7%

calcium chloride solution at room temperature on a stir plate. As the solid melted, Ca^{2+} came into contact at the interface and the cations diffused inwards to crosslink the alginate chains. Within 6 h, an alginate gel in the shape of a cylinder was obtained. Chitosan gels were made by a similar method. 2% chitosan was dissolved in 0.15 M acetic acid. Then the solution was frozen at –20°C overnight. The vial was then broken and the frozen solid was placed in a 0.5 M NaOH solution. As the solid melted, OH^- diffused in and chitosan chains got deprotonated and thereby crosslinked into a gel due to hydrogen bonding.

PVA gels were made by freeze-thaw cycling. 10% PVA was dissolved in DI water at ~ 90°C. Upon cooling to room temperature, a viscous solution was obtained. This solution was then subjected to two freeze-thaw cycles. For each cycle, the solution was frozen at –20°C overnight and then thawed at room temperature. The freeze-thaw cycling induced the PVA to form a robust gel due to the formation of crystallites at junctions between the chains.

SA gels were made by free-radical polymerization. 10% monomer, 0.03% BIS (crosslinker), and 2.0 μL/g TEMED (accelerator) were dissolved in DI water. After sufficient mixing, 0.02% initiator KPS was quickly mixed into the solution. Then the solution was placed under a nitrogen atmosphere for at least 30 min, whereupon it was polymerized into a gel. Then the SA gel was taken out of its container and washed with DI water once.

Electric-Field-Induced Shrinkage of Hydrogels. Hydrogels to be tested were made into a cylindrical shape (~ 2 cm diameter) and cut to a certain height (from 1 to 4 cm). Two polished graphite slabs (2 × 3 cm) were placed in contact with top and bottom of the gel. The two slabs were connected as electrodes to the positive and negative terminals of a BK Precision 9104 DC power supply. A DC voltage of typically 20 V was applied and the shrinkage of the gel was observed.

Electro-carving hydrogels. One graphite rod as the working electrode was connected to the positive terminal of the DC power supply, while a graphite slab as the counter electrode was connected to the negative terminal. The counter electrode was placed in contact with random location on an agar gel to be carved, and the tip of the working electrode was located where the gel needed to be carved. By moving the working electrode along certain pathway, the gel shrank along the trajectory of the working electrode and deformed into a certain 3D shape.

5.3 Results and Discussion

5.3.1 Electric-Field Induced Deformation on Agar Gels

We first studied the effect of electrolysis on agar gels. Two pieces of graphite sheets as electrodes are placed on either side of a cylindrical 1% agar gel (2 cm diameter × 4 cm height). 20 V is applied across the gel and the shape change of the gel is observed. Overall, the gel gradually shrinks over time, and its height reduces to less than a half of its original state. More interestingly, a distinct boundary appears in the middle of the gel while the shrinkage proceeds. A half of the gel near the anode (+) is more shrunken in size, while water leaks out from the other half near the cathode (–). A distinct difference in thickness appears at the boundary. Figure 5.1 shows the decrease in size of the gel and its deformation.

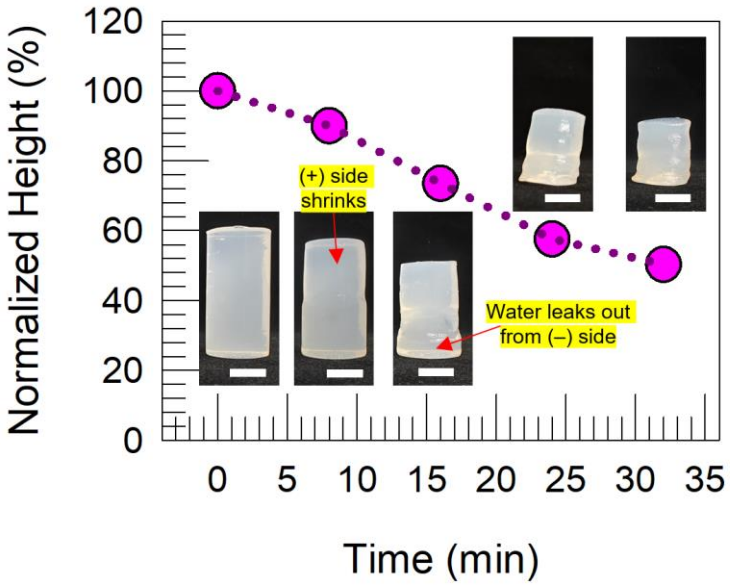

Figure 5.1. Shrinkage of Agar in Electric Field. A 4-cm-tall agar gel is placed between two graphite slabs as electrodes, and 20 V is applied. Half of the gel near the anode shrinks and water leaks out of the other half near the cathode. The gel collapses to half of its height in ~30 min. Scale bars are 1 cm.

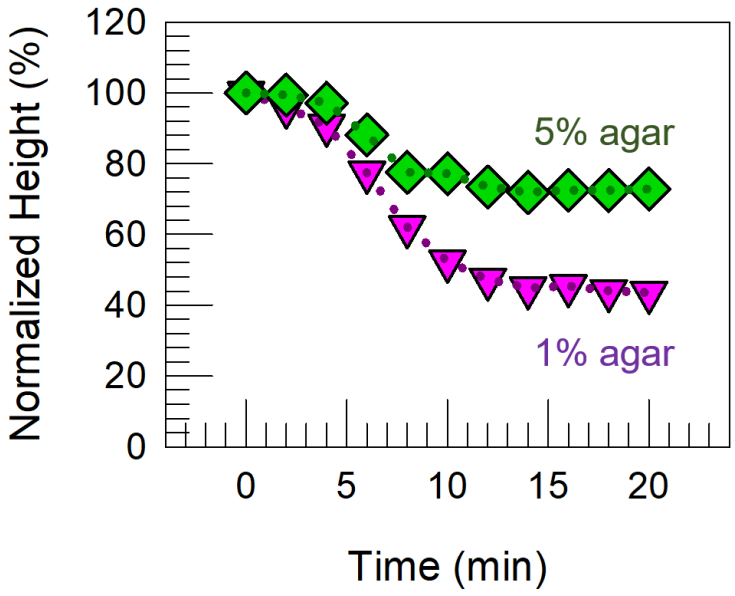

Figure 5.2. Shrinkage Profile of Agar Gels with Different Concentration. 2-cm-tall agar gels of 1% and 5% concentration are electrolyzed under 20 V voltage. Heights of agar gels normalized to original height is plotted against time. Gels with higher concentration shrink slower and to a less extent in electric field.

5.3.2 Factors that Affect Shrinkage of Agar in Electric Field

We examined different factors that affect this shrinkage phenomenon induced by electric field. The first variable is the concentration of agar in the gel. At different agar concentrations, the gels show the same behavior (i.e., shrinkage on the anode (+) side and water leakage on the cathode (–) side) but at different rates. Figure 5.2 compares the shrinkage of 1% & 5% agar gels. The gel with higher concentration not only shrinks slower, but also shrinks less when it stops shrinking. This could be attributed to the stiffness of the gel counteracts with the electric effect which results in deformation.

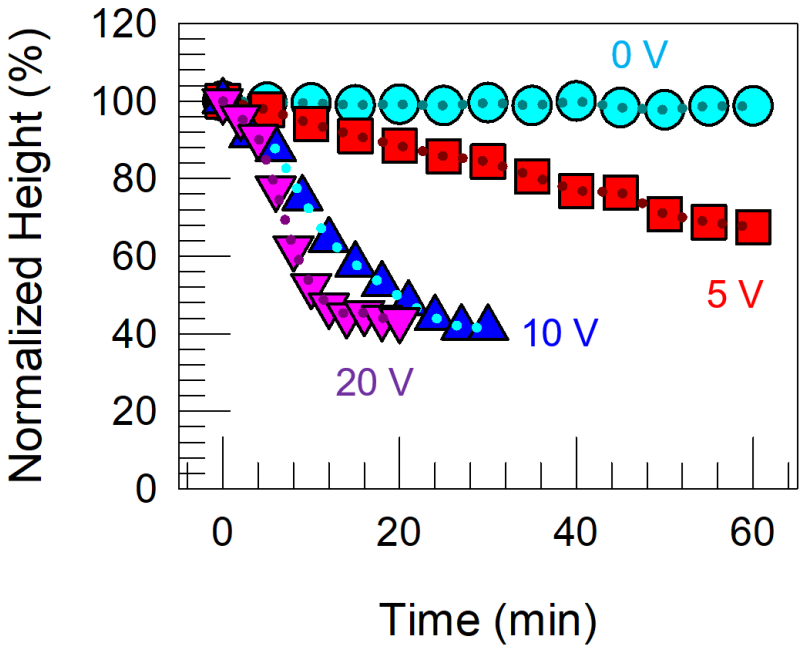

Figure 5.3. Shrinkage Profile of Agar Gels under Different Voltages. 2-cm-tall agar gels of 1% concentration are electrolyzed under 0 ~ 20 V voltage. Heights of agar gels normalized to original height is plotted against time. Without an electric field, there is no observable shrinkage. As voltage increases, agar shrinks faster in the electric field.

Voltage is another factor that affects the shrinkage of agar gels. Figure 5.3 shows the shrinkage curve of a 2-cm-tall 1% agar gel under different voltages. As one would imagine, the higher the voltage is, the faster the shrinkage will be. When no voltage is applied, there is no observable shrinkage of the gel. When 5 V is applied across the 2-cm-tall agar gel, shrinkage of the gel lasts for more than 1 h. When the voltage is increased to 10 or 20 V, the time required for shrinkage reduces significantly to ~ 10 min.

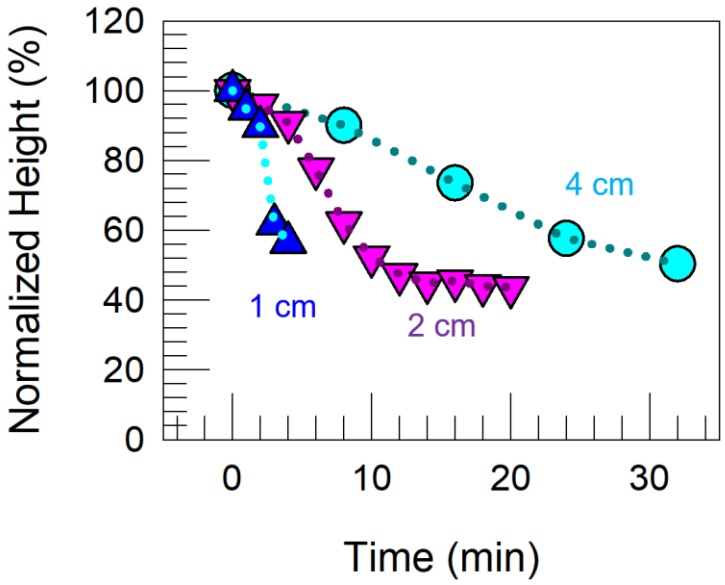

Figure 5.4. Shrinkage Profile of Agar Gels with Different Initial Height. 1% agar gels of different height are electrolyzed under 20 V voltage. Height of agar gels normalized to original height is plotted against time. Taller gels shrink relatively slower in electric field.

We also tested the effect of gel dimension on the shrinking rate. Under the same voltage of 20 V, a smaller distance between the electrodes leads to larger electric field strength, thereby resulting in faster shrinkage. As shown in Figure 5.4, when the height of the gel decreases from 4 cm to 1 cm, the time needed for the agar gel to shrink also decreases significantly from ~30 min to ~5 min. For the ease of experiment and observation, the gels used in this study are mostly 2-cm tall if not specifically mentioned.

Apart from the variables mentioned above, we also found that salt concentration in the agar gel makes a difference. Higher salt concentration leads to a higher conductivity, therefore resulting in a higher current. However, despite the higher current observed, we find that an agar gel with 1% additional NaCl does not shrink under 5 V voltage. (Figure 5.5) Comparing the effect of voltage and that of NaCl concentration,

increasing the voltage increases both the current and shrinking rate, while increasing NaCl concentration increases current but decreases shrinking rate. This suggests that current is not the crucial parameter that drives the shrinkage. Adding extra free charge carriers into the gel does not contribute to the shrinkage. Instead, higher ionic strength appears to counteract with the electric field in terms of the effect on gel deformation.

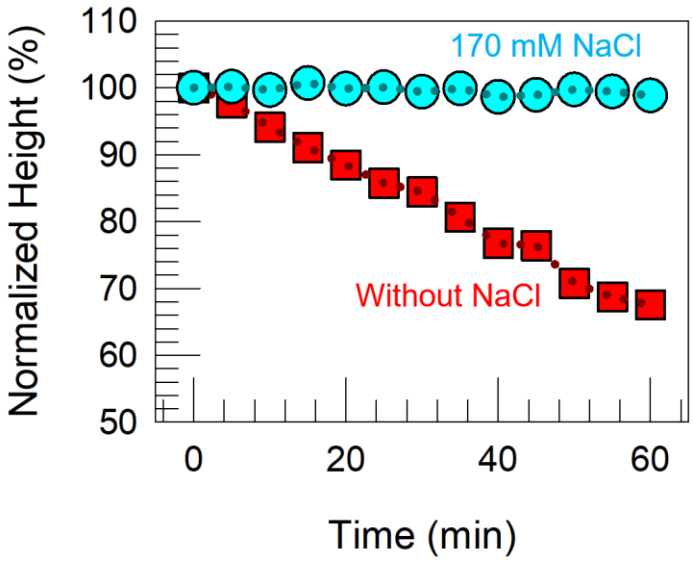

Figure 5.5. Shrinkage Profile of Agar Gels with Different NaCl Concentration. 1% (170 mM) NaCl is added to 1% agar gel, and the shrinkage profile under 5 V voltage is compared to that of an agar gel without NaCl. Adding NaCl to 170 mM inhibits shrinkage of the agar gel.

Since electrolysis of a hydrogel always involves pH changes on both electrodes, the effect of pH cannot be overlooked. We added a pH indicator, Alizarin Red S, to the agar gel and conducted the shrinking experiment. (Figure 5.6A) Alizarin Red S is yellow under acidic conditions, orange or red around neutral, and pink or purple under basic conditions. Before being electrolyzed, the agar gel with indicator shows a yellowish orange color, indicating a weakly acidic nature. When electrolysis starts, H^+ is generated

from the anode (+) and OH^- from the cathode. At ~ 3 min, the gel becomes half yellow and half pink, indicating that H^+ and OH^- are electrophoresed deep into the gel and neutralize each other in the middle. Most importantly, the boundary that separates the acidic half and the basic half of the gel exactly indicates which part of the gel shrinks, i.e., the yellow-colored acidic half is more shrunken while the pink-colored basic half is more swollen, with the boundary of the color being exactly the boundary of deformation. As electrolysis proceeds, it is observed that water leaking out from the gel has a pink color, confirming that it is the cathode side where water leaks out. This relationship between pH and deformation indicates that pH must contribute to the different behavior of different sides of the gel.

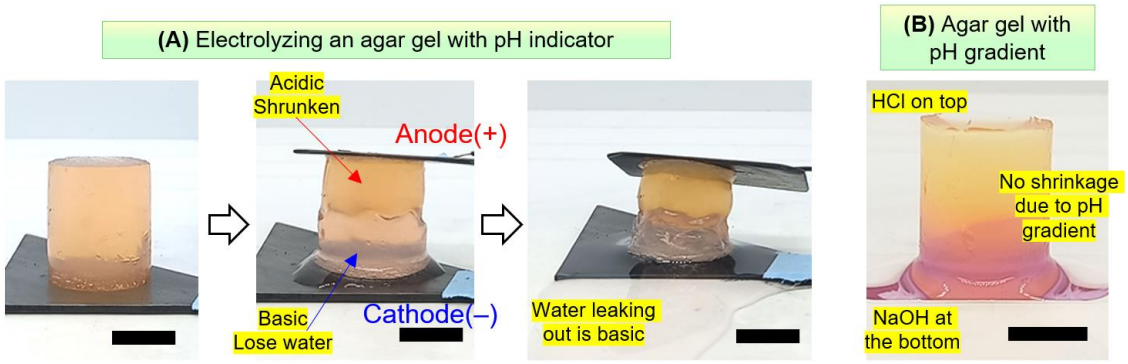

Figure 5.6. Effect of pH on Shrinkage of Agar Gels. (A) A 1% agar gel (2 cm height) with a pH indicator Alizarin Red S is electrolyzed under 20 V. The indicator shows that the gel becomes half acidic and half basic during electrolysis. The acidic half shrinks, while the basic half loses water. Water leaking out from the gel shows a basic color. (B) A pH gradient is generated in a 1% agar gel by diffusion without an electric field. 1 M HCl is added onto the top and 1 M NaOH to the bottom of the gel. In 1 h, the gel becomes also half acidic half basic, while no deformation is observed.

Based on the observation above, is it pH difference alone that results in the shrinkage of the gel? A pH gradient is created in an agar gel to see if it shrinks without an

electric field. (Figure 5.6B) Several droplets of 1 mol/L NaOH solution are added onto the bottom of an agar gel with Alizarin Red S, while the same amount of 1 mol/L HCl solution is dropped onto the top. The yellow color from the top and the pink color from the bottom expand slowly for ~ 1 h and meet in the middle. During the whole process, no shrinkage of the gel is observed. This demonstrates that pH alone is not the reason for deformation of the agar gel, and the electric field must have some further effect on the gel.

5.3.3 Electric-Field-Induced Shrinkage on Other Gels

Apart from agar, does the same phenomenon occur on other gels? We tested several other gels to see if the electrically induced shrinkage is a general phenomenon. As shown in Figure 5.7, some gels do shrink, while some others do not. Agarose, alginate and poly(sodium acrylate) (SA) gels show the same phenomenon as agar does, i.e. shrinkage from the anode (+) side and water leakage from the cathode (–) side. However, polyacrylamide (AAm), chitosan (gelled by NaOH), gelatin and poly(vinyl alcohol) (PVA) gels have neither shrinkage nor water leakage in the electric field. Note that the gels that do not shrink are all non-ionic, while the ones that shrink in electric field could mostly be regarded as anionic. The only apparent exception is agarose, which is non-ionic. Agarose is a polysaccharide extracted from agar, which has another component, agaropectin. Commercially available agarose may contain some amount of impurity anionic agaropectin, which makes the gel overall slightly anionic. This difference between ionic and non-ionic gels suggests that the shrinkage is related to the interaction of the electric field on the backbone charge of the gels.

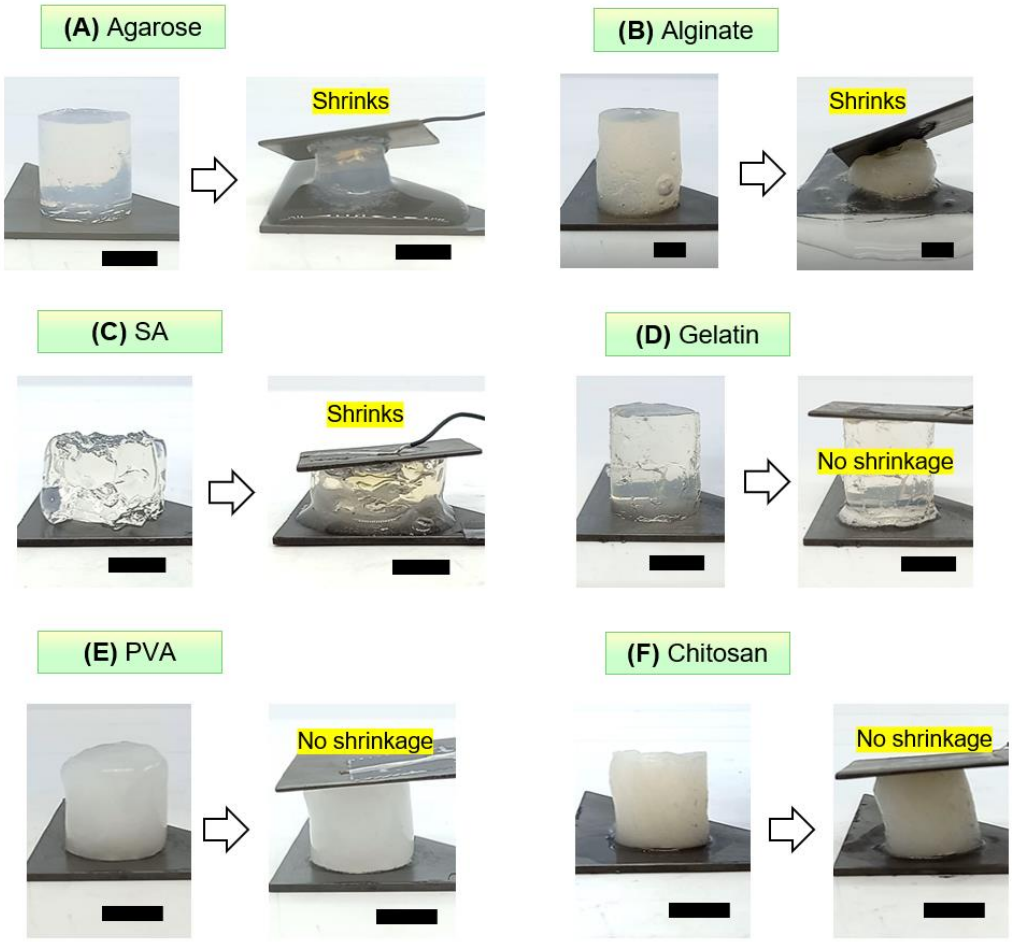

Figure 5.7. Electric-Field-Induced Effects on Other Gels. Various gels are electrolyzed under 20 V for 15 min and examined for shrinkage. (A) Agarose, (B) alginate and (C) SA gels shrink as agar gels do, while (D) gelatin, (E) PVA and (F) chitosan (gelled by NaOH) gels undergo no visible deformation.

5.3.4 Mechanism of Electric-Field-Induced Shrinkage

A curious question is the mechanism of the electrically induced shrinkage, i.e., why gels shrink in electric field. Agar is known to be a thermosensitive gel which melts at ~ 80 ℃ and gels again when cooled down to room temperature. Despite the fact that current generates heat, the leaking water, falling out of the circuit and cooling down, does not gel again. Also, the temperature rise during the shrinking process is measured to be

several degrees, far less than what is required to melt the agar gel. Furthermore, some non-thermosensitive gels such as alginate and SA gels also shrink in electric field. Therefore, temperature change cannot be the mechanism.

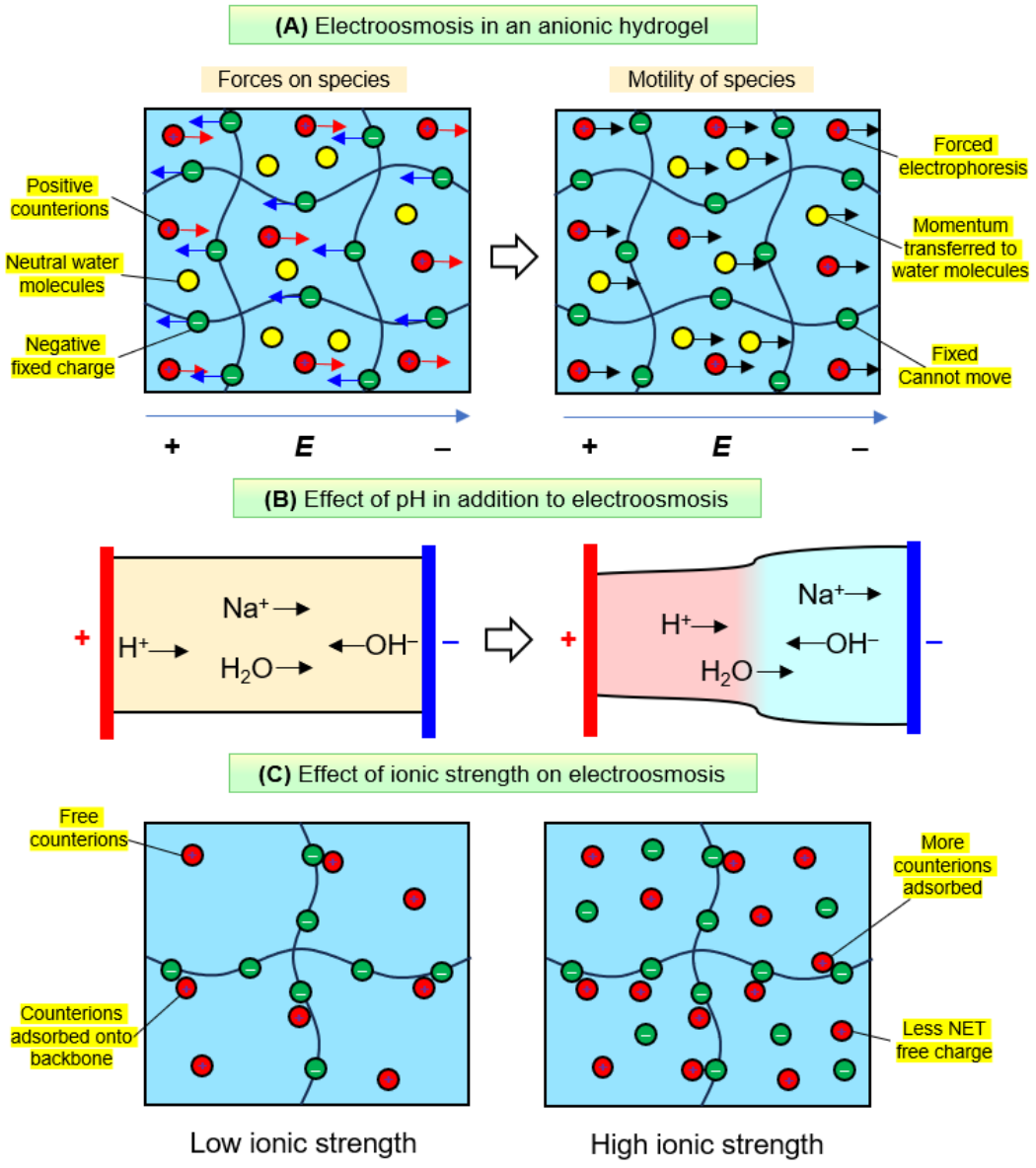

Figure 5.8. Schematics of Mechanism of Electric-Field-Induced Shrinkage. (A) Electroosmosis in an anionic gel. Negative charges are fixed on the gel backbone. Positive counterions and neutral solvent water are mobile. When an electric field is applied, the polyanion of the backbone cannot move, while mobile cations are forced to move along the field direction. Due to thermal motion, the cations collide with neutral

molecules and transfer momentum to them, making the solvent migrate towards the same direction. (B) Effect of pH. H^+ is generated on the anode and OH^- on the cathode. To balance the charge, counterions Na^+ are pumped to the basic side. By electroosmosis as illustrated in (A), water is pumped along with Na^+ from the acidic half to the basic half, making the acidic half shrink and the basic half swell. (C) Effect of salt. Counterions can be either mobile or adsorbed onto the gel backbone due to electrostatic attraction. As the ionic strength increases, more counterions are adsorbed onto the gel backbone, resulting in less net free mobile charge. Since electroosmosis is due to net mobile charge, increasing ionic strength decreases electroosmosis.

We have demonstrated that pH plays a role in the shrinkage since the pH difference corresponds to the different shrinkage behaviors of the two halves of the gel, but pH alone does not lead to shrinkage. Our observations also indicate that the loss of water is related to the ionic nature of the gel, and that ionic strength counteracts with the electric field. Based on this, we propose a combined effect of pH and electroosmosis as the mechanism. The agar gel as an anionic hydrogel has negative charge on its backbone and mobile cations as counterions. When the gel is placed in an electric field, the fixed charge on the gel backbone cannot move, while the mobile cations (most likely Na^+) are forced to move from the anode (+) side to the cathode (–) side. Because of thermal motion, the cations collide with water molecules and their translational momentum is transferred to water molecules. As a result, the liquid inside the gel moves from anode (+) to cathode (–) as a whole. This electroosmosis effect results in shrinkage on the anode side and gain in water on the cathode side. When more water than the gel can withhold is driven to the cathode side, excess liquid leaks out of the gel. (Figure 5.8A)

How pH affects the shrinkage of the agar gel is illustrated in Figure 5.8B. Since electroosmosis is an effect on the net mobile charge, its intensity should depend on

electric field strength and also gel composition. Consider the acidic half of the gel. As H^+ is generated from the anode, the mobile cations become excess, so Na^+ has to be electrophoresed away. On the contrary, the basic half of the gel has to gain Na^+ to balance the charge of OH^- generated from the cathode. Therefore, by electroosmosis Na^+ must drive water from the acidic half to the basic half. The acidic half loses water as a whole while the basic half gains water as a whole, thus generating a distinct boundary due to differential shrinkage.

The effect of extra salt on electroosmosis is illustrated in Figure 5.8C. When a higher concentration of salt is present in an anionic gel, more cations will be adsorbed onto the gel backbone. Therefore, less net mobile charge (cancelling out the positive and negative charges) will be present in the gel. Since electroosmosis is due to the net mobile charge, its intensity should be less. Thus increasing salt concentration prevents electrically induced shrinkage.

5.3.5 Electro-Carving Hydrogels into 3D Structures

Using this electrically induced shrinkage, we can "sculpt" a hydrogel into 3D shapes by focusing the electric field to shrink desired locations. Figure 5.9 shows a "smiley face" carved on a plate-shaped agar gel. A graphite rod is used as the anode (+) and a graphite plate is used as the cathode (–). Because the plate has much larger contact area with the gel than the rod does, the electric field is the most intense at the tip of the anode. So the gel shrinks most significantly at the anode (+) tip, while the deformation is negligible elsewhere. Therefore, the anode serves as a "knife" to "sculpt" patterns on the

agar gel. By moving the anode along a certain pathway, a smiley face is carved on top of the gel.

Figure 5.9. "Smiley Face" by Electro-Carving with a Rod Electrode. An agar gel plated is "sculpted" with a graphite rod anode as working electrode and a graphite plate as the counter electrode. 20 V is applied and the tip of the working electrode has the greatest intensity of electric field, making the gel shrink most intensely at the tip. By moving the electrode on the gel surface, a "smiley face" is carved on the gel plate within ~2.5 min.

5.4 Conclusions

In conclusion, we developed a novel strategy to carve hydrogels into 3D shapes using an electric field. An agar gel shrinks when it is electrolyzed between two graphite electrodes. We have found that half of the gel close to the anode shrinks, while water leaks out from the other half close to the cathode. As the electric field strength increases, the gel shrinks faster. With a higher agar concentration, the gel shrinks slower. Increasing the ionic strength of the gel prohibits the shrinkage under electric field. The same phenomenon occurs on various anionic hydrogels besides agar, such as alginate and poly(sodium acrylate) gels, while non-ionic hydrogels show no deformation. This shrinkage under electric field is attributed to a combined effect of pH and electroosmosis. We demonstrate that by focusing the electric field at the tip of a rod electrode, the shrinkage can be localized at designated locations on a hydrogel. Therefore, an electric field can be used as a “knife” to “sculpt” hydrogels into specific 3D shapes. This electro-carving method could be an alternative to current hydrogel 3D-printing strategies. As a top-down method that eliminates excess parts from a bulk material, electro-carving could be beneficial when fabricating certain structures, since it avoids building up materials from scratch as in bottom-up strategies like 3D-printing.

Chapter 6
Recommendations and Future Work

6.1 Project Summary

In this dissertation, we studied various different responses that an electric field could trigger on different polymeric materials. Based on the effects of electric field, we developed different strategies to modulate the polymeric materials. By utilizing a DC electric voltage of 5~20 V, different effects on polymeric materials, including adhesion to a hard solid electrode, change of physical state from solution to gel, and spatially resolved shrinkage, could be triggered in a facile manner. From the scientific aspect, this work broadens the knowledge base of electrochemistry of polymeric materials, regarding both electrochemical reactions and electrophoretic effects. From the technical standpoint, this work develops novel and facile strategies to fabricate complex structures with soft materials, either hybrid structures with hard and soft materials or 3D-structured hydrogels. These strategies could potentially be useful in robotics, energy storage, underwater adhesion, tissue engineering and so on.

In Chapter 3, we have reported a facile method for adhering soft, aqueous materials to hard materials. The soft material needs to be an ionic conductor, which typically means it must have water and ions (salt). Examples of such soft materials include hydrogels as well as animal-based tissues (meat from cows, pigs, and chickens) and plant-based tissues (fruits and vegetables). The hard material must be an electronic conductor like a metal or graphite, allowing it to serve as electrodes in a simple

electrochemical setup. Our method, which we term *hard-soft electro-adhesion* or **EA**$^{[HS]}$, is to bring the hard and soft materials into contact and apply a low DC electric voltage (e.g., 5 V) for a short time (e.g., 3 min). Depending on the nature of the hard and soft materials, adhesion is induced at the anode (+), cathode (–), both electrodes, or neither. After the field is removed, this adhesion still persists. If adhesion is observed only to one electrode, switching the polarity of the field typically reverses the adhesion. The adhesion strength increases with increasing voltage, time in the field, and ionic conductivity of the gel. The ultimate adhesion strength is limited only by the strength of the gel. Metals that can be adhered via **EA**$^{[HS]}$ to AAm gels (all at the anode) have reduction potentials above a critical value. This correlation to the electrochemical series suggests that **EA**$^{[HS]}$ is due to chemical bonds between the gel and the anode induced by electrochemical reactions. FTIR data on chemical changes at the interface supports this conclusion. Finally, the versatility of this phenomenon is shown through various examples. **EA**$^{[HS]}$ could enable applications in robotics, energy storage, and underwater adhesion.

In Chapter 4, we introduce a nozzle-free 3D-printing technique which uses an electric field for solidification of bio-ink. When an alginate solution is electrolyzed with inert electrodes, a gel is formed at the anode with spatial and temporal resolution. Using a moving working electrode, multiple alginate gels can be formed at different locations. These gels serve as building blocks or “voxels” and merge together spontaneously, thereby forming 3D structures. This electro-gelation strategy is fast and at low cost compared to regular 3D-bioprinting. Resolution of electro-gelation can be fine-tuned to hundreds of micron scale. Cell studies confirmed that cells can adhere to and survive on

printed gels. Electro-gelation could also apply to other ionic biopolymers such as chitosan. This strategy may provide a facile alternative to currently available 3D-bioprinting techniques.

In Chapter 5, we developed a novel strategy to "sculpt" hydrogels into 3D shapes with an electric field as the "knife". An agar gel shrinks while electrolyzed between two graphite electrodes. We have found that half of the gel close to the anode shrinks, while water leaks out from the other half close to the cathode. The gel shrinks faster as the field strength increases or the polymer concentration decreases. Increasing the ionic strength of the gel prohibits the shrinkage under electric field. Anionic hydrogels besides agar such as alginate and poly(sodium acrylate) gels also shrink in electric field, while non-ionic hydrogels do not. This phenomenon is attributed to a combined effect of pH and electroosmosis. By focusing the electric field at the tip of a rod electrode, we can localize the shrinkage at designated locations on a hydrogel. Therefore, an electric field can be used as a "knife" to "sculpt" hydrogels into specific 3D shapes. This electro-carving strategy could be an alternative to current hydrogel 3D-printing strategies. As a top-down method, it eliminates excess parts from a bulk material, while bottom-up strategies like 3D-printing build up materials from scratch. Electro-carving could be beneficial when fabricating certain structures, since it may save time from building mass amount of materials compared to 3D-bioprinting.

6.2 Recommendations for Future Work

6.2.1 3D-printing hybrid hydrogels by electro-gelation

In Chapters 4, we demonstrate that an electric stimulus can be utilized in 3D-printing technique as the solidification method. A homogeneous structure can be easily printed with one single bio-ink. However, practically, structures with multiple compartments could be more useful in many cases, as different compartments could have synergetic effects and thus enable special functions.

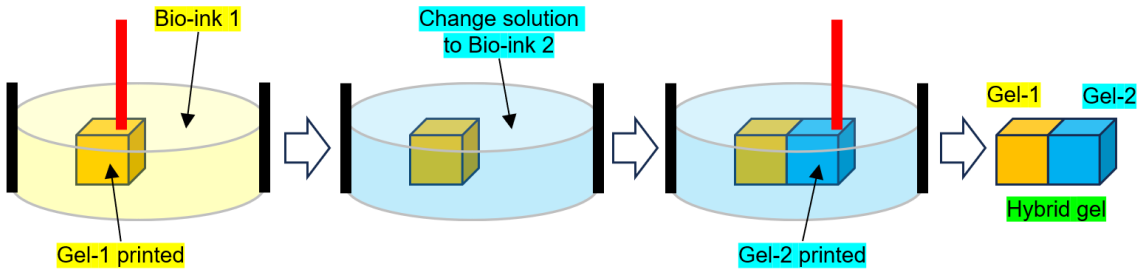

Figure 6.1. Proposed 3D-printing of hybrid gels. Gel-1 is printed by electro-gelation with a first bio-ink. Then the surrounding bio-ink is removed and replaced with a second bio-ink. Afterwards gel-2 is printed by electro-gelation. The resulting gel should be a combination of gel-1 and gel-2.

In principle, it is also possible for electro-gelation to print multi-compartment structures by switching the bio-ink as in extrusion-based printing techniques. We propose to first print one compartment of a structure with a first bio-ink, and then change the solution in the container to the second bio-ink and print the next compartment. In this way, hybrid structures should be formed, which adds to the flexibility of electro-gelation as a 3D-printing strategy. The compartments can differ from each other in various ways. For instance, they can be printed with alginate solutions of different concentrations. This

will lead to different mechanical properties at different locations of the gel. Or different compartments can be loaded with different cargos such as nanoparticles, enzymes and so on. It would also be interesting to see if electro-gelation can combine different biopolymers into a hybrid gel as different compartments.

6.2.2 4D-printing using electric stimuli

3D-printing is a spatially resolved material fabrication technique. Apart from the three spatial dimensions, researchers also extend the concept to the dimension of time, which leads to 4D-printing. The concept of 4D-printing is as follows.[105,106] A stimuli-responsive material is first printed by 3D-printing. Then the resulting structure is subjected to an appropriate stimulus so that it deforms and becomes the desired structure. Typically, the printed structure can transform back to its original shape as printed upon a reversed stimuli. In this way, the printed structure has a deformation "dimension" in addition to the three spatial dimensions, and thus the technique is termed "4D-printing". Such stimuli-responsive materials could be beneficial as their different 3D shapes before and after triggered transformation could be suitable in different circumstances. For instance, a flat geometry is convenient for storage and transportation since it takes up less space, while 3D shapes are typically required for functioning. When a 4D-printed material is not in use, it can stay in its flat geometry, while when its functionality is needed, a stimulus can be easily applied so that it transforms into the required 3D shape.

We demonstrated in Chapter 4 that 3D-printing of hydrogels can be achieved by electro-gelation. In the literature, it is also reported that an electric field can trigger

hydrogels to fold or bend. This provides a possibility that the two steps of 4D-printing, i.e., printing of the material and triggered transformation, can both be realized with electric field. We propose to first fabricate a stimuli-responsive structure using electro-gelation and then apply electric stimuli to make it transform into a desired shape. This idea may broaden the possibility of our electro-gelation technique as it includes one more dimension of flexibility.

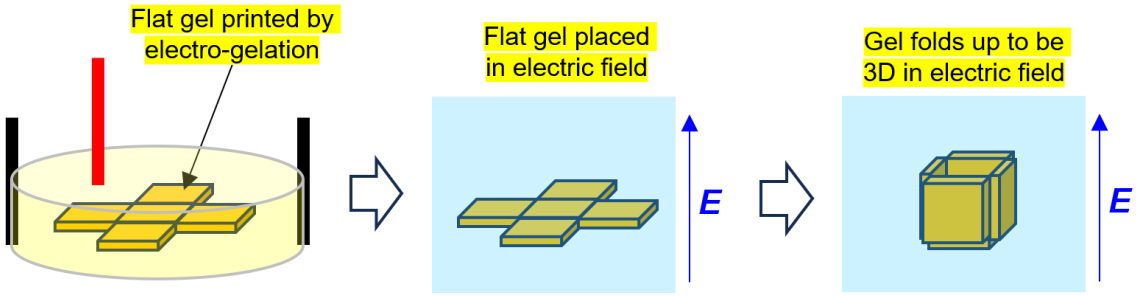

Figure 6.2. Proposed 4D-printing. A flat structure should be printed with electro-gelation using an electro-responsive soft material. When an appropriate electric field is applied afterwards, it should bend or fold up to be a 3D structure.

6.2.3 Combining electro-adhesion and 3D-shaping of hydrogels

In chapter 3, we observed that a strong adhesion can be triggered by an electric stimulus between a soft polymeric material and a hard solid. This combination of hard and soft materials, in some sense, is analogous to naturally existing skeletomuscular system, where soft muscles are adhered to hard bones to enable body motion. Yet muscles are much more complex than synthetic hydrogels, in terms of both chemistry and structure. To really mimic the functionality of naturally existing systems, well-designed 3D structures of the soft material is often required. Therefore, we propose to use the

fabrication strategies in Chapter 4 & 5 to make 3D-shaped hydrogels and then electro-adhere the hydrogels to hard solids. This could result in more functionalities than simply combining cuboid or cylindrical gels with hard solids.

6.2.4. Electrochemistry between electrodes and gel backbone

In Chapter 3, we show that the adhesion between hard solids and soft gels results from chemical bonds between the electrode and the gel backbone generated by electrochemical reactions. Electrochemical reactions in aqueous solutions have been studied for centuries, and electrochemical organic synthesis is also of interest. But direct electrochemical reactions between electrodes and polymer chains instead of small molecules are seldom reported. We show that polymeric gel backbone can also adsorb onto the electrode and exchange electrons with the electrode without small molecules to mediate the reaction. Also, in common electrochemical reaction mechanisms, after electron exchange the products should detach from the electrode. Yet in the case of $\mathbf{EA}^{[HS]}$, the adsorbed species is the final product without detachment step. We believe that the reaction mechanism of polymers or gel backbones on an electrode would be interesting in terms of broadening the knowledge base of electrochemistry.

References

[1] Kwon, G. H.; Park, J. Y.; Kim, J. Y.; Frisk, M. L.; Beebe, D. J.; Lee, S. H. "Biomimetic soft multifunctional miniature aquabots." *Small* **2008**, *4*, 2148-53.

[2] Lim, H. L.; Chuang, J. C.; Tran, T.; Aung, A.; Arya, G.; Varghese, S. "Dynamic Electromechanical Hydrogel Matrices for Stem Cell Culture." *Adv. Funct. Mater.* **2011**, *21*, 55-63.

[3] Markx, G. H. "The use of electric fields in tissue engineering: A review." *Organogenesis* **2008**, *4*, 11-7.

[4] Wadhwa, R.; Lagenaur, C. F.; Cui, X. T. "Electrochemically controlled release of dexamethasone from conducting polymer polypyrrole coated electrode." *J. Control. Release* **2006**, *110*, 531-41.

[5] Morales, D.; Palleau, E.; Dickey, M. D.; Velev, O. D. "Electro-actuated hydrogel walkers with dual responsive legs." *Soft Matter* **2014**, *10*, 1337-1348.

[6] Brannonpeppas, L.; Peppas, N. A. "Equilibrium Swelling Behavior of Ph-Sensitive Hydrogels." *Chem. Eng. Sci.* **1991**, *46*, 715-722.

[7] Koetting, M. C.; Peters, J. T.; Steichen, S. D.; Peppas, N. A. "Stimulus-responsive hydrogels: Theory, modern advances, and applications." *Mat. Sci. Eng. R* **2015**, *93*, 1-49.

[8] Matsuo, E. S.; Tanaka, T. "Patterns in Shrinking Gels." *Nature* **1992**, *358*, 482-485.

[9] Peppas, N. A.; Hilt, J. Z.; Khademhosseini, A.; Langer, R. "Hydrogels in biology and medicine: From molecular principles to bionanotechnology." *Adv. Mater.* **2006**, *18*, 1345-1360.

[10] Peppas, N. A.; Huang, Y.; Torres-Lugo, M.; Ward, J. H.; Zhang, J. "Physicochemical, foundations and structural design of hydrogels in medicine and biology." *Annu. Rev. Biomed. Eng.* **2000**, *2*, 9-29.

[11] Qiu, Y.; Park, K. "Environment-sensitive hydrogels for drug delivery." *Adv. Drug Deliver. Rev.* **2012**, *64*, 49-60.

[12] Tokarev, I.; Minko, S. "Stimuli-responsive hydrogel thin films." *Soft Matter* **2009**, *5*, 511-524.

[13] Harris, R. D.; Auletta, J. T.; Motlagh, S. A. M.; Lawless, M. J.; Perri, N. M.; Saxena, S.; Weiland, L. M.; Waldeck, D. H.; Clark, W. W.; Meyer, T. Y.

"Chemical and Electrochemical Manipulation of Mechanical Properties in Stimuli-Responsive Copper-Cross-Linked Hydrogels." *ACS Macro Lett.* **2013**, *2*, 1095-1099.

[14] Liu, Y.; Genzer, J.; Dickey, M. D. ""2D or not 2D": Shape-programming polymer sheets." *Prog. Polym. Sci.* **2016**, *52*, 79-106.

[15] Gargava, A.; Xu, W. H.; Raghavan, S. R. "Electrically Induced Bursting of Aqueous Capsules Made from Biopolymers: 'Switching On' the Release of Payloads." *Adv. Funct. Mater.* **2022**, *32*, 2206029.

[16] Svirskis, D.; Travas-Sejdic, J.; Rodgers, A.; Garg, S. "Electrochemically controlled drug delivery based on intrinsically conducting polymers." *J. Control. Release* **2010**, *146*, 6-15.

[17] Zinger, B.; Miller, L. L. "Timed Release of Chemicals from Polypyrrole Films." *J. Am. Chem. Soc.* **1984**, *106*, 6861-6863.

[18] Shi, X. W.; Tsao, C. Y.; Yang, X. H.; Liu, Y.; Dykstra, P.; Rubloff, G. W.; Ghodssi, R.; Bentley, W. E.; Payne, G. F. "Electroaddressing of Cell Populations by Co-Deposition with Calcium Alginate Hydrogels." *Adv. Funct. Mater.* **2009**, *19*, 2074-2080.

[19] Haider, S.; Park, S. Y.; Saeed, K.; Farmer, B. L. "Swelling and electroresponsive characteristics of gelatin immobilized onto multi-walled carbon nanotubes." *Sensor. Actuat. B-Chem.* **2007**, *124*, 517-528.

[20] Hirose, Y.; Giannetti, G.; Marquardt, J.; Tanaka, T. "Migration of Ions and pH Gradients in Gels under Stationary Electric-Fields." *J. Phys. Soc. Jpn.* **1992**, *61*, 4085-4097.

[21] Tanaka, T.; Nishio, I.; Sun, S. T.; Uenonishio, S. "Collapse of Gels in an Electric-Field." *Science* **1982**, *218*, 467-469.

[22] Palleau, E.; Morales, D.; Dickey, M. D.; Velev, O. D. "Reversible patterning and actuation of hydrogels by electrically assisted ionoprinting." *Nat. Commun.* **2013**, *4*, 2257.

[23] Asoh, T. A.; Kawamura, E.; Kikuchi, A. "Stabilization of electrophoretically adhered gel-interfaces to construct multi-layered hydrogels." *RSC Adv.* **2013**, *3*, 7947-7952.

[24] Asoh, T. A.; Kikuchi, A. "Electrophoretic adhesion of stimuli-responsive hydrogels." *Chem. Commun.* **2010**, *46*, 7793-7795.

[25] Asoh, T. A.; Kikuchi, A. “Rapid fabrication of reconstructible hydrogels by electrophoretic microbead adhesion.” *Chem. Commun.* **2012**, *48*, 10019-10021.

[26] Asoh, T. A.; Kinoshita, H.; Shoji, T.; Kikuchi, A.; Tsuboi, Y. “Rapid hydrogel repair utilizing microgel architectures.” *Mater. Chem. Front.* **2017**, *1*, 1594-1599.

[27] Borden, L. K.; Gargava, A.; Kokilepersaud, U. J.; Raghavan, S. R. “Universal way to "glue" capsules and gels into 3D structures by electroadhesion.” *ACS Appl. Mater. Interfaces* **2023**, *15*, 17070-17077.

[28] Gargava, A.; Ahn, S.; Bentley, W. E.; Raghavan, S. R. “Rapid Electroformation of Biopolymer Gels in Prescribed Shapes and Patterns: A Simpler Alternative to 3-D Printing.” *ACS Appl. Mater. Interfaces* **2019**, *11*, 37103-37111.

[29] Borden, L. K.; Gargava, A.; Raghavan, S. R. “Reversible electroadhesion of hydrogels to animal tissues for suture-less repair of cuts or tears.” *Nat. Commun.* **2021**, *12*, 4419.

[30] Tanaka, T. “Gels.” *Sci. Am.* **1981**, *244*, 124-&.

[31] Li, J.; Mooney, D. J. “Designing hydrogels for controlled drug delivery.” *Nat. Rev. Mater.* **2016**, *1*, 16071.

[32] Sikdar, P.; Uddin, M. M.; Dip, T. M.; Islam, S.; Hoque, M. S.; Dhar, A. K.; Wu, S. “Recent advances in the synthesis of smart hydrogels.” *Mater. Adv.* **2021**, *2*, 4532-4573.

[33] Quesada-Pérez, M.; Maroto-Centeno, J. A.; Forcada, J.; Hidalgo-Alvarez, R. “Gel swelling theories: the classical formalism and recent approaches.” *Soft Matter* **2011**, *7*, 10536-10547.

[34] Colombani, D. “Chain-growth control in free radical polymerization.” *Prog. Polym. Sci.* **1997**, *22*, 1649-1720.

[35] Banik, S. J.; Fernandes, N. J.; Thomas, P. C.; Raghavan, S. R. “A new approach for creating polymer hydrogels with regions of distinct chemical, mechanical, and optical properties.” *Macromolecules* **2012**, *45*, 5712-5717.

[36] Tako, M. “The principle of polysaccharide gels.” *Adv. Biosci. Biotechnol.* **2015**, *6*, 22.

[37] Pawar, S. N.; Edgar, K. J. “Alginate derivatization: A review of chemistry, properties and applications.” *Biomaterials* **2012**, *33*, 3279-3305.

[38] Grant, G. T.; Morris, E. R.; Rees, D. A.; Smith, P. J. C.; Thom, D. "Biological Interactions between Polysaccharides and Divalent Cations - Egg-Box Model." *FEBS Lett.* **1973**, *32*, 195-198.

[39] Djabourov, M. "Architecture of gelatin gels." *Contemp. Phys.* **1988**, *29*, 273-297.

[40] Jaipan, P.; Nguyen, A.; Narayan, R. "Gelatin-based hydrogels for biomedical applications." *MRS Commun.* **2017**, *7*, 416-426.

[41] Bhattarai, N.; Gunn, J.; Zhang, M. Q. "Chitosan-based hydrogels for controlled, localized drug delivery." *Adv. Drug Deliver. Rev.* **2010**, *62*, 83-99.

[42] Tako, M.; Nakamura, S. "Gelation mechanism of agarose." *Carbohyd. Res.* **1988**, *180*, 277-284.

[43] Salati, M. A.; Khazai, J.; Tahmuri, A. M.; Samadi, A.; Taghizadeh, A.; Taghizadeh, M.; Zarrintaj, P.; Ramsey, J. D.; Habibzadeh, S.; Seidi, F.; Saeb, M. R.; Mozafari, M. "Agarose-based biomaterials: Opportunities and challenges in cartilage tissue engineering." *Polymers* **2020**, *12*, 1150.

[44] Bard, A. J.; Faulkner, L. R. *Electrochemical Methods : Fundamentals and Applications*, 2nd ed.; John Wiley: New York, 2001.

[45] OpenStaxCollege *Biology*; Downloadable at http://cnx.org/content/col11448/latest/, 2013.

[46] Levental, I.; Georges, P. C.; Janmey, P. A. "Soft biological materials and their impact on cell function." *Soft Matter* **2007**, *3*, 299-306.

[47] Alberts, B. *Molecular Biology of the Cell*, 4th ed.; Garland Publishers: New York, 2002.

[48] Felsenthal, N.; Zelzer, E. "Mechanical regulation of musculoskeletal system development." *Development* **2017**, *144*, 4271-4283.

[49] Li, Z. W.; Seo, Y.; Aydin, O.; Elhebeary, M.; Kamm, R. D.; Kong, H.; Saif, M. T. A. "Biohybrid valveless pump-bot powered by engineered skeletal muscle." *Proc. Natl. Acad. Sci. USA* **2019**, *116*, 1543-1548.

[50] Raman, R.; Cvetkovic, C.; Bashir, R. "A modular approach to the design, fabrication, and characterization of muscle-powered biological machines." *Nat. Protoc.* **2017**, *12*, 519-533.

[51] Sun, Z. Q.; Li, Z. H.; Qu, K. Y.; Zhang, Z. Z.; Niu, Y. Z.; Xu, W. L.; Ren, C. G. "A review on recent advances in gel adhesion and their potential applications." *J. Mol. Liq.* **2021**, *325*, 115254.

[52] Shao, H.; Stewart, R. J. "Biomimetic underwater adhesives with environmentally triggered setting mechanisms." *Adv. Mater.* **2010**, *22*, 729-733.

[53] Muir, B. V.; Myung, D.; Knoll, W.; Frank, C. W. "Grafting of cross-linked hydrogel networks to titanium surfaces." *ACS Appl. Mater. Interfaces* **2014**, *6*, 958-966.

[54] Sekine, T.; Takashima, Y.; Harada, A. "Direct covalent bond formation between materials using copper(I)-catalyzed azide alkyne cycloaddition reactions." *RSC Adv.* **2015**, *5*, 56130-56135.

[55] Wang, Y. M.; Huang, F. R.; Chen, X. B.; Wang, X. W.; Zhang, W. B.; Peng, J.; Li, J. Q.; Zhai, M. L. "Stretchable, conductive, and self-healing hydrogel with super metal adhesion." *Chem. Mater.* **2018**, *30*, 4289-4297.

[56] Li, A.; Jia, Y.; Sun, S.; Xu, Y.; Minsky, B. B.; Stuart, M. A. C.; Colfen, H.; von Klitzing, R.; Guo, X. "Mineral-enhanced polyacrylic acid hydrogel as an oyster-inspired organic-inorganic hybrid adhesive." *ACS Appl. Mater. Interfaces* **2018**, *10*, 10471-10479.

[57] Rao, P.; Sun, T. L.; Chen, L.; Takahashi, R.; Shinohara, G.; Guo, H.; King, D. R.; Kurokawa, T.; Gong, J. P. "Tough hydrogels with fast, strong, and reversible underwater adhesion based on a multiscale design." *Adv. Mater.* **2018**, *30*, 1801884.

[58] He, X. Y.; Liu, L. Q.; Han, H. M.; Shi, W. Y.; Yang, W.; Lu, X. Q. "Bioinspired and microgel-tackified adhesive hydrogel with rapid self-healing and high stretchability." *Macromolecules* **2019**, *52*, 72-80.

[59] Li, W.; Liu, X.; Deng, Z.; Chen, Y.; Yu, Q.; Tang, W.; Sun, T. L.; Zhang, Y. S.; Yue, K. "Tough bonding, on-demand debonding, and facile rebonding between hydrogels and diverse metal surfaces." *Adv. Mater.* **2019**, *31*, 1904732.

[60] Yu, J.; Wei, W.; Danner, E.; Ashley, R. K.; Israelachvili, J. N.; Waite, J. H. "Mussel protein adhesion depends on interprotein thiol-mediated redox modulation." *Nat. Chem. Biol.* **2011**, *7*, 588-590.

[61] Lee, H.; Lee, B. P.; Messersmith, P. B. "A reversible wet/dry adhesive inspired by mussels and geckos." *Nature* **2007**, *448*, 338.

[62] Lv, R.; Bei, Z. W.; Huang, Y.; Chen, Y. W.; Zheng, Z. Q.; You, Q. L.; Zhu, C.; Cao, Y. P. "Mussel-inspired flexible, wearable, and self-adhesive conductive hydrogels for strain sensors." *Macromol. Rapid Comm.* **2020**, *41*, 1900450.

[63] Guo, J. L.; Leng, J. S.; Rossiter, J. “Electroadhesion technologies for robotics: A comprehensive review.” *IEEE Trans. Robotics* **2020**, *36*, 313-327.

[64] Rajagopalan, P.; Muthu, M.; Liu, Y. L.; Luo, J. K.; Wang, X. Z.; Wan, C. Y. “Advancement of electroadhesion technology for intelligent and self-reliant robotic applications.” *Adv. Intell. Syst.* **2022**, *4*, 2200064.

[65] Johnsen, A.; Rahbek, K. “A physical phenomenon and its applications to telegraphy, telephony, etc.” *J. Inst. Elect. Eng.* **1923**, *61*, 713-725.

[66] Shintake, J.; Rosset, S.; Schubert, B.; Floreano, D.; Shea, H. “Versatile soft grippers with intrinsic electroadhesion based on multifunctional polymer actuators.” *Adv. Mater.* **2016**, *28*, 231-238.

[67] Levine, D. J.; Iyer, G. M.; Daelan Roosa, R.; Turner, K. T.; Pikul, J. H. “A mechanics-based approach to realize high-force capacity electroadhesives for robots.” *Sci. Robot.* **2022**, *7*, eabo2179.

[68] Qiu, X.; Huang, X.; Zhang, L. “Electrochemical bonding of hydrogels at rigid surfaces.” *Small Methods* **2022**, *6*, e2201132.

[69] Adelnia, H.; Ensandoost, R.; Moonshi, S. S.; Gavgani, J. N.; Vasafi, E. I.; Ta, H. T. “Freeze/thawed polyvinyl alcohol hydrogels: Present, past and future.” *Eur. Polym. J.* **2022**, *164*, 110974.

[70] Comyn, J. *Adhesion Science*; The Royal Society of Chemistry: Cambridge, UK, 1997.

[71] Martin, L. B. B.; Rose, J. K. C. “There's more than one way to skin a fruit: Formation and functions of fruit cuticles.” *J. Exp. Bot.* **2014**, *65*, 4639-4651.

[72] Enev, V.; Sedlacek, P.; Rihak, M.; Kalina, M.; Pekar, M. “IR-Supported Thermogravimetric Analysis of Water in Hydrogels.” *Front. Mater.* **2022**, *9*, 931303.

[73] Stuart, B. *Infrared Spectroscopy: Fundamentals and Applications*; John Wiley & Sons, Ltd, 2004.

[74] Mallakpour, S.; Azadi, E.; Hussain, C. M. “State-of-the-art of 3D printing technology of alginate-based hydrogels-An emerging technique for industrial applications.” *Adv. Colloid Interface Sci.* **2021**, *293*, 102436.

[75] Zhu, W.; Ma, X. Y.; Gou, M. L.; Mei, D. Q.; Zhang, K.; Chen, S. C. “3D printing of functional biomaterials for tissue engineering.” *Curr. Opin. Biotechnol.* **2016**, *40*, 103-112.

[76] Murphy, S. V.; Atala, A. "3D bioprinting of tissues and organs." *Nat. Biotechnol.* **2014**, *32*, 773-785.

[77] Browne, M. P.; Redondo, E.; Pumera, M. "3D Printing for Electrochemical Energy Applications." *Chem. Rev.* **2020**, *120*, 2783-2810.

[78] Goh, G. D.; Sing, S. L.; Yeong, W. Y. "A review on machine learning in 3D printing: applications, potential, and challenges." *Artif. Intell. Rev.* **2021**, *54*, 63-94.

[79] Le Duigou, A.; Correa, D.; Ueda, M.; Matsuzaki, R.; Castro, M. "A review of 3D and 4D printing of natural fibre biocomposites." *Mater. Design* **2020**, *194*, 108911.

[80] Li, J. H.; Wu, C. T.; Chu, P. K.; Gelinsky, M. "3D printing of hydrogels: Rational design strategies and emerging biomedical applications." *Mater. Sci. Eng. R Rep.* **2020**, *140*, 100543.

[81] Nadagouda, M. N.; Rastogi, V.; Ginn, M. "A review on 3D printing techniques for medical applications." *Curr. Opin. Chem. Eng.* **2020**, *28*, 152-157.

[82] Keerthana, K.; Anukiruthika, T.; Moses, J. A.; Anandharamakrishnan, C. "Development of fiber-enriched 3D printed snacks from alternative foods: A study on button mushroom." *J. Food Eng.* **2020**, *287*, 110116.

[83] Melocchi, A.; Uboldi, M.; Maroni, A.; Foppoli, A.; Palugan, L.; Zema, L.; Gazzaniga, A. "3D printing by fused deposition modeling of single- and multi-compartment hollow systems for oral delivery - A review." *Int. J. Pharm.* **2020**, *579*, 119155.

[84] Prendergast, M. E.; Burdick, J. A. "Recent Advances in Enabling Technologies in 3D Printing for Precision Medicine." *Adv. Mater.* **2020**, *32*, 1902516.

[85] Boland, T.; Mironov, V.; Gutowska, A.; Roth, E. A.; Markwald, R. R. "Cell and organ printing 2: Fusion of cell aggregates in three-dimensional gels." *Anat. Rec. Part A* **2003**, *272A*, 497-502.

[86] Wilson, W. C.; Boland, T. "Cell and organ printing 1: Protein and cell printers." *Anat. Rec. Part A* **2003**, *272A*, 491-496.

[87] Mironov, V.; Kasyanov, V.; Markwald, R. R. "Organ printing: from bioprinter to organ biofabrication line." *Curr. Opin. Biotechnol.* **2011**, *22*, 667-673.

[88] Mironov, V.; Visconti, R. P.; Kasyanov, V.; Forgacs, G.; Drake, C. J.; Markwald, R. R. "Organ printing: Tissue spheroids as building blocks." *Biomaterials* **2009**, *30*, 2164-2174.

[89] Lu, Y.; Mapili, G.; Suhali, G.; Chen, S. C.; Roy, K. “A digital micro-mirror device-based system for the microfabrication of complex, spatially patterned tissue engineering scaffolds.” *J. Biomed. Mater. Res. A* **2006**, *77A*, 396-405.

[90] Zhang, A. P.; Qu, X.; Soman, P.; Hribar, K. C.; Lee, J. W.; Chen, S. C.; He, S. L. “Rapid Fabrication of Complex 3D Extracellular Microenvironments by Dynamic Optical Projection Stereolithography.” *Adv. Mater.* **2012**, *24*, 4266.

[91] Doraiswamy, A.; Narayan, R. J.; Harris, M. L.; Qadri, S. B.; Modi, R.; Chrisey, D. B. “Laser microfabrication of hydroxyapatite-osteoblast-like cell composites.” *J. Biomed. Mater. Res. A* **2007**, *80A*, 635-643.

[92] Koch, L.; Deiwick, A.; Schlie, S.; Michael, S.; Gruene, M.; Coger, V.; Zychlinski, D.; Schambach, A.; Reimers, K.; Vogt, P. M.; Chichkov, B. “Skin tissue generation by laser cell printing.” *Biotechnol. Bioeng.* **2012**, *109*, 1855-1863.

[93] Liao, Y.; Song, J. X.; Li, E.; Luo, Y.; Shen, Y. L.; Chen, D. P.; Cheng, Y.; Xu, Z. Z.; Sugioka, K.; Midorikawa, K. “Rapid prototyping of three-dimensional microfluidic mixers in glass by femtosecond laser direct writing.” *Lab Chip* **2012**, *12*, 746-749.

[94] Bajaj, P.; Schweller, R. M.; Khademhosseini, A.; West, J. L.; Bashir, R. “3D Biofabrication Strategies for Tissue Engineering and Regenerative Medicine.” *Annu. Rev. Biomed. Eng.* **2014**, *16*, 247-276.

[95] Fu, H. H.; Liu, Y. Z.; Adrià, F.; Shao, X. G.; Cai, W. S.; Chipot, C. “From Material Science to Avant-Garde Cuisine. The Art of Shaping Liquids into Spheres.” *J. Phys. Chem. B* **2014**, *118*, 11747-11756.

[96] Nojoomi, A.; Jeon, J.; Yum, K. “2D material programming for 3D shaping.” *Nat. Commun.* **2021**, *12*, 603.

[97] Schmidt, F. “The Art of Shaping Materials.” *Art Percept.* **2020**, *8*, 407-433.

[98] Shaked, T.; Bar-Sinai, K. L.; Sprecher, A. “Adaptive robotic stone carving: Method, tools, and experiments.” *Autom. Constr.* **2021**, *129*, 103809.

[99] Yin, F. C.; Ji, Q. Z.; Wen, C. W. “An adaptive terminal sliding mode control of stone-carving robotic manipulators based on radial basis function neural network.” *Appl. Intell.* **2022**, *52*, 16051-16068.

[100] Molloy, B.; Mödlinger, M. “The Organisation and Practice of Metal Smithing in Later Bronze Age Europe.” *J World Prehist.* **2020**, *33*, 169-232.

[101] Vijayaram, T. R.; Sulaiman, S.; Hamouda, A. M. S.; Ahmad, M. H. M. "Numerical simulation of casting solidification in permanent metallic molds." *J. Mater. Process. Technol.* **2006**, *178*, 29-33.

[102] del Barrio, E.; Sánchez-Somolinos, C. "Light to Shape the Future: From Photolithography to 4D Printing." *Adv. Opt. Mater.* **2019**, *7*, 1900598.

[103] Miller, A.; Mumford, L. *Stone and Marble Carving: A Manual for the Student Sculptor*; Univ. of California Press, 1948.

[104] Evans, J. M. *The Lives of Sumerian Sculpture: An Archaeology of the Early Dynastic Temple*; Cambridge University Press, 2012.

[105] Gladman, A. S.; Matsumoto, E. A.; Nuzzo, R. G.; Mahadevan, L.; Lewis, J. A. "Biomimetic 4D printing." *Nat. Mater.* **2016**, *15*, 413-+.

[106] Skylar, T.; Carrie, M.; Carlos, O.; Daniel, D.; Shai, H. "4D Printing and Universal Transformation." *Proceedings of the 34th Annual Conference of the Association for Computer Aided Design in Architecture* **2014**, 539-548.

List of Publications

Publications:

[1] Xu, W. H.; Burni, F. A.; Raghavan, S. R. “Electrically Induced Adhesion of Hard and Soft Materials: A Simple Way to Reversibly Stick Metals or Graphite to Gels or Tissues.” *ACS Cent. Sci.* **2024**, *10*, 695-707.

[2] Ma, P.; Jia, X.; Xu, W.; He, Y.; Tarwa, K.; Alharbi, M. O.; Wei, C.-I.; Wang, Q. “Enhancing salmon freshness monitoring with sol-gel cellulose nanocrystal colorimetric paper sensors and deep learning methods.” *Food Biosci.* **2023**, *56*, 103313.

[3] Gargava, A.; Xu, W. H.; Raghavan, S. R. “Electrically Induced Bursting of Aqueous Capsules Made from Biopolymers: 'Switching On' the Release of Payloads.” *Adv. Funct. Mater.* **2022**, *32*, 2206029.

[4] Ma, P. H.; Xu, W. H.; Teng, Z.; Luo, Y. G.; Gong, C.; Wang, Q. “An Integrated Food Freshness Sensor Array System Augmented by a Metal-Organic Framework Mixed-Matrix Membrane and Deep Learning.” *ACS Sensors* **2022**, *7*, 1847–1854.

[5] Ma, P. H.; Zhang, Z.; Xu, W. H.; Teng, Z.; Luo, Y. G.; Gong, C.; Wang, Q. “Integrated Portable Shrimp-Freshness Prediction Platform Based on Ice-Templated Metal-Organic Framework Colorimetric Combinatorics and Deep Convolutional Neural Networks.” *ACS Sustain. Chem. Eng.* **2021**, *9*, 16926-16936.

Manuscripts in preparation:

[1] Xu, W. H.; Burni, F. A.; Aroom, K.; Raghavan, S. R. “3D-printing biopolymer gels with an electric field - A simple route that avoids nozzles, heat and UV light.” *In preparation.*

[2] Xu, W. H.; Burni, F. A.; Nader, M.; Raghavan, S. R. “Electro-carving of hydrogels: Using a focused electric field to "sculpt" 3D structures.” *In preparation.*

List of Presentations

[1] Xu, W. H.; Raghavan, S. R. “3D-printing biopolymer gels with an electric field - A simple route that avoids nozzles, heat and UV light.” MRS Spring Meeting 2023, April, San Francisco, California.

[2] Xu, W. H.; Gargava, A.; Raghavan, S. R. “Electrically induced bursting of aqueous capsules made from biopolymers: ‘Switching on’ the release of payloads.” MRS Spring Meeting 2023, April, San Francisco, California.

[3] Raghavan, S. R.; Xu, W. H. “Creating biopolymer gels in 3D using electric fields: 3D-printing without heat or light.” 97th ACS Colloid and Surface Science Symposium 2023, June Raleigh, North Carolina.

[4] Xu, W. H.; Raghavan, S. R. “Strong adhesion of hard solids to soft gels by applying an electric field.” ACS Fall 2022, August, Chicago, Illinois.